Contents

Chapter 1

Abstract

Diblock copolymers dissolved in a selective solvent self-assemble into micellar aggregates. These aggregates consists of a diffuse corona of the dissolved blocks and a dense core of the insoluble blocks. The corona scattering has been investigated using the Monte Carlo simulation technique. The corona was represented as a number of chains tethered to a spherical core, chains interacted through excluded volume interactions and they were excluded from the core region. The corona scattering of a micelle contains information about single chain properties, such as the radius of gyration, as well as overall properties such as the radial monomer profile. The corona scattering can be separated into two contributions, one due to intra-chain and another due to inter-chain scattering. The corona scattering can, furthermore, be regarded as being caused by an average radial profile (as in a core-shell model) and a scattering contribution due to density fluctuation correlations about this average radial density profile. These fluctuations are caused by chain connectivity and chain-chain interaction effects such as the "correlation hole". The fluctuation scattering carries information about the compressibility of the corona.

Simulations were performed systematically varying the number of chains in the corona, the chain length, and core radius corresponding to surface coverages in the experimentally accessible regime for diblock copolymer micelles. During simulations the partial scattering contributions due to intra-chain and inter-chain scattering as well as the scattering due to the radial profile were sampled. Properties such as the single-chain radius of gyration, chain center-of-mass distance to the core, and the radial monomer profile were also sampled.

The model of micelle scattering due to Pedersen and Gerstenberg [J.S. Pedersen and M.C. Gerstenberg, Macromolecules (1996), 29, p. 1363] neglects the effects of excluded volume interactions. The validity of this model, which can estimate the chain radius of gyration and center-of-mass distance from the core, was investigated using simulated scattering data. The conclusion was that the model provides accurate estimates of for low surface coverages, but that the estimates get progressively worse as the surface coverage is increased.

Using a self-consistent analysis of the simulation data it was shown that the corona scattering can be very accurately represented by a weighted average between a core-shell model and a Random Phase Approximation (RPA) expres-

sion, where the core-shell model represents the scattering contribution due to the radial profile, and the RPA expression describes the fluctuation scattering contribution. The RPA approximation depends on the intra-chain scattering and an excluded volume parameter proportional to the apparent second virial coefficient. The resulting expression is denoted solution profile scattering as it has the interpretation of being the scattering from a two dimensional layer of dilute/semi-dilute polymer solution confined in a shell around the micelle surface with some radial density profile. The polymer solution can be regarded as being two dimensional since the width of corona is comparable to the radius of gyration of the corona chains.

The forward scattering due to density fluctuations can easily be obtained in this approach, and this provides the osmotic compressibility of the corona. The compressibility obtained from the self-consistent analysis shows an universal dependence on the reduced surface coverage, since compressibilities obtained from simulations varying number of chains, chain length, or core radius collapse onto a common curve. The corresponding apparent second virial coefficient follows an approximate power law as function of reduced surface coverage. The corona compressibility shows a surface coverage dependence analogous to that of a polymer solution as function of reduced concentration c/c^*. This validates that the micellar corona can be regarded as a quasi-two dimensional polymer solution.

The solution profile scattering expression has also been used for fitting the Monte Carlo simulation data. The expression depends on the single chain radius of gyration, an excluded volume coefficient, and a radial profile of the corona. Excellent fits were obtained within the entire range of experimentally available surface coverages using a Maximum Entropy estimate for the corona profile. The radius of gyration and the corona profile were estimated by the fits, and these were found to be in very good agreement with results obtained directly from the Monte Carlo simulation.

A formalism for the form factor and structure factor of connected acyclic polymer structures was developed based on a generalization of a diagrammatic interpretation of the micelle scattering model due to Pedersen and Gerstenberg. Some examples of structures described by this formalism includes micelles with an arbitrary core geometry, branched polymers, and copolymer stars. The formalism include excluded volume effects on the level of a linear chain, and an expression for the form factor of a copolymer with excluded volume interactions is given. Expressions for the form factor of a triblock copolymer star with and without excluded volume interactions have been derived using the formalism, and fitted to Monte Carlo simulations results for the scattering without excluded volume for $f = 2, 3$, and 6 arms. Scattering was sampled for the entire star as well as the individual blocks yielding scattering for four different contrasts in total. The simulated scattering results with excluded volume interactions for triblock copolymer stars with $f = 2$ arms have also been fitted. These fits show an excellent agreement between the simulated scattering results and the theoretical form factor.

Chapter 2

Resumé

Når diblokcopolymere opløses i et opløsningsmiddel, der er godt for den ene blok og dårlig for den anden blok, danner copolymerene en micelle bestående af en diffus korona af den opløste blok og en tæt kerne af den uopløselige blok. Koronaspredningen er blevet undersøgt med Monte Carlo simulationsteknikker. I simulationerne blev koronaen repræsenteret som et antal af kæder, der sidder fast på en kugleformet kerne. Kæderne vekselvirkede med "excluded volume" vekselvirkninger, og var udelukket fra kernen.

Koronaspredningen fra en micelle indeholder information om enkeltkæde egenskaber så som kædernes gyrationsradius og radialfordelingen af monomerer. Koronaspredningen har to bidrag, et fra intrakæde og et fra interkæde spredning, dvs. spredning fra den enkelte kæde og spredning mellem kæder. Koronaspredningen kan også opfattes som værende summen af to bidrag fra spredningen fra gennemsnits radialprofilen (en kerne-skal model) og fra korrelationer af tæthedsfluktuationer. Disse fluktuationer skyldes, at kæderne er sammenhængende og kæde-kæde vekselvirkninger som for eksempel "korrelations hullet". Fluktuationsspredningsbidraget indeholder information om koronaens kompressibilitet.

Simulationer er blevet udført, hvor antallet af kæder, kædelængde og kerneradius systematisk er blevet varieret svarende til de overfladetætheder, der kan opnås eksperimentelt for diblokcopolymer miceller. Under simulationerne blev spredningsbidrag så som intrakæde- og interkædespredningen samt spredningen fra radial profilen indsamlet. Egenskaber som enkeltkæde gyrationsradius, den gennemsnitlige afstand fra kædernes massemidtpunkt til kernen og radialprofilen af monomere blev også indsamlet.

Modellen for micellespredningen, der er foreslået af Pedersen og Gerstenberg [J.S. Pedersen and M.C. Gerstenberg, Macromolecules (1996), 29, p. 1363], negligerer effekterne af excluded volume vekselvirkninger. Gyldigheden af denne model er blevet undersøgt ved hjælp af data fra simulationer. Konklusionen var, at for små overfladetætheder giver modellen præcise estimater for enkeltkæde gyrationsradius og kædernes massemidtpunkts afstand til kernen, men at estimaterne bliver dårligere, som overfladetætheden øges.

Ved hjælp af en selvkonsistent analyse af simulationsdata blev det vist, at koronaspredningen kan repræsenteres meget præcist som et vægtet gennemsnit

mellem en kerne-skals model og et Random Phase Approximation (RPA) udtryk, hvor kerne-skals modellen repræsenterer spredningsbidraget fra koronaens profil, mens RPA-udtrykket beskriver spredningsbidraget fra tæthedsfluktuationer. RPA-udtrykket afhænger af intrakæde spredningen og af en excluded volume parameter, der kan vises at være proportional med den anden virial koefficient. Det resulterende udtryk kan fortolkes som spredningen fra et to-dimensionalt lag af en "dilute/semi-dilute" polymeropløsning med en vis radialprofil. Udtrykket kaldes derfor opløsningsprofilspredning. Polymeropløsningen kan opfattes som værende to-dimensional fordi koronaens tykkelse er sammenlignelig med koronakædernes gyrationsradius.

Den fremadrettede spredning fra tæthedsfluktuationerne kan let udregnes med opløsningsprofilsprednings udtrykket, og det giver den osmotiske kompressibilitet af micellens korona. Kompressibiliteten fra den selvkonsistente analyse har en universal afhængighed af den reducerede overfladetæthed fra simulationer, hvor antallet af kæder, kædelængde og kerneradius falder på den samme kurve. Korona kompressibiliteten har en overfladetæthedsafhængighed, der er analog med koncentrationsafhængigheden af c/c^* for en polymeropløsning. Dette indikere at micelle koronaen kan opfattes som en kvasi-to-dimensional polymeropløsning.

Opløsningsprofiludtrykket er også blevet fittet til Monte Carlo simulationsdata. Udtrykket afhænger af enkeltkæde gyrationsradius, en excluded volume parameter og et udtryk for koronaens radialprofil. Ved hjælp af et Maximum Entropi estimat for koronaens radialprofil er der opnået fortræffelige fits for alle simulationer. Fra disse fits blev enkeltkæde gyrationsradius og koronaens radialprofil fundet, og disse er i meget god overensstemmelse med resultaterne, der blev indsamlet under Monte Carlo simulationerne.

På basis af en diagrammatisk fortolkning af det af Pedersen og Gerstenberg foreslået modeludtryk for micelle spredningen er en formalisme for udregningen af formfaktorer og strukturfaktorer af sammenhængende acykliske polymer strukturerer blevet udviklet. Miceller med en arbitrær kernegeometri, forgrenede polymere og copolymerstjerner er nogle af de strukturere, hvis spredning kan udregnes med formalismen. Formalismen kan inkludere excluded volume vekselvirkninger på samme niveau som for en lineær kæde, og et udtryk for formfaktoren af copolymer med excluded volume vekselvirkninger gives. Ved hjælp af denne formalisme er formfaktoren for en triblokcopolymerstjerne udregnet med og uden excluded volume vekselvirkninger. Disse udtryk er blevet fittet til Monte Carlo simulationsresultater for spredningen uden excluded volume vekselvirkninger for $f = 2, 3$ og 6 arme, og med excluded volume vekselvirkninger for $f = 2$. Under simulationerne blev spredningen indsamlet for hele stjernen samt for de tre blokke svarende til spredningsbidragene for fire forskellige kontraster, og alle fire kontraster blev fittet samtidigt. Disse fits viser en fortræffelig overensstemmelse mellem simulerede spredningsresultater og de teoretiske udtryk.

Chapter 3

Introduction

Complex fluids exhibit many interesting phenomena. They have structures on a mesoscopic scale, and the presence of these structures yield a surprising response to the presence of external fields such as shear, electrical, or magnetic fields. Some examples are for instance shear-induced birefringence of polymers solutions, electrical field-induced birefringence of liquid crystals, and the ordering of ferro-liquids in external magnetic fields [1, 2, 3]. Complex fluids can also behave as solids on short time scales, and as fluids on long time scales. Examples of complex fluids are mud, toothpaste, paint, shampoo, and liquid crystals as well as many biological fluids such as cell cytoplasm and blood. Thus complex fluids are quite common, but their behaviour are qualitatively different from "simple" fluids.

Complex fluids consisting of a colloid suspension of large particles or molecules can self-assemble in numerous structures, depending on the shape of the colloidal particles or molecules and their interactions. Solutions and melts of polymers and copolymers offer a system, where the architecture and chemical properties of the polymers can be designed and numerous structures can be obtained as a result [4].

A copolymer consists of a sequence of chemically different blocks of polymers joined end-to-end forming a long linear molecule. Copolymers are unable to undergo macroscopic phase separations, but micro-phase separations are possible. The structure of the micro-phase separated domains are determined by a minimisation of the surface energy between domains of different blocks, however, the entropy of stretching polymers chains also affects the shape of these domains[5]. Diblock copolymers can also self-assemble into micellar aggregates in a solvent that is selective for one block [6]. Many possible core geometries such as spherical, elliptical, and cylindrical cores are possible. Spherical micelles can, furthermore, order in crystalline structures such as body-centered or face-centered cubic crystals depending on the range of the micelle-micelle interactions, and cylindrical micelles can order into hexagonal rod structures [7, 8].

Polymers are also used for modifying the mechanical, chemical or biological properties of solid or liquid surfaces [9, 10, 11]. Diblock copolymers, for instance, provides a macromolecular analogy of amphiphilic molecules [12], and can be

used to modify the properties of a liquid surface or by adsorbing at a solid interface.

Grafting polymers onto the surface of a colloid aggregate introduces a repulsive interaction between aggregates, which inhibit coagulation and/or coalescence behaviour. The repulsive interactions is due to the fact that the polymer configurational degrees of freedom is reduced if it is squeezed between two colloidal aggregates. This leads to a decrease of the configurational entropy [13], and is the cause of the repulsive interactions between the colloidal particles. Tethering polymers to a surface can act as a lubricant or an adhesive between surfaces [14, 15], and tethered polymers can increase biocompatibility and inhibit protein adsorption [10, 16]. Lipid vesicles (liposomes) protected by diblock copolymers have also been suggested for drug delivery systems. Drug molecules, dissolved in the lipid layer or the interior, are protected from enzymatic degradation by the copolymers, and from being filtered from the blood stream in the liver or kidneys [17].

Advances in polymer synthesis allow good control over the polymerisation process, and existing techniques can realize many polymer architectures such as those shown in figure 3.1. Structures can be mapped out in terms of structural phase-diagrams by systematically varying the polymer architecture and experimental parameters such as concentration, solvent quality, and temperature. These can be used to formulate and test theories that relate polymer architecture and experimental parameters to structure, and test theories predicting the macroscopic mechanical, rheological, electric or magnetic properties of the complex fluids. This yields information about the basic physical processes that leads to the emergence of structures in complex fluids, and an understanding the physical processes allows the structure of complex fluids to be designed for practical applications.

Various techniques exist for probing the structure of complex fluids [18], however, small-angle X-ray and neutron scattering techniques are ideally suited for obtaining detailed structural information. Unfortunately scattering techniques do not yield a picture of the structure such as real space methods like microscopy, nor is there in general an easy way of inverting the results from a scattering experiment to obtain the structure. This is in a very real sense due to a very complex and convoluted dependence of the measured scattering on the structure of the complex fluid.

One way to infer structure from scattering data is to fit structural models to the observed scattering. Each model represents the expected scattering from an analytical model of a structure or is the result of a parametrisation of results from simulations. This provides a "tool box" of models that can be fitted to the experimental data, i.e. free the model parameters must be optimised in order for the model scattering to agree with the experimentally observed scattering. If a good agreement is obtained, it suggests that the structure present in the sample is the same structure as that represented by the model, and that the parameters estimated by the fit procedure are most likely to correspond to the "real" values of those parameters [19].

The aim of the present thesis is to present and validate an expression for the scattering from dilute solutions of diblock copolymer micelles with a spherical

core. Monte Carlo simulations of a mesoscopic micelle model has been used to obtain the scattering that would be obtained from an almost ideal scattering experiment. Hence, any scattering expression can be compared to the scattering from a micelle in the ideal case, where in principle the scattering is exact (except for statistics due to a finite number of samples) and the real values of all parameters are known in advance.

3.1 Polymers

Polymers are string-like objects consisting of a long sequence of monomers. The most important property of a polymer is the conformational entropy associated with the many internal degrees of freedom of a chain [4]. The entropically favoured configuration of a polymer is that of a random walk, however, the configuration is also influenced by the difference between monomer-monomer and monomer-solvent interactions. These are effectively the same in a Θ-solvent and as a result monomers are approximately non-interacting, in which case the configuration is only determined by the entropy.

In a bad solvent monomer-solvent interactions are very unfavourable compared to monomer-monomer interactions, and as a result compact "collapsed" polymer configurations are energetically favourable. However, in a good solvent monomer-solvent interactions are negligible compared to monomer-monomer interactions in which case the each monomer will be surrounded by a volume from which other monomers are excluded. Hence the name "excluded volume" interactions. The preferred configuration of a polymer in a good solvent will be that of a self-avoiding random walk, and the chain will swell relative to an non-interacting random walk. In the limit where the monomer-monomer potential can be regarded as a hard-sphere potential, the enthalpy is either infinite or zero, and the free energy is independent of temperature i.e. an athermal solvent.

Varying the polymer concentration in a good solvent yield three qualitative different regimes [20, 21]: dilute solution, semi-dilute solution, and a melt. In a dilute solution each polymer is far from other polymers and the solution can be regarded as an ideal gas of hard spheres, where each hard sphere has a characteristic size given by the radius of gyration of the polymer. The solution enters the semi-dilute regime when the polymer density exceeds the overlap density, which is defined by the inverse of the volume occupied by one polymer chain in an unperturbed configuration. Polymers will inter-penetrate each other forming a transient network of intermeshed chains above the overlap density. The characteristic chain size of dilute solutions is replaced by a characteristic mesh size or correlation length in semi-dilute solutions, which defines a length scale above which no correlations due to polymer connectivity persists, and below which interactions between different chains are negligible. If no solvent is present, i.e. the volume fraction of polymer is unity, polymers will be in a melt state. The preferred chain conformation will be that of a non-interacting random walks as predicted by Flory [22]. This can be understood as follows: in a good solvent the enthalpy contribution from monomer-monomer interactions decreases as the chain swells, however, in a melt swelling would not decrease

the number of the monomer-monomer contacts as there is no free space to swell into. As a result the enthalpy is unaffected by swelling, and the preferred configurations will be the non-interacting random walk configurations favoured by the entropy .

3.2 Tethered chains

Polymers can be tethered to a surface by one end, thus forming a diffuse layer on the surface [9]. Some tethered chain structures are shown in figure 3.2. The equilibrium properties of a tethered polymer layer at an impenetrable surface in a good solvent follow from the balance between entropic forces and excluded volume interactions. The latter favour a state with a minimum of monomer-monomer contacts, e.g. a state with a low density of monomers. Such a state can be achieved by increasing the available volume per chain, i.e. by the chain stretching away from the surface. Entropic forces, however, will tend to maximise the number of available chain configurations by opposing the chain stretching and by shifting the corona away from the surface to some extent. If the interface is convex a chain can get a relative larger available volume by stretching compared to flat interfaces. As a result, surface curvature has a large impact on the monomer density distribution away from the surface, and tends to reduce chain stretching for convex surfaces.

At low surface coverage, polymers will have a mushroom like shape due to surface expulsion, however, at very high surface coverage excluded volume interactions dominate and chains will be strongly stretched forming a polymeric brush. A broad crossover region of intermediate surface coverages exists between these limits and experiments are typically carried out in this regime.

Many theoretical techniques have been applied to the problem of tethered chains on a planar or curved surfaces. Scaling theories treat polymers as close packed blobs with a size given by the local correlation length. It is implicitly assumed that the local polymer concentration throughout the polymer layer is in the semi-dilute regime. From the blob description, density profiles can be obtained as well as predictions of the dependence of the width of the tethered chain layer as function of chain length and surface coverage. Daoud and Cotton [23] made a model for the profile of star polymers using a blob description, which was modified by Halperin to describe small finite size cores [24].

Self-consistent field (SCF) methods [25, 26, 27, 28, 29] can be derived from the statistical physics of chain molecules [30]. From SCF methods the profiles can be obtained for moderately high surface coverages and weakly interacting chains. SCF methods break down in the presense of large density fluctuations, for instance at lower surface coverages. In the limit of extreme stretching lateral fluctuations are weak and the path of a polymer chain can be mapped onto a classical mechanical problem of a falling particle in a potential as originally shown by Semenov [31].

The thermodynamics of polymers layers at flat interfaces has been investigated by Carignano and Szleifer [10, 32, 33] using a single-chain mean field theory. This approach includes all the intra-chain interactions within the cho-

sen chain model, and a mean field approach is used for solvent molecules and other chains. This approach provides the osmotic pressure profile away from the surface and pressure-area isotherms.

Tethered polymers at flat and curved interfaces have been investigated by Molecular Dynamics and Monte Carlo methods [34, 35, 36]. Computer simulations have primarily been used for obtaining density profiles as function of various parameters. Common for all these approaches, at least as they are currently applied, are that none of them produce expressions that can be used for analysing experimental scattering data. However, Monte Carlo and Molecular Dynamics simulations can easily be modified to sample scattering corresponding to an ideal scattering experiment with contrast variation.

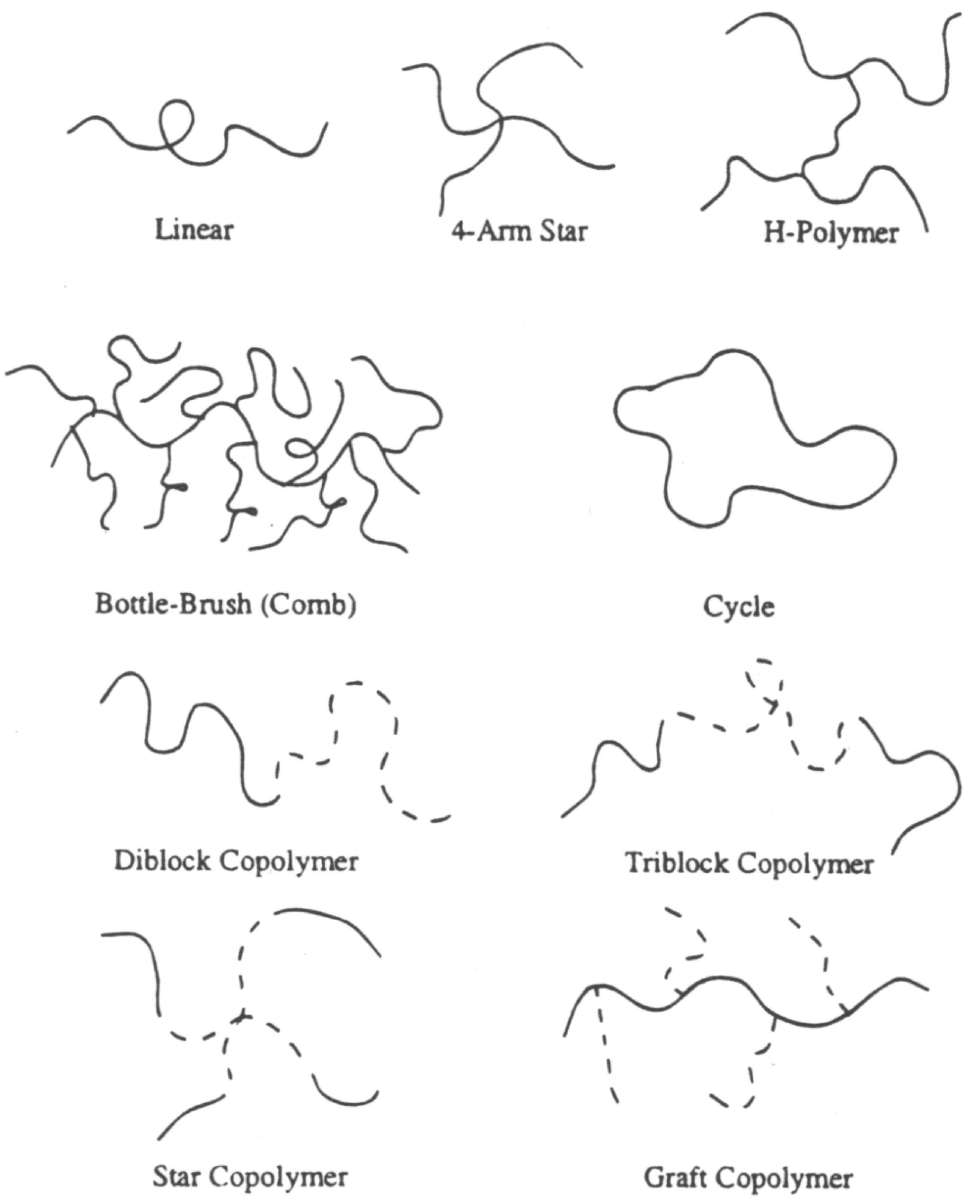

Figure 3.1: Different polymer structures (from [4]).

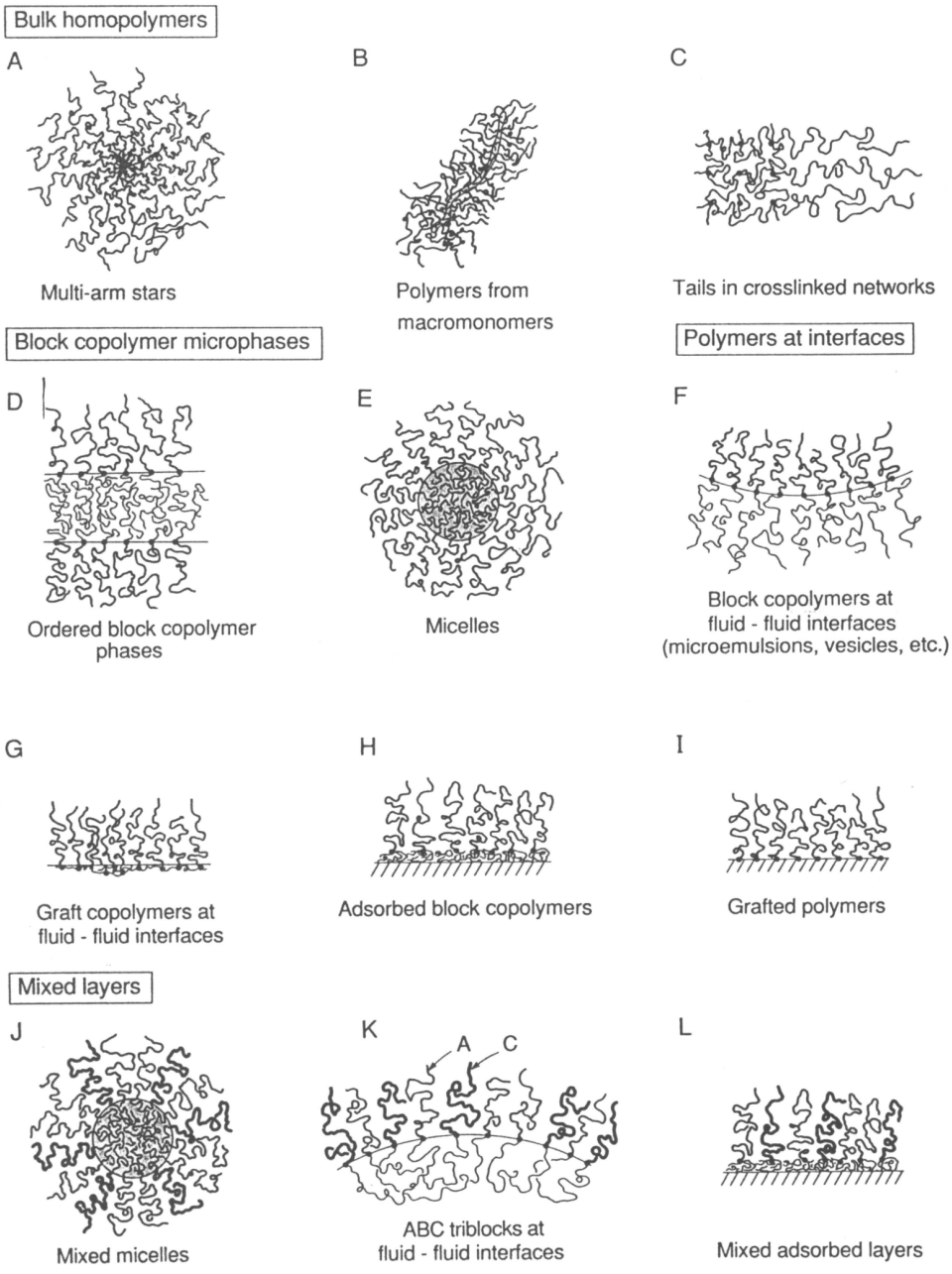

Figure 3.2: An illustration of some tethered chain structures (from [9]).

Chapter 4

Theory

This chapter introduces the theoretical background for the summary of articles, and the articles themselves. First basic scattering theory including contrast variation techniques and the scattering from a solution of different particles are introduced. The relation between scattering, correlation functions, and thermodynamics is derived. Two sections derive expressions for the scattering from dilute and semi-dilute polymer solutions. The main topic of the thesis is scattering from aggregates in solution especially micellar aggregates and models of the micellar scattering, and this is introduced after a section on core-shell models. The chapter is concluded with a brief remark on the interpretation of scattering data, and a heuristic introduction to Maximum Entropy methods. For further information the reader is referred to the literature on scattering theory and applications to fluids and soft condensed matter, see e.g. [18, 37, 38, 39].

4.1 Basic scattering theory

In a general scattering experiment a beam of incident radiation illuminates a volume of matter, and the scattered radiation is detected at a certain angle relative to the transmitted beam. The observed scattering depends on the interaction between the beam and matter within the scattering volume. Typical beams consist of laser light, X-rays from a synchrotron or conventional source, or neutrons from a reactor or spallation source.

The incident radiation is represented as a plane wave with a wave vector $\mathbf{k}_i$ and the scattered radiation is approximated by a plane wave with wave vector $\mathbf{k}_s$, which is defined by the position of the detector relative to the transmitted beam. Assuming that the scattering process is elastic i.e. $k = |\mathbf{k}_i| = |\mathbf{k}_s|$, and that the scattering is weak such that multiple scattering events can be neglected, it follows from quantum mechanics using the first Born approximation [37, 40] that the detected intensity is given by the differential cross section

$$\frac{\mathrm{d}\sigma}{\mathrm{d}\Omega} \propto |\langle \mathbf{k}_s | U(\mathbf{r}) | \mathbf{k}_i \rangle|^2 .$$

Here $U(\mathbf{r})$ is the interaction potential between radiation and matter. Assuming that the potential is caused by many different scatterers located at positions

$\mathbf{r}_j$. Then the potential can be expressed as the sum $U(\mathbf{r}) = \sum_j U_j(\mathbf{r} - \mathbf{r}_j)$, where U_j is the interaction potential between the j'th scatterer and the incident radiation. This yields a matrix element

$$\langle \mathbf{k}_s | U | \mathbf{k}_i \rangle = \sum_j U_j(\mathbf{q}) e^{-i\mathbf{q}\cdot\mathbf{r}_j},$$

where the scattering vector $\mathbf{q}$ is defined as $\mathbf{q} = \mathbf{k}_i - \mathbf{k}_s$. The momentum transfer of the scattering process is given by $\hbar\mathbf{q}$. The length of the $\mathbf{q}$ vector is directly related to the angle 2θ between the transmitted beam and the scattered beam measured at the detector position as $|\mathbf{q}| = 2k\sin(\theta)$, and the wavelength of the incident radiation is $\lambda = 2\pi/k$. The scattering due to structures with a longer length scale than the incident radiation is located very close to the transmitted beam. Accordingly, scattering techniques of measuring structures longer length scale than the incident radiation are known as small-angle scattering techniques.

Neutrons are scattered from the atom nuclei, and it is a good approximation to assume that the spatial extension of the potentials is small compared to the wavelength of the incident radiation, in which case the scatterers can be regarded as point-like, and the neutron interaction potential can be approximated by a delta function

$$U_j(\mathbf{r}) = \frac{2\pi\hbar^2}{m} b_j \delta(\mathbf{r}),$$

where b_j is the scattering length. This potential is also known as the Fermi pseudo-potential. The scattering length of neutrons has a complicated dependence on the atom number, isotope and spin state, and can even be negative. The scattering from a number of point-like scatterers becomes

$$\frac{\mathrm{d}\sigma}{\mathrm{d}\Omega}(\mathbf{q}) \propto \left| \sum_j b_j e^{-i\mathbf{q}\cdot\mathbf{r}_j} \right|^2.$$

By defining the scattering length density $\pi(\mathbf{r})$, the sum is replaced by an integral over the scattering volume and the result is

$$\frac{\mathrm{d}\sigma}{\mathrm{d}\Omega}(\mathbf{q}) \propto \left| \int \mathrm{d}\mathbf{r} \pi(\mathbf{r}) e^{-i\mathbf{q}\cdot\mathbf{r}} \right|^2.$$

The discrete expression can easily be retrieved from the continuum description using a density defined as $\pi(\mathbf{r}) = \sum_j b_j \delta(\mathbf{r} - \mathbf{r}_j)$.

The observed scattering is the square of the Fourier transform of the scattering length density distribution. Any periodic structure, such as crystal, will have a large Fourier component for the corresponding $\mathbf{q}$ vector, and this will give rise to a strong scattering. As a result a very important application for scattering techniques has been the determination of crystal structures. A crystal can be rigidly mounted in a scattering experiment, however, if the scatterers are polymers or aggregates suspended in a solvent then many different configurations of scatterers are possible. Let $\pi_\alpha(\mathbf{r})$ denote the scattering length density when the system is in the α'th state, where the state is used to collectively denote

the configuration of molecules or aggregates. $\langle X_\alpha(\mathbf{r})\rangle_\alpha$ denotes a configurational average over all the possible states α of the quantity X_α. Translational or orientational averages, will be denoted by subscript "t" and "o", respectively. Thus $\langle X_\alpha(\mathbf{r}_1,\mathbf{r}_2)\rangle_{\alpha to}$ is the configurational, translational, and orientational average of the function $X_\alpha(\mathbf{r}_1,\mathbf{r}_2)$, while a translational and orientational average is denoted $\langle X_\alpha(\mathbf{r})\rangle_{to}$.

For particles, molecules or aggregates suspended in a solvent the configurational, orientational, and translational average of the of the scattering is

$$\frac{\mathrm{d}\sigma}{\mathrm{d}\Omega} \propto \left\langle \left| \int \mathrm{d}\mathbf{r}\pi_\alpha(\mathbf{r}) e^{-i\mathbf{q}\cdot\mathbf{r}} \right|^2 \right\rangle_{\alpha to}.$$

For convenience the scattering length density is replaced by $\pi_\alpha(\mathbf{r}) = \Delta\pi_\alpha(\mathbf{r}) + \pi_{solvent}$ where $\Delta\pi_\alpha(\mathbf{r})$ is the excess scattering length density of the scatterers relative to that of the solvent $\pi_{solvent}$. The excess scattering length density is given by $\Delta\pi_\alpha(\mathbf{r}) = \sum_i \Delta b_i \rho_\alpha^{(i)}(\mathbf{r})$, where $\rho_\alpha^{(i)}(\mathbf{r})$ is the number density of the i'th species of scatterer and Δb_i the excess scattering length of that species, where a scatterer could be an atom, a molecule or an aggregate of molecules. Separating the contributions due to species and solvent the scattering is

$$\frac{\mathrm{d}\sigma}{\mathrm{d}\Omega}(q) \propto \left\langle \left| \sum_i \Delta b_i \int \mathrm{d}\mathbf{r}\rho_\alpha^{(i)}(\mathbf{r}) e^{-i\mathbf{q}\cdot\mathbf{r}} + \pi_{solvent} \int \mathrm{d}\mathbf{r} e^{-i\mathbf{q}\cdot\mathbf{r}} \right|^2 \right\rangle_{\alpha to}.$$

Defining the Fourier transform of the density distribution as

$$\rho_\alpha^{(i)}(\mathbf{q}) = \int \mathrm{d}\mathbf{r}\rho_\alpha^{(i)}(\mathbf{r}) e^{-i\mathbf{q}\cdot\mathbf{r}},$$

where integrals are restricted to the scattering volume V, and using the definition of the delta function the differential scattering cross section becomes

$$\propto \left\langle \left| \sum_i \Delta b_i \rho_\alpha^{(i)}(\mathbf{q}) + \pi_{solvent} V\delta(\mathbf{q}) \right|^2 \right\rangle_{\alpha to}.$$

Hence, the scattering due to the solvent will be confined to the forward direction $\mathbf{q} = 0$, where it is indistinguishable from the transmitted part of the incident beam, and as a result the $\delta(\mathbf{q})$ term can be ignored. In the rest of this chapter the argument of a function is used to distinguish between functions and their Fourier transforms, such that $f(\mathbf{q})$ denotes the Fourier transform of a function $f(\mathbf{r})$.

Using neutron scattering techniques it is possible to selectively cancel scattering contributions from certain species by matching the solvent scattering length density to the scattering length density of that species. Scattering contrast can be enhanced by changing the isotope composition of a species, for instance by substituting hydrogen atoms with deuterium as often done for polymers or biomolecules. This can be used for investigating the structure of an object, that consists of different types of scatterers for instance different species of polymer molecules, such as a star polymer or a micelle consisting of block copolymers [41], a complex biological structure such as a virus [42] or a biomolecule

such as a ribosome, which can consist of both RNA, DNA, and proteins. This is the basis for neutron contrast variation studies [18, 43, 44], which yield more information about the structural arrangements of constituent species compared to what can be obtained by, for instance, X-ray techniques.

4.2 Form and Structure factor

Neglecting the forward scattering contribution due to the solvent the differential cross section for neutron scattering is given by

$$\frac{\mathrm{d}\sigma}{\mathrm{d}\Omega} \propto \left\langle \left| \sum_i \Delta b_i \rho_\alpha^{(i)}(\mathbf{q}) \right|^2 \right\rangle_{\alpha to}.$$

If the sample consists of a number M objects suspended in a liquid, such that they located at $\mathbf{R}_i^\alpha$, in the configuration denoted by α, the scattering length density distribution is

$$\pi_\alpha(\mathbf{r}) = \sum_{i=1}^{M} \beta_i \rho_\alpha^{(i)}(\mathbf{r} - \mathbf{R}_i^\alpha),$$

where $\rho^{(i)}(\mathbf{r})$ is the density distribution and $\beta_i = \Delta b_i \int \mathrm{d}\mathbf{r} \rho^{(i)}(\mathbf{r})$ is the total excess scattering length of the i'th object, in which case it is easy to derive

$$\frac{\mathrm{d}\sigma}{\mathrm{d}\Omega}(q) = \frac{1}{M} \left\langle \left| \sum_{i=1}^{M} \beta_i \rho_\alpha^{(i)}(\mathbf{q}) e^{-i\mathbf{q}\cdot\mathbf{R}_i^\alpha} \right|^2 \right\rangle_{\alpha to} \tag{4.1}$$

$$= \frac{1}{M} \left\langle \sum_{i=1}^{M} \beta_i^2 \rho_\alpha^{(i)}(\mathbf{q}) \rho_\alpha^{(i)}(-\mathbf{q}) + 2 \sum_{i>j}^{M} \beta_i \beta_j \rho_\alpha^{(i)}(\mathbf{q}) \rho_\alpha^{(j)}(-\mathbf{q}) e^{-i\mathbf{q}\cdot(\mathbf{R}_i^\alpha - \mathbf{R}_j^\alpha)} \right\rangle_{\alpha to}.$$

Assuming that the position of an object is not correlated with its orientation, and that the orientation of different objects is uncorrelated, the average can be rewritten as

$$\frac{1}{M} \sum_{i=1}^{M} \left\langle \beta_i^2 \rho_\alpha^{(i)}(\mathbf{q}) \rho_\alpha^{(i)}(-\mathbf{q}) \right\rangle_{\alpha o} + \frac{2}{M} \sum_{i>j}^{M} \langle \beta_i \rho_\alpha^{(i)}(\mathbf{q}) \rangle_{\alpha o} \langle \beta_j \rho_\alpha^{(j)}(\mathbf{q}) \rangle_{\alpha o} \left\langle e^{-i\mathbf{q}\cdot(\mathbf{R}_i^\alpha - \mathbf{R}_j^\alpha)} \right\rangle_{\alpha to}.$$

The form factor of the i'th object is defined as $F_i(q) = \left\langle \rho_\alpha^{(i)}(\mathbf{q}) \rho_\alpha^{(i)}(-\mathbf{q}) \right\rangle_{\alpha o}$, the form factor amplitude as $A_i(q) = \langle \rho_\alpha^{(i)}(\mathbf{q}) \rangle_{\alpha o}$, and the center-to-center structure factor as $H_{ij}(q) = \left\langle \exp[-i\mathbf{q} \cdot (\mathbf{R}_i^\alpha - \mathbf{R}_j^\alpha)] \right\rangle_{\alpha to}$. Using these abbreviations the scattering function can be stated as

$$\frac{\mathrm{d}\sigma}{\mathrm{d}\Omega}(q) = \frac{1}{M} \sum_{i=1}^{M} \beta_i^2 F_i(q) + \frac{2}{M} \sum_{i>j}^{M} \beta_i \beta_j A_i(q) H_{ij}(q) A_j(q). \tag{4.2}$$

The form factor describes the scattering from two sites within the same object, while the second term describes the interference scattering from sites

belonging to different objects. If the positions of the different objects are uncorrelated as it will be in a very dilute solution, then $H_{ij}(q) = 0$ and only the scattering due to the form factor is observed. The second term is a product of Fourier transforms, and by virtue of the Fourier convolution theorem this corresponds to a convolution of distributions. Thus the second term can be interpreted in real space as the convolution of three distance distributions: $A_i(r)$, which is the distribution of distances between sites in object i and its center, and $H_{ij}(r)$ is the distribution of distances between the center of object i and j, and a distribution of distances between the center and sites within object j. The generalisation of this interpretation is presented in article IV.

In the special case where only one type of object is present, eq. (4.2) yields

$$\frac{\mathrm{d}\sigma}{\mathrm{d}\Omega}(q) = F(q)S_{app}(q),$$

where the apparent structure factor is $S_{app}(q) = A^2(q)H(q)/F(q) + 1$. $H(q)$ is the center-to-center structure factor, i.e. the Fourier transform of center-to-center distances between different objects. In the special case where the objects are spherically symmetric $F(q) = A^2(q)$ (see section 4.9) and the apparent structure factor is $S_{app}(q) = H(q)+1$. The form factor carries information about distances within a object and thus indirectly interactions within that object, whereas the structure factor carries information about the distances between different objects, and thus carries information about object-object interactions. Using the Ornstein-Zernike relation the structure factor can be calculated for a known pair-potential between objects given a suitable closure relation [39].

In general the scattering length density depends on the interaction between the incident radiation and the atoms in the sample volume [18, 43]. Light and X-ray photons are scattered from electrons, while neutrons, on the other hand, interact with the atomic nuclei via weak short-ranged nuclear forces. It is also possible to define scattering length densities in the case of light and X-ray scattering, and the result is that an equation exactly as that of neutron scattering is obtained, except with different expressions for the scattering lengths. For X-rays the scattering length b_i is the atomic form factor of the i'th atom and depends on $\mathbf{q}$, while $\pi(\mathbf{r})$ is proportional to the electron density distribution in the sample. The interpretation of the scattering length for light scattering is more complex, but it is related to the polarizability of the scatterers, and this can be expressed using the derivative of the index of refraction with respect to concentration.

In order to simplify the notation it will be assumed that only one species of scatterer is present, in which case a scattering function $S(\mathbf{q})$ can be defined as

$$S(\mathbf{q}) = \frac{1}{N}\left\langle \left| \int \mathrm{d}\mathbf{r}\rho_\alpha(\mathbf{r})e^{-i\mathbf{q}\cdot\mathbf{r}} \right|^2 \right\rangle_{\alpha to}, \tag{4.3}$$

where N is the number of scatterers given by $N = \int \mathrm{d}\mathbf{r}\rho_\alpha(\mathbf{r})$. The number of scatterers is assumed to be fixed and independent of state α. The scattering function is independent of the type of radiation that is used. The differential cross section is related to the scattering function by the excess scattering length, which depends on the type of radiation, as

$$\frac{\mathrm{d}\sigma}{\mathrm{d}\Omega} \propto N\Delta b^2 S(\mathbf{q})$$

At this level no assumptions have been made about the nature of the scatterers. They could be aggregates, polymers molecules, or individual atoms. Nor has any assumptions been made about the structural arrangements of objects.

4.3 Correlation functions

This section introduces correlation functions of densities corresponding to a single species of scatterer, and no assumptions are made regarding the nature of the scatterers. They could be atoms, molecules, or aggregates. The correlation functions will be related to the scattering function and later to a general statistical physical property. Results presented in the following sections are correct even in the absence of orientational and translational averages, and as a result the these averages are described in a separate section.

Expanding the norm square in the scattering expression eq. (4.3) the scattering function can be rewritten as

$$NS(\mathbf{q}) = \left\langle \int \mathrm{d}\mathbf{r}_1 \rho_\alpha(\mathbf{r}_1) e^{i\mathbf{q}\cdot\mathbf{r}_1} \times \int \mathrm{d}\mathbf{r}_2 \rho_\alpha(\mathbf{r}_2) e^{-i\mathbf{q}\cdot\mathbf{r}_2} \right\rangle_\alpha = \langle \rho_\alpha(\mathbf{q})\rho_\alpha(-\mathbf{q})\rangle_\alpha ,$$

here $\rho_\alpha(\mathbf{q})$ is the Fourier transform of the number density distribution in the α'th state. Using the fact that the configurational average and Fourier transformation are both linear operations and can be interchanged, the scattering function can be rewritten as

$$NS(\mathbf{q}) = \int \mathrm{d}\mathbf{r}_1 \mathrm{d}\mathbf{r}_2 \left\langle \rho_\alpha(\mathbf{r}_1)\rho_\alpha(\mathbf{r}_2)\right\rangle_\alpha e^{i\mathbf{q}\cdot(\mathbf{r}_1-\mathbf{r}_2)}$$

$$\equiv \int \mathrm{d}\mathbf{r}_1 \mathrm{d}\mathbf{r}_2 C(\mathbf{r}_1,\mathbf{r}_2) e^{i\mathbf{q}\cdot(\mathbf{r}_1-\mathbf{r}_2)} = C(\mathbf{q}),$$

where $C(\mathbf{r}_1,\mathbf{r}_2) \equiv \langle \rho_\alpha(\mathbf{r}_1)\rho_\alpha(\mathbf{r}_2)\rangle_\alpha$ defines the density-density correlation function, and $C(\mathbf{q}) = \langle \rho_\alpha(\mathbf{q})\rho_\alpha(-\mathbf{q})\rangle_\alpha$ its Fourier transform. The scattering function $S(\mathbf{q})$ is given by the Fourier transformed density-density correlation function $C(\mathbf{q})$. The correlation function contains information about to what extend the density at one point $\mathbf{r}_1$ is "related to" the density at another point $\mathbf{r}_2$. In the absense of interactions, either direct or indirect, between particles at the two positions, they will be statistically independent. Thus correlations can be regarded as a measure of the structures imposed by interactions between particles. The correlation function becomes $C(\mathbf{r}_1,\mathbf{r}_2) \to \langle \rho_\alpha(\mathbf{r}_1)\rangle_\alpha \langle \rho_\beta(\mathbf{r}_2)\rangle_\beta$ for $|\mathbf{r}_1 - \mathbf{r}_2| \to \infty$ as interactions are assumed to be of a short range. This assumption is not correct for crystalline materials, where there is long ranged order.

The density distribution of the α'th state $\rho_\alpha(\mathbf{r})$ can be expressed in terms of the configurationally averaged density $\rho(\mathbf{r}) = \langle \rho_\beta(\mathbf{r})\rangle_\beta$ and a density fluctuation $\delta\rho_\alpha(\mathbf{r})$ defined as $\rho_\alpha(\mathbf{r}) = \rho(\mathbf{r}) + \delta\rho_\alpha(\mathbf{r})$. Inserting this in the definition of the correlation function and expanding using $\langle \delta\rho_\beta(\mathbf{r})\rangle_\beta = 0$ yields

$$C(\mathbf{r}_1, \mathbf{r}_2) \equiv \langle \rho_\alpha(\mathbf{r}_1)\rho_\alpha(\mathbf{r}_2)\rangle_\alpha = \rho(\mathbf{r}_1)\rho(\mathbf{r}_2) + \langle \delta\rho_\alpha(\mathbf{r}_1)\delta\rho_\alpha(\mathbf{r}_2)\rangle_\alpha .$$

The density correlation function is the sum of two contributions, one originating from the product of average densities, and another originating from the fluctuations of individual configurations about the average density. The density fluctuation correlation function (also known as the Ursell function) is here defined as

$$D(\mathbf{r}_1, \mathbf{r}_2) \equiv \langle \delta\rho_\alpha(\mathbf{r}_1)\delta\rho_\alpha(\mathbf{r}_2)\rangle_\alpha = C(\mathbf{r}_1, \mathbf{r}_2) - \rho(\mathbf{r}_1)\rho(\mathbf{r}_2),$$

for large distances the fluctuation correlation function converges to zero. Inserting the correlation function in the expression for the scattering function yields

$$NS(\mathbf{q}) = \int \mathrm{d}\mathbf{r}_1 \mathrm{d}\mathbf{r}_2 C(\mathbf{r}_1, \mathbf{r}_2) e^{i\mathbf{q}\cdot(\mathbf{r}_1 - \mathbf{r}_2)},$$

$$= \left| \int \mathrm{d}\mathbf{r} \rho(\mathbf{r}) e^{i\mathbf{q}\cdot\mathbf{r}} \right|^2 + \int \mathrm{d}\mathbf{r}_1 \mathrm{d}\mathbf{r}_2 \, \langle \delta\rho_\alpha(\mathbf{r}_1)\delta\rho_\alpha(\mathbf{r}_2)\rangle_\alpha \, e^{i\mathbf{q}\cdot(\mathbf{r}_1 - \mathbf{r}_2)},$$

$$= \rho(\mathbf{q})\rho(-\mathbf{q}) + ND(\mathbf{q}).$$

The scattering function has two contributions, one is the configurationally averaged density distribution $|\rho(\mathbf{q})|^2$, and another due to density fluctuations about the average density, this latter contribution is given by

$$D(\mathbf{q}) = \frac{1}{N} \langle \delta\rho_\alpha(\mathbf{q})\delta\rho_\alpha(-\mathbf{q})\rangle_\alpha .$$

The density fluctuation correlations are typically short ranged, and the Fourier integral can be regarded as an integral over a number of cells with some characteristic size. The Fourier integral will be proportional to the number of cells, and the definition of the fluctuation scattering includes an inverse factor N, such that it is independent of number of scatteres in the large volume limit, i.e. $D(\mathbf{q})$ becomes an intensive quantity.

4.4 Statistical Physics

In order to understand the physical information contained in the fluctuation correlation function, a relation between correlation functions and statistical physics has to be established (the following derivation is inspired by [38]). An average over possible states can be expressed as

$$\langle X_\alpha \rangle_\alpha = \frac{\sum_\alpha X_\alpha e^{-\beta H_\alpha}}{\sum_\alpha {}_\alpha e^{-\beta H_\alpha}}, \tag{4.4}$$

where H_α is the Hamiltonian of system when it is in the α'th state and $\beta = 1/(k_b T)$, where k_b is the Boltzmann constant, and T is the absolute temperature. We are interested in ensemble averages of densities and correlation functions

between densities, the grand canonical ensemble which depend on the volume V, temperature T, and an external chemical potential field $\mu(\mathbf{r})$ is a good choice. The grand canonical partition function is given by

$$\Xi[\mu(\mathbf{r})] = \sum_{\alpha} \exp\left(-\beta H_\alpha + \beta \int \mathrm{d}\mathbf{r}\rho_\alpha(\mathbf{r})\mu(\mathbf{r})\right).$$

How this sum is evaluated, and how the Hamiltonian and the number density of a state ρ_α for an actual polymer or polymer aggregate is expressed is outside the scope of this thesis (see e.g. [45, 46, 47, 48]). Variational calculus [49] can be used to calculate the response of the grand canonical partition function to infinitesimal variations of the external chemical potential, which shows it can be used as a generating function for correlation functions. For example

$$\frac{\delta}{\beta\delta\mu(\mathbf{r}_1)} \ln \Xi[\mu(\mathbf{r})] = \frac{1}{\beta\Xi} \frac{\delta}{\delta\mu(\mathbf{r}_1)} \Xi[\mu(\mathbf{r})]$$

$$= \frac{1}{\Xi} \sum_{\alpha} \exp\left(-\beta H_\alpha + \beta \int \mathrm{d}\mathbf{r}\rho_\alpha(\mathbf{r})\mu(\mathbf{r})\right) \frac{\delta}{\delta\mu(\mathbf{r}_1)} \int \mathrm{d}\mathbf{r}\rho_\alpha(\mathbf{r})\mu(\mathbf{r}).$$

Using the definition $\delta\mu(\mathbf{r})/\delta\mu(\mathbf{r}_1) = \delta(\mathbf{r} - \mathbf{r}_1)$ [39, 38] in the integral, the following result is obtained

$$\frac{1}{\Xi[\mu(\mathbf{r})]} \sum_{\alpha} \rho_\alpha(\mathbf{r}_1) \exp\left(-\beta H_\alpha + \beta \int \mathrm{d}\mathbf{r}\rho_\alpha(\mathbf{r})\mu(\mathbf{r})\right),$$

which for $\mu(\mathbf{r}) = 0$ reduces to

$$\frac{\sum_\alpha \rho_\alpha(\mathbf{r}_1) \exp\left(-\beta H_\alpha\right)}{\sum_\alpha \exp\left(-\beta H_\alpha\right)} = \langle \rho_\alpha(\mathbf{r}_1) \rangle_\alpha .$$

The linear response of $\ln\Xi$, i.e. the grand potential, to a variation in the external chemical potential, is the configurational average of the density. The following relations can be deduced with relative ease in a similar manner

$$\frac{\delta}{\beta\delta\mu(\mathbf{r}_1)} \ln \Xi[\mu(\mathbf{r})]\bigg|_{\mu=0} = \langle \rho_\alpha(\mathbf{r}_1) \rangle_\alpha = \rho(\mathbf{r}_1), \tag{4.5}$$

$$\frac{1}{\Xi[\mu(\mathbf{r})]} \frac{\delta}{\beta\delta\mu(\mathbf{r}_1)} \frac{\delta}{\beta\delta\mu(\mathbf{r}_2)} \Xi[\mu(\mathbf{r})]\bigg|_{\mu=0} = \langle \rho_\alpha(\mathbf{r}_1)\rho_\alpha(\mathbf{r}_2) \rangle_\alpha = C(\mathbf{r}_1, \mathbf{r}_2),$$

and

$$\frac{\delta}{\beta\delta\mu(\mathbf{r}_1)} \frac{\delta}{\beta\delta\mu(\mathbf{r}_2)} \ln \Xi[\mu(\mathbf{r})]\bigg|_{\mu=0} = \langle \delta\rho_\alpha(\mathbf{r}_1)\delta\rho_\alpha(\mathbf{r}_2) \rangle_\alpha = D(\mathbf{r}_1, \mathbf{r}_2). \tag{4.6}$$

The derivation shows that the average density, the density correlation function, and the density fluctuation correlation functions can all be regarded as functionals of the external chemical potentials, which in the $\mu = 0$ limit corresponds to the previously defined correlation functions. In particular a comparison of eq. (4.5) and eq. (4.6) shows that the following relation is valid

$$\chi(\mathbf{r}_1, \mathbf{r}_2) \equiv \frac{\delta\rho(\mathbf{r}_1)}{\beta\delta\mu(\mathbf{r}_2)} = D(\mathbf{r}_1, \mathbf{r}_2). \tag{4.7}$$

$\chi(\mathbf{r}_1, \mathbf{r}_2)$ is a generalised susceptibility as it relates response of the average density at $\mathbf{r}_1$ to a change in the external chemical potential at $\mathbf{r}_2$, and this is identical to the density fluctuation correlation function. This follows directly from the definition of the grand canonical partition function, and in general the linear response of the density of an extensive parameter with respect to its conjugate field is given by the fluctuation correlations of that extensive density. This type of relation is known as a fluctuation-dissipation theorem [38, 39, 50].

A connection to the isothermal compressibility follows when Taylor expanding the density in the external chemical potential field as

$$\rho[\mathbf{r}_1; \mu(\mathbf{r})] = \rho[\mathbf{r}_1; \mu = 0] + \int \mathrm{d}\mathbf{r}_2 \, \frac{\delta}{\delta\mu(\mathbf{r}_2)} \rho[\mathbf{r}_1; \mu(\mathbf{r})]\Big|_{\mu(\mathbf{r})=0} \delta\mu(\mathbf{r}_2) + \cdots$$

$$= \rho[\mathbf{r}_1; \mu = 0] + \beta \int \mathrm{d}\mathbf{r}_2 D(\mathbf{r}_1, \mathbf{r}_2)\delta\mu(\mathbf{r}_2) + \cdots.$$

In the special case where the chemical potential is a small constant $\delta\mu(\mathbf{r}_2) = \delta\mu$, this becomes

$$\frac{\partial\rho(\mathbf{r}_1)}{\partial\mu} = \frac{\rho(\mathbf{r}_1; \delta\mu) - \rho(\mathbf{r}_1; \mu = 0)}{\delta\mu} = \beta \int \mathrm{d}\mathbf{r}_2 D(\mathbf{r}_1, \mathbf{r}_2) + \cdots,$$

using the definition for $D(\mathbf{q})$ and the mean density $\rho = N/V = V^{-1} \int \mathrm{d}\mathbf{r}_1 \rho(\mathbf{r}_1)$ the equation can be rewritten as

$$\frac{\partial\rho}{\partial\mu} = \frac{1}{V} \int \mathrm{d}\mathbf{r}_1 \frac{\partial\rho(\mathbf{r}_1)}{\partial\mu} = \frac{\beta}{V} \int \mathrm{d}\mathbf{r}_1 \mathrm{d}\mathbf{r}_2 D(\mathbf{r}_1, \mathbf{r}_2) = \beta\rho D(\mathbf{q} = 0).$$

The response of the average density to a change in a constant external chemical potential is given by the $\mathbf{q} = 0$ limit of the density fluctuation correlation function. This result can can be related to the isothermal compressibility κ_T, which is defined as

$$\kappa_T \equiv -\frac{1}{V} \frac{\partial V}{\partial p}\bigg|_{T,N} = \rho^{-2} \frac{\partial\rho}{\partial\mu}\bigg|_T.$$

Here the Gibbs-Duhem relation $V dp = N d\mu + S dT$ and $\rho = N/V$ was used to rewrite the expression. The isothermal compressibility can be related to the Fourier transform of the density fluctuation correlation function as

$$\kappa_T = \beta\rho^{-1} D(\mathbf{q} = 0).$$

The osmotic pressure Π can be expanded in the density in a virial expansion

$$\beta\Pi = \rho + A_2\rho^2 + A_3\rho^3 + \cdots,$$

where the virial coefficients $A_2, A_3, \ldots$ contains information about interactions. If the particles are non-interacting, e.g. as they are in an ideal gas, then $A_2 =$

$A_3 = \ldots = 0$ and the expansion reduces to the ideal gas law. The isothermal compressibility can be expressed using the virial expansion as follows

$$\kappa_T = \left(\rho \frac{\partial \Pi}{\partial \rho}\right)^{-1} = \frac{\beta}{\rho}\left(1 + 2A_2\rho + 3A_3\rho^2 + \ldots\right)^{-1}.$$

Hence, by obtaining the forward scattering due to density fluctuation correlations, the virial coefficients can be obtained as

$$\frac{1}{D(q=0)} = 1 + 2A_2\rho + 3A_3\rho^2 + \ldots = 1 + 2A_2(\rho)\rho. \tag{4.8}$$

Here the apparent second virial coefficient $A_2(\rho) = A_2 + \frac{3}{2}A_3\rho + \cdots$ was used to absorb all higher order terms. By doing series of scattering experiments at increasing densities, and extrapolating to obtain the forward scattering, the virial coefficients can in principle be obtained [51, 52]. In practice multiple scattering sets an upper limit for the densities that can be probed in particular for light scattering.

The configurational average of a polymer solution is a homogeneous density distribution, as a result the scattering due to the average density is in the forward direction, and all the observed scattering will be due to the density fluctuation correlation function, and as a result the observed scattering can extrapolated to $\mathbf{q} = 0$ to yield the osmotic compressibility $\partial\Pi/\partial\rho$ [51, 20].

4.5 Positional and orientational averages

Objects suspended in a liquid medium are not fixed, and as a result of this translationally invariance, the correlation function $C(\mathbf{r}_1, \mathbf{r}_2)$ can only depend on the relative vector $C(\mathbf{r}_2 - \mathbf{r}_1) = \langle C(\mathbf{r}_1, \mathbf{r}_2)\rangle_t$. Nor is there a fixed orientation, as a result of this rotational invariance the correlation function can only depend on the length of the relative vector as $C(|\mathbf{r}_2 - \mathbf{r}_1|) = \langle C(\mathbf{r}_2 - \mathbf{r}_1)\rangle_o = \langle C(\mathbf{r}_1, \mathbf{r}_2)\rangle_{to}$. Thus positional and orientational average can be performed by inserting $V^{-1}\delta(r - |\mathbf{r}_2 - \mathbf{r}_1|)$ in any $\int \mathrm{d}\mathbf{r}_1\mathrm{d}\mathbf{r}_2 \cdots$ integral, where the factor V^{-1} is due to the translational invariance. For instance

$$\langle C(\mathbf{r}_1, \mathbf{r}_2)\rangle_{to} \equiv V^{-1}\int \mathrm{d}\mathbf{r}_1\mathrm{d}\mathbf{r}_2 C(\mathbf{r}_1, \mathbf{r}_2)\delta(r - |\mathbf{r}_2 - \mathbf{r}_1|),$$

$$= V^{-1}\int \mathrm{d}\mathbf{r}_1\mathrm{d}(\mathbf{r}_2 - \mathbf{r}_1) C(\mathbf{r}_2 - \mathbf{r}_1)\delta(r - |\mathbf{r}_2 - \mathbf{r}_1|).$$

The integrand is independent of $\mathbf{r}_1$, and the $\mathbf{r}_1$ integral yields a factor of volume, that is cancelled by the prefactor. Expressing the relative vector $\mathbf{r}_2 - \mathbf{r}_1$ in spherical representation yields

$$= \int \mathrm{d}(\cos\theta)\,\mathrm{d}\phi r^2 C(r) = 4\pi r^2 P(r).$$

$4\pi r^2 P(r)$ is the pair-distance distribution between the objects, e.g. it gives the number of particles in a spherical shell between r and $r + \mathrm{d}r$ around any

object. The scattering function of a fixed radial shell can be derived using the same procedure as

$$S(q,r) \propto V^{-1} \int \mathrm{d}\mathbf{r}_1 \mathrm{d}\mathbf{r}_2 C(\mathbf{r}_1,\mathbf{r}_2)\delta(r-|\mathbf{r}_2-\mathbf{r}_1|)e^{-i\mathbf{q}\cdot(\mathbf{r}_2-\mathbf{r}_1)}$$

$$= \int \mathrm{d}(\cos\theta)\mathrm{d}\phi\, r^2 P(r) e^{-iqr\cos\theta} = 4\pi r^2 \frac{\sin(qr)}{qr} P(r).$$

The scattering is only a function of q, and performing the radial integral of the pair-distance distribution yields the normalised scattering function as

$$S(q) = \frac{\int \mathrm{d}r 4\pi r^2 \frac{\sin(qr)}{qr} P(r)}{N \int \mathrm{d}r 4\pi r^2 P(r)}.$$

This expression can be used for calculating the scattering from a polymer chain when an expression for the pair-distance distribution is available.

4.6 Polymer models

Polymers are connected string-like objects, which gives rise to connectivity correlations between different sites on the same chain. Polymers also consist of monomers, which interact with neighbouring monomers, this interaction gives rise to rigidity of the polymer back bone, due to the torsional potential of the bonds and possible steric interactions from side groups on the monomers. Monomers far from each other along the chain, can be spatially close due to the conformation of the polymer chain, and this leads to excluded volume interactions. Finally, monomers interact with the solvent molecules, which means that the preferred polymer conformations show a strong dependence on solvent quality and temperature [4].

A chain with contour length L from end-to-end or correspondingly n segments, can be regarded as a polymer conformation given by a vectors $\mathbf{R}_i$ which denote the position of a i'th site/segment along the chain. One parameter that describes a polymer is the mean square site-site distance which is defined as

$$\left\langle R_{ij}^2 \right\rangle = \left\langle \left| \mathbf{R}_i^\alpha - \mathbf{R}_j^\alpha \right|^2 \right\rangle_\alpha ,$$

where the average is over all conformations of the polymer, and $\mathbf{R}_i^\alpha - \mathbf{R}_j^\alpha$ denotes the separation vector from site j to site i when the chain is in the α'th configuration. From this expression the Hausdorff dimension d_H [53] can be defined as

$$\sqrt{\langle R_{ij}^2 \rangle} \propto |i-j|^{\frac{1}{d_H}}.$$

The "true" Hausdorff dimension is obtained for $|i-j| \to \infty$. For chains of finite length there will be corrections to the Hausdorff dimension. A special case of the site-to-site distance is the end-to-end distance, which is defined as

$$\left\langle R_{ee}^2 \right\rangle = \left\langle |\mathbf{R}_0^\alpha - \mathbf{R}_n^\alpha|^2 \right\rangle_\alpha ,$$

Another quantity is the radius of gyration, which is defined by

$$\left\langle R_g^2 \right\rangle = \left\langle \frac{1}{n} \sum_i^n |\mathbf{R}_i^\alpha - \mathbf{R}_{cm}^\alpha|^2 \right\rangle_\alpha \quad \text{where} \quad \mathbf{R}_{cm}^\alpha = \frac{1}{n} \sum_i^n \mathbf{R}_i^\alpha .$$

The radius of gyration is the mean square distance from a site on the chain to the chain center of mass, and it is a measure of the spatial extension of the chain. The radius of gyration can also be shown to be [54]

$$\left\langle R_g^2 \right\rangle = \frac{1}{n^2} \left\langle \sum_{i,j}^n \left| \mathbf{R}_i^\alpha - \mathbf{R}_j^\alpha \right|^2 \right\rangle_\alpha .$$

The most simple model of a polymer is a flexible chain model, i.e. a random walk. In this model the step length l_0 of the random walk must be longer than the length scale over which chain orientation information persists in a real polymer, and hence the flexible chain model only captures large scale properties of a real polymer. The model includes effects due to connectivity, however, effects due to chain-chain and chain-solute interactions are neglected, and thus it corresponds to the physical case of a polymer in a Θ-solvent, where polymer interactions can approximately be neglected. From basic random walk theory it follows that the mean square site-to-site distance $\langle R_{ij}^2 \rangle = |i-j| l_0^2$, where l_0 is the segment length. In particular $\langle R_{ee}^2 \rangle = l_0 L$, and from this equation it follows that $d_H = 2$. The radius of gyration can be shown to be $\langle R_g^2 \rangle = l_0 L/6$ in the limit of many segments [54]. From basic random walk theory it can further more be shown that the pair-distance distribution between sites on a random walk is Gaussian distribution in the large n limit.

The angle θ between successive segments is free for the flexible chain model, fixing this angle introduces semi-flexibility in the chain, hence known as the semi-flexible chain model, this model also neglects interactions between different segments. Flory [54] has shown that the expressions for the average end-to-end distance and radius of gyration for a flexible chain (in the large n limit) are also valid for a semi-flexible chain, however, with the segment length replaced by the Kuhn Length b as

$$\left\langle R_{ee}^2 \right\rangle = Lb, \quad \text{and} \quad \left\langle R_g^2 \right\rangle = \frac{Lb}{6}.$$

The Kuhn length b is given by

$$b = \frac{1+\cos(\theta)}{1-\cos(\theta)} l_0 .$$

The Kuhn length is the length scale on which the orientation of subsequent segments is uncorrelated. e.g. it is the step length of the equivalent flexible chain. An approximate expression for the pair-distance distribution of a semi-flexible chain has been derived by Daniels [55, 56].

The Kratky-Porod chain model is obtained from the semi-flexible chain model in the limit where $n_b \to \infty$, $l_0 \to 0$, and $\theta \to 0$ such that the number of statistical independent segments $n_b = L/b$ is fixed, in that case [54, 57, 58]

$$\left\langle R_{ee}^2 \right\rangle = Lb \left\{ 1 - \frac{1}{2n_b} \left(1 - e^{-2n_b} \right) \right\},$$

and

$$\left\langle R_g^2 \right\rangle = \left(1 - \frac{3}{2n_b} + \frac{3}{2n_b^2} - \frac{3}{4n_b^3} \left(1 - e^{-2n_b} \right) \right) \frac{Lb}{6}.$$

These expressions reduce to the semi-flexible chain result in the limit of large n_b. The previous models were analytically tractable, however, including excluded volume effects for both a flexible and semi-flexible chain model leads to a model, that is very difficult to handle analytically. The excluded volume interaction is a very strong and long-ranged interaction for polymers in three dimensions. There are three approaches which can yield results for chains with excluded volume: one is simulation techniques such as Molecular Dynamics or Monte Carlo simulations, see e.g. [59, 60, 61, 62], another approach is functional integrals [30], and a third method is renormalization group techniques, see e.g. [46, 48, 63, 64].

Simulation techniques are limited by the computer time it takes to perform a simulation, at present, however, it is possible to perform simulations on very complex chain models. It is also possible to simulate chains confined to pores [65], or chains tethered to surfaces. The disadvantage of simulation techniques are that results are obtained for a particular set of parameters, and repeated simulation runs sweeping the parameter space are necessary before general conclusions can be made just like performing a series of experiments.

Functional integrals provide a statistical physical description of polymer chains. Polymers are represented as a continuous curve $\mathbf{R}(l)$, with an energy functional given by an Edwards Hamiltonian $H_E[\mathbf{R}(l)]$ [66]. The chain partition function can be obtained by integrating over all continuous curves (hence the name functional integrals) where each curve is weighted by the Boltzmann factor $\exp(-H_E[\mathbf{R}(l)]/k_bT)$. Functional integrals of both flexible and semi-flexible chains can be formulated. A functional integral can be reexpressed in terms of a diffusion equation, and the problem of excluded volume chains can be expressed as a self-consistent solution of a diffusion equation i.e. a SCF theory [66, 67].

Renormalization group techniques (RGT) attack the problem of excluded volume by expanding the functional integral in powers of the site-site interaction parameter. This expansion is divergent in three dimensions, however, in four dimensions the excluded volume interaction can be regarded as a perturbation. Heuristically this can be explained by the fact that the Hausdorff dimension of a excluded volume chain is less than two (it is $d_H \approx 1.7$ [68]), two planes ($d_H = 2$) will almost always cross each other in a four dimensional space, while they will almost never cross each other in a five dimensional space. Similarly two self-avoiding chains will rarely overlap if the dimension is four [21]. The expansion can furthermore be expanded in ϵ given by the dimensionality $d = 4 - \epsilon$. Through

the renormalization procedure singular terms around $d = 4$ are absorbed in a series of relations relating microscopic (bare) quantities to effective macroscopic quantities. Hence the ill-behaved microscopic model is reformulated into a well-behaved effective model that depends only on macroscopic quantities, and these can then be evaluated for $\epsilon = 1$ i.e. in three dimensions.

Using a simple mean field argument Flory predicted a simple scaling relation $\langle R_{ee}^2 \rangle = b^2 n^{2\nu}$ between mean-end-to-end distance and the number of statistical segments for a flexible chain with excluded volume interactions [21]. Here b is the Kuhn length, n is the number of segments which is assumed to be large. Flory also gave an expression for the critical exponent $\nu = 3/(d+2)$. This expression gives the correct value for one and two dimensions. In three dimensions Flory predicted $v = 0.6$, while RGT predicts a value of $\nu = 0.588$ [63, 68]. For 4 four dimensions or more $\nu = 0.5$. RGT also provides an expression for the pair-distance distribution [60, 64, 69] from which the radius of gyration can be calculated [70] as

$$\left\langle R_g^2 \right\rangle = \frac{b^2 n^{2\nu}}{2(1+\nu)(1+2\nu)}.$$

Later studies have shown that different exponents exist for end-to-end, end-to-internal point and internal-to-internal point distributions [60, 64]. The result for a flexible random walk is retrieved in the limit of $\nu \to 0.5$. The Hausdorff or fractal dimension of a chain is given by $d_H = \nu^{-1}$, and this is related to the volume occupied by a chain in the long chain limit.

4.7 Scattering from a dilute solution of flexible polymers

In a dilute polymer solution we can neglect the correlations between positions, orientation, and configuration of individual chains, and as a result the scattering can be calculated from the pair-distance distribution of a single chain ($H(q) = 0$). For a long flexible polymer without interactions between any sites the pair-distance distribution is given by a Gaussian distribution as

$$P(r,l)4\pi r^2 \mathrm{d}\mathbf{r} = \left(\frac{3}{2\pi\langle R_{ee}^2(l)\rangle}\right)^{\frac{3}{2}} \exp\left(-\frac{3r^2}{2\langle R_{ee}^2(l)\rangle}\right) 4\pi r^2 \mathrm{d}\mathbf{r}.$$

This results follows from the fact that the problem of a non-interacting flexible polymer can be mapped onto the problem of a random walker, where the time in the random walk problem corresponds to contour length for the polymer. $P(r,l)$ is the distance distribution for two arbitrary sites on the chain separated by a distance l along the contour. The scattering contribution from two fixed sites separated by a fixed contour length l is $\sin(qr)/(qr)$ averaged over all possible separations r as

$$\Psi(q,l) = \int_0^\infty \mathrm{d}r 4\pi r^2 \frac{\sin(qr)}{qr} P(r,l) = \exp\left(-\frac{blq^2}{6}\right).$$

$\Psi(q,l)$ is a configurational averaged phase factor for fixed contour length. The full scattering is obtained by averaging the phase factor over all possible sites (l_1 and l_2) on the chain as

$$F_{Debye}(q) = \int_0^L \frac{\mathrm{d}l_1 \mathrm{d}l_2}{L^2} \Psi(q, |l_1 - l_2|) = \int_0^L \mathrm{d}l \frac{2(L-l)}{L^2} \exp\left(-\frac{blq^2}{6}\right)$$

$$= \frac{2\left(e^{-x} - 1 + x\right)}{x^2},$$

where the abbreviation $x = bLq^2/6 = (qR_g)^2$ was introduced. This result was first derived by Debye in 1947 [71]. In a similar manner the form factor of any polymer chain with a given pair-distance distribution can in principle be derived. Results for the Daniels and des Cloizeaux distributions [55, 60] are given in article IV and shown in figure 4.1.

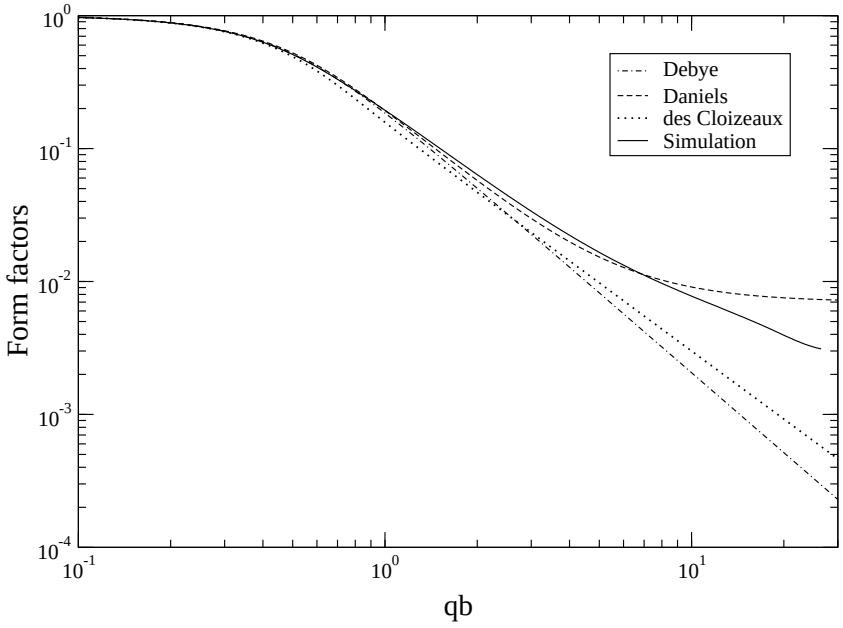

Figure 4.1: Form factors for different pair-distance distributions for $R_g = 3.11b$ and $L/b = 38$ corresponding to the simulation.

The form factor of flexible chains with and without interactions, semi-flexible chains without interactions, and simulation results with excluded volume interactions and semi-flexibility are shown in figure 4.1. The Daniels approximation breaks down around $qb \simeq 3$ values, but the remaining three form factors shows power law behaviour at high q values. This is caused by the different chain statistics

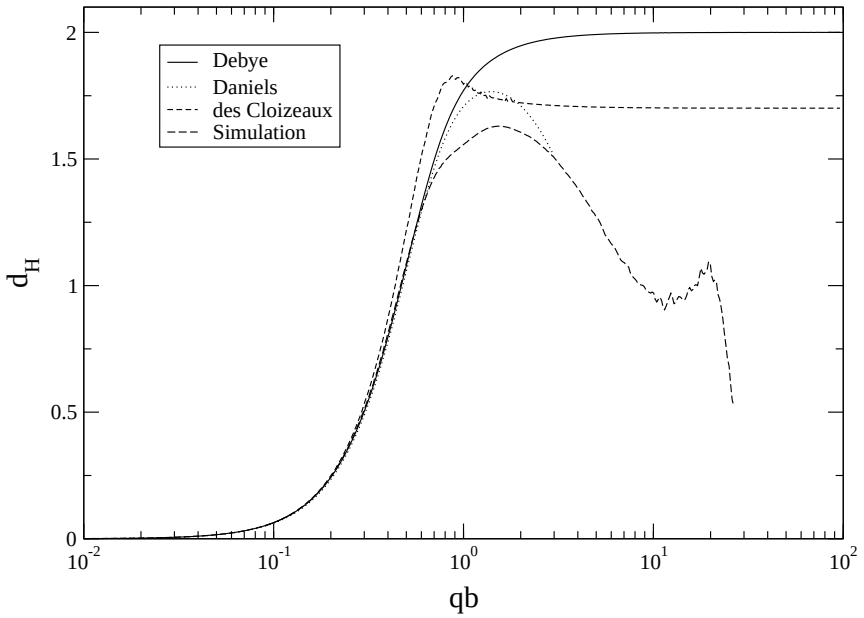

Figure 4.2: Scale dependent Hausdorff dimension corresponding to form factors shown in figure 4.1.

$$\left\langle \left(R_i^\alpha - R_j^\alpha \right)^2 \right\rangle_\alpha \propto |i-j|^{\frac{2}{d_h(|i-j|)}},$$

where $d_h(|i-j|)$ is the scale dependent Hausdorff dimension, which can also be derived from the form factor as as $d_H(q) = -\mathrm{d}(\log_{10}(F_c))/\mathrm{d}(\log_{10}(q))$, and this is shown in figure 4.2. For small qb values the chain is probed on very long length scales compared to the radius of gyration, where chains are point-like objects with Hausdorff dimension is zero. For large values of qb very short length scales are probed, the Debye and des Cloizeaux distributions do not include semi-flexibility, and they converge to the long chain limit of a random walk and a self-avoiding random walk, which yields Hausdorff dimensions of two ($\nu = 0.5$) and 1.7 ($\nu = 0.588$), respectively. The Hausdorff from the simulation has a peak at the length scales where the random walk nature of the chain is probed, but the simulations includes effects of semi-flexibility, which leads to $d_H = 1$ at large values of qb. An extended range of powerlaw behaviour is not observed because of the finite number of segments and few vertices per Kuhn length.

4.8 Scattering from a semi-dilute solution of flexible polymers

Assuming that N identical polymers each with n segments/scattering sites is dissolved in a volume V. Assuming further that $\mathbf{R}_{ij}^{\alpha}$ is the position of the j'th segment on the i'th chain when the collective configurations of all the chains is denoted α (in the following the indices i, l range from $1, \ldots, N$ and j, k from $1, \ldots, n$ in order to simplify notation). This means that the instantaneous density distribution of the α'th state is given by

$$\rho_{\alpha}(\mathbf{r}) = \sum_{i=1}^{N} \sum_{j=1}^{n} \delta(\mathbf{r} - \mathbf{R}_{ij}^{\alpha}),$$

while the mean density of scattering sites in the volume is $\rho = nN/V$. The solution will be in the semi-dilute regime if $4\pi R_g^3 N/(3V) > 1$, where R_g is the radius of gyration of an unperturbed chain. The semi-dilute regime is characterized by chain densities so large that there are more than one chain within the volume occupied by an unperturbed chain.

The scattering function was shown to consist of two contributions due to the configurationally averaged density and density fluctuation correlations. The average density is constant, and as a result the scattering from the average density is proportional to a delta function at $\mathbf{q} = 0$, and it will be neglected. The scattering function $S(q)$ is the density fluctuation correlation function $D(q)$, and is given by

$$S(q) = \frac{1}{nN} \left\langle \left| \int \mathrm{d}\mathbf{r} \rho_{\alpha}(\mathbf{r}) e^{-i\mathbf{q}\cdot\mathbf{r}} \right|^2 \right\rangle_{\alpha} = \left\langle \frac{1}{nN} \left| \sum_{i}^{N} \sum_{j}^{n} e^{-i\mathbf{q}\cdot\mathbf{R}_{ij}^{\alpha}} \right|^2 \right\rangle_{\alpha}$$

$$= \frac{1}{nN} \sum_{i}^{N} \sum_{j,k}^{n} \left\langle e^{-i\mathbf{q}\cdot(\mathbf{R}_{ij}^{\alpha} - \mathbf{R}_{ik}^{\alpha})} \right\rangle_{\alpha} + \frac{1}{nN} \sum_{i \neq l}^{N} \sum_{j,k}^{n} \left\langle e^{-i\mathbf{q}\cdot(\mathbf{R}_{ij}^{\alpha} - \mathbf{R}_{lk}^{\alpha})} \right\rangle_{\alpha},$$

which can be written as

$$S(q) = \omega(q) + \rho h(q). \tag{4.9}$$

We have thus written the total scattering function as the contribution from intra-chain correlations, and inter-chain correlations. The intra-chain scattering contribution is defined as

$$\omega(q) = \frac{1}{nN} \sum_{i}^{N} \sum_{j,k}^{n} \left\langle e^{-i\mathbf{q}\cdot(\mathbf{R}_{ij}^{\alpha} - \mathbf{R}_{ik}^{\alpha})} \right\rangle_{\alpha},$$

which is simply the Fourier transform of the distance distribution between sites on the same chain. If chain-chain interactions are weak, for instance for sufficiently low densities within the semi-dilute regime, and if we neglect semi-flexibility and excluded volume interactions, then $\omega(q) = nNF_{Debye}(qR_g)$. The

inter-chain scattering contribution is the Fourier transform of the distance distribution between sites on different chains

$$h(q) = \frac{V}{(nN)^2} \sum_{i \neq l}^{N} \sum_{j,k}^{n} \left\langle e^{-i\mathbf{q}(\mathbf{R}_{ij}^{\alpha} - \mathbf{R}_{lk}^{\alpha})} \right\rangle_{\alpha} .$$

Inter-chain correlations are long-ranged on the length scale of the characteristic inter-chain length scale. This is caused by indirect interactions mediated by neighbouring polymer chains. As a result an effective inter-chain correlation function between sites on pairs of polymers can be introduced, which is called the direct correlation function, and denoted $c(q)$, this should not to be confused by the Fourier transform of the average density distribution $C(q)$. The direct correlation function is introduced in an attempt to decompose the correlations induced by indirect interactions, mediated by the medium consisting by all other polymers, into an effective pair correlation that includes only direct interactions between pairs of chains. The direct correlation function is expected to have a characteristic length scale comparable to the inter-chain distances. In reality each pair of sites on two chains have a direct correlation function, but an average is often performed over all sites producing a site-averaged direct correlation function. This is the equivalent site approximation.

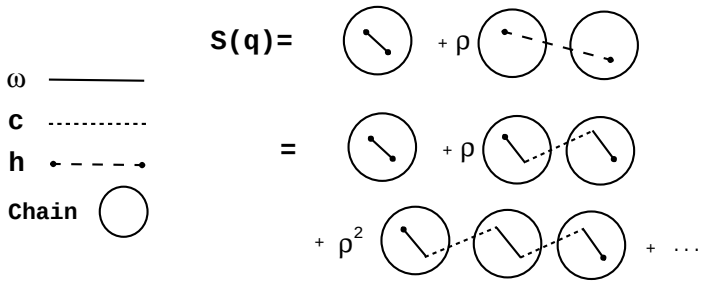

Figure 4.3: Diagrammatic expansion of the PRISM equation in terms of intra-chain correlations $\omega(q)$, and direct correlation function $c(q)$.

Following this approach, the scattering can be resolved into contributions from the individual chain ω, a contribution from the correlation between two polymers $\rho\omega c\omega$. A diagrammatic expansion is shown in figure 4.3, where the scattering is interpreted as the correlation created by a jump from one site to another site on the same chain (providing a factor ω), a jump from that site to another site on another chain (ρc), and finally a jump to another site on the other chain (ω). Taking higher order terms into account the result is an expansion of the scattering function as

$$S(q) = \omega + \rho\omega c\omega + \rho^2 \omega c\omega c\omega + \rho^3 \omega c\omega c\omega c\omega + \cdots \tag{4.10}$$

This equation can be regarded as the definition of the direct correlation function. Comparing eq. (4.9) and (4.10) shows that the total inter-molecular correlation function can be written

$$h(q) = \omega c\omega + \rho\omega c\omega c\omega + \rho^2\omega c\omega c\omega c\omega + \cdots = \omega c\left(\omega + \rho h\right), \tag{4.11}$$

which is the Polymer Reference Interaction Site Model (PRISM) equation [72, 73, 74, 75]. In PRISM theory an expression for $\omega(q)$ is assumed, as well as a closure relation, which relates the direct correlation function $c(r)$ to an interaction potential. From the closure relation the total correlation function $h(q)$ can then be obtained via the PRISM equation. Solving eq. (4.9) and eq. (4.11) for the intra-chain correlation function ω and the direct correlation function $c(q)$ yields

$$S(q) = \frac{\omega(q)}{1 - \rho c(q)\omega(q)}.$$

If the direct correlation function is short ranged, the Fourier transform will essentially be constant, so we can introduce the approximation $\rho\nu(\rho) = -n\rho c(q = 0)$, where ν is the excluded volume parameter. The assumption that the excluded volume parameter is a function of the density was originally suggested by Daoud et al. [20] and rigorously shown by Benoit et al. [76]. A normalised intra-correlation function is defined as $\overline{\omega}(q) = \omega(q)/n$ such that $\overline{\omega}(q = 0) = 1$. This has the effect of turning the PRISM expression for the scattering into the form of an Random Phase Approximation (RPA) [73, 76]

$$S(q) = n\frac{\overline{\omega}(q)}{1 + \rho\nu(\rho)\overline{\omega}(q)}.$$

Thus

$$\frac{n}{S(q = 0)} = 1 + \nu(\rho)\rho.$$

The left hand side is the scattering per polymer molecule rather than per scatterer. The excluded volume parameter $\nu(\rho)$, which should not be confused to the critical length exponent. A comparison of this expression with eq. (4.8) shows that $\nu(\rho) = 2A_2(\rho)$. The excluded volume parameter can be shown to depend only on the reduced polymer concentration c/c^* [21, 73].

4.9 Core-shell models

Core-shell models describe the scattering as being caused by a number of concentric shells, see e.g. [70, 77]. Assuming the shells to be of infinitesimal width, the core-shell model assumes knowledge of the $\rho(s)$ area density of scatterers on the s sized shell. The normalised core-shell form factor amplitude ($A_{shell}(\mathbf{q} = 0) = 1$) is given by

$$A_{shell}(\mathbf{q}) = \rho^{-1}\int_0^\infty \mathrm{d}s A(s)\Psi_s(\mathbf{q}, s)\rho(s) \quad \text{with} \quad \rho = \int_0^\infty \mathrm{d}s A(s)\rho(s), \tag{4.12}$$

where $A(s)$ is the area and $\Psi_s(\mathbf{q}, s)$ is the phase factor of a s sized shell given by

$$\Psi_s(\mathbf{q}, s) = A(s)^{-1} \int \mathrm{d}\mathbf{r}\delta[f(\mathbf{r}, s)]e^{-i\mathbf{q}\cdot\mathbf{r}},$$

where $f(\mathbf{r}, s)$ is a shape-function. The shape function is zero if and only if the point $\mathbf{r}$ is on the shell with size s. The area of the shell $A(s)$ is given by $A(s) = \int \mathrm{d}\mathbf{r}\delta[f(\mathbf{r}, s)]$. The orientationally averaged form factor and form factor amplitude of a shell structure is

$$F_{shell}(q) = \langle A_{shell}(\mathbf{q})A_{shell}(-\mathbf{q})\rangle_o \quad \text{and} \quad A_{shell}(q) = \langle A_{shell}(\mathbf{q})\rangle_o .$$

An example: For the special case of a spherical shell the shape function is $f(\mathbf{r}, s) = |\mathbf{r}| - s$, in this case the phase factor is easy to calculate as

$$\Psi_{sphere}(q, s) = A(s)^{-1} \int \mathrm{d}\mathbf{r}\delta[|\mathbf{r}| - s]e^{-i\mathbf{q}\cdot\mathbf{r}}$$

$$= \frac{1}{4\pi s^2} \int \mathrm{d}\phi\mathrm{d}(\cos\theta)e^{-iqs\cos\theta} = \frac{\sin(qs)}{qs}.$$

Assuming a homogeneous spherical object the radial density is $\rho(s) = 1$ for $s < r$ and 0 elsewhere. The radial integral becomes

$$A_{sphere}(q) = \frac{3}{4\pi r^3} \int_0^r \mathrm{d}s 4\pi s^2 \frac{\sin(qs)}{qs}$$

$$= \frac{3[\sin(qr) - qr\cos(qr)]}{(qr)^3} = \Phi(qr).$$

This result was first obtained by Lord Rayleigh [78]. The form factor amplitude for a homogeneous sphere is the simplest possible core-shell structure and will denoted $\Phi(qr)$ in the rest of this thesis. Since the form factor amplitude only depends on the magnitude of the $\mathbf{q}$ vector the form factor of a sphere is $F_{sphere}(q) = \Phi^2(qr)$. The form factor will always be the square of the form factor amplitude for any spherical symmetric distribution.

A core-shell model of a micelle with a spherical core assumes $F_{micelle}(q) = (\beta_{cor}A_{cor}(q) + \beta_{co}\Phi(qR_{co}))^2$, where the corona form factor amplitude A_{cor} is given by eq. (4.12) using some assumed corona profile $\rho(r)$. Hence core-shell models includes scattering due to an average shell densities ($C(q)$), but neglects the scattering scattering due to density fluctuations ($D(q)$) caused by chain connectivity, and chain interactions such as the correlation hole [20] are neglected. The next section demonstrates how some of these effects can be taken into account.

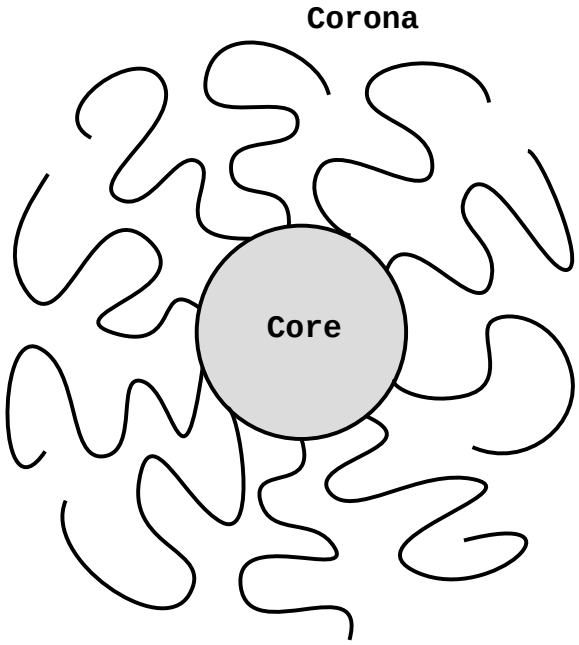

Figure 4.4: Illustration of a micelle consisting of a spherical core and a corona of dissolved chains.

4.10 Scattering from a micellar aggregate

A micelle consists of a core with some geometrical shape such as spherical, elliptical or cylindrical, and a corona of dissolved polymer chains. Assuming that the core is homogeneous then it can be described by a core-shell model $A_s(\mathbf{q})$. The normalised ($A^\alpha_{cor}(q=0)=1$) corona form factor amplitude is

$$A^\alpha_{cor}(\mathbf{q}) = \frac{1}{Nn}\sum_{i=1}^{N}\sum_{k=1}^{n} e^{-i\mathbf{q}\cdot\mathbf{R}^\alpha_{ik}},$$

where $\mathbf{R}^\alpha_{ik}$ is the location of the k'th vertex on the i'th chain in the corona when the corona is in the α'th state. N is the number of chains, and n is the number of scattering sites per chain (in the rest of this section all i and j sums are over chains, i.e. they range from $1,\ldots,N$). The normalised [$F_{micelle}(q=0)=1$] scattering of a micelle can then be written as

$$F_{micelle}(q) = (\beta_{ch}+\beta_{co})^{-2}\left\langle\left|\beta_{ch}A^\alpha_{cor}(\mathbf{q})+\beta_{co}A_s(\mathbf{q})\right|^2\right\rangle_{\alpha o}, \tag{4.13}$$

where the average is over all configurations ("α") of the chains in the corona and orientations ("o") of the micelle. The two terms describe the corona and core, respectively. β_{ch} and β_{co} are the total excess scattering lengths of the whole corona and core. These can be written $\beta_{ch}=NV_{ch}\Delta\pi_{ch}$ and $\beta_{co}=N_{co}V_{co}\Delta\pi_{co}$ where N, N_{co}, V_{ch} and V_{co} are the number of chains in the corona and core, respectively, and the specific volume of a single corona and core chain, respectively. The excess scattering length densities of a corona chain is $\Delta\pi_{ch}=\pi_{corona,chain}-\pi_{solvent}$

and for core chain $\Delta\pi_{co} = \pi_{core,chain} - \pi_{solvent}$, where $\pi_{corona,chain}$,$\pi_{core,chain}$, and $\pi_{solvent}$ are the scattering length densities of a single chain in the corona, of a single chain in the core, and of the solvent, respectively. Assuming that the core form factor $A_s(\mathbf{q})$ is real, which is the case if the core has a parity ($\mathbf{R} \to -\mathbf{R}$) symmetry, then the micellar scattering can be expressed as

$$F_{micelle}(q) = (\beta_{ch} + \beta_{co})^{-2} \left\langle \beta_{ch}^2 A_{cor}^{\alpha}(\mathbf{q}) A_{cor}^{\alpha}(-\mathbf{q}) \right.$$

$$\left. + \beta_{co}^2 A_s^{\alpha}(\mathbf{q})^2 + 2\beta_{ch}\beta_{co} A_s(\mathbf{q}) \mathrm{Re}\left(A_{cor}^{\alpha}(\mathbf{q})\right) \right\rangle_{\alpha o}.$$

These three scattering terms correspond to the corona form factor, the core form factor, and an corona-core interference scattering, respectively. A normalised corona form factor is defined by

$$F_{cor}(q) = \left\langle |A_{cor}^{\alpha}(\mathbf{q})|^2 \right\rangle_{\alpha o}. \tag{4.14}$$

The corona-core interference scattering can be defined as

$$S_{cs}(q) = \langle A_s(\mathbf{q}) \mathrm{Re}\left(A_{cor}^{\alpha}(\mathbf{q})\right) \rangle_{\alpha o}.$$

In the special case of a spherical core $S_{cs}(q) = \Phi(qr) A_{cor}(q)$ and $A_{cor}(q) = \langle A_{cor}^{\alpha}(\mathbf{q}) \rangle_{\alpha o}$. Using these definitions, the micellar scattering for a spherical core is

$$F_{micelle}(q) = \beta_{ch}^2 F_{cor}(q) + \beta_{co}^2 \Phi^2(qr) + 2\beta_{ch}\beta_{co}\Phi(qr) A_{cor}(q).$$

The physical interpretation of these three terms is that they, respectively, correspond to the Fourier transform of the pair-distance distribution between two scattering sites in the corona, two scattering sites in the core, or between two scattering sites in the core and in the corona. In the special case of a spherical core, the vector between a site in the corona and a site in the core can be written as a sum of a vector from the corona site to the core center, and from the core center to the core site. Due to the rotational symmetry these two vectors will be statistically independent and independent on orientation. As a result the pair-distance distribution factorises into the product of a corona-site-to-core-center (A_{cor}) and center-to-core-site (Φ) probability distributions, the Fourier transform of which is $S_{cs}(q)$.

The corona scattering can separated into contributions using several choices for the separation. One possibility is to separate the corona scattering in terms of scattering from the configurationally average density, and scattering from the density fluctuation about this average. Another approach is to separate the scattering in terms of inter-chain scattering and of intra-chain scattering as

$$F_c(q) = \left\langle \frac{1}{N} \sum_i |A_i^{\alpha}(\mathbf{q})|^2 \right\rangle_{\alpha o}, \quad \text{and}$$

$$H(q) = \left\langle \frac{1}{N(N-1)} \sum_{i \neq j} A_i^{\alpha}(\mathbf{q}) A_j^{\alpha}(-\mathbf{q}) \right\rangle_{\alpha o}, \tag{4.15}$$

where the phase sum A_i^α of the i'th chain when the corona is in the α'th configurational state is defined as

$$A_i^\alpha(\mathbf{q}) = \frac{1}{n}\sum_{k=1}^{n} e^{-i\mathbf{q}\cdot\mathbf{R}_{ik}^\alpha}.$$

The corona form factor is the following weighted average

$$F_{cor}(q) = \frac{1}{N}F(q) + \frac{N-1}{N}H(q). \tag{4.16}$$

The physical interpretation of these two terms is as follows: $F(q)$ is the average single chain form factor, e.g. the Fourier transformed pair-distance distribution between sites within the same chain. This carries information about the chain radius of gyration, chain length, chain stiffness, and the number of statistical independent segments. It also contains information about chain connectivity such as the fractal dimension of the chain. The Fourier transform of the pair-distance distributions between sites on different chains $H(q)$ contains information about the radial profile of the corona, but also chain-chain interactions such as the correlation hole, which is present in ordinary three dimensional polymer solutions [20, 21].

4.11 Interpretation of scattering

Scattering techniques are very sensitive to the structural arrangements of the scatterers, especially periodic structures. As a result scattering techniques are ideally suited to probe structural arrangements. However, the basic problem of scattering tehniques is the inverse problem of how to deduce structure from the experimental data of the scattering $S(\mathbf{q})$, since phase information is lost in the measuring process only the pair-distance distribution can be reconstructed, and from from which structure must be inferred.

Furthermore, the scattering is only known in a certain range of $\mathbf{q}$ vectors due to instrumental limitations. Data are subject to instrumental smearing due to finite beam collimation (how well defined are directions of $\mathbf{k}_s$ and $\mathbf{k}_i$), wavelength spread (how narrow is the energy distribution e.g. $|\mathbf{k}_i|$ for instance from a neutron source), and finite detector resolution. Finally there are statistically errors on the experimental scattering data. All these sources of error make a direct inversion of $S(\mathbf{q})$ very difficult in general. Only in the special case of a spherically symmetric arrangement of scatterers is it possible to analytically invert the scattering, as in that case the Fourier transform is a real function, and no phase information is lost due to the norm square except for an overall sign.

Two types of methods exist for inferring the physical structure producing the observed scattering; these are model fitting and free-form analysis [19]. In free-form analysis the pair distance distribution is obtained for example by the indirect Fourier transform method introduced by Glatter [79]. The method works as follows: the pair distance distribution is represented as a linear combination of cubic splines, typically with some 50 spline functions. The coefficients are obtained by fitting the Fourier transformed basis functions to the observed

scattering data. Finally, if the scattering objects are centro-symmetric the radial excess scattering length density distribution can be obtained from square-root deconvolution, also introduced by Glatter [80]. Instrumental effect can furthermore be incorporated in the fit. The "free form" name of the method follows from the fact that the indirect Fourier transform method is independent on any a-priori assumed model expressions, just like maximum entropy methods.

Model fits using least-squares methods [81, 82, 83, 84] is another way of inferring the structure [85]. A particular model is assumed, for instance a model describing the scattering expected from a solution of micellar aggregates. The model will depend on a number of parameters, and the most likely set of parameters are obtained from fitting the model scattering to the experimental data. The goodness-of-fit is typically estimated by the reduced chi-square statistic χ^2_{red}, which is defined as

$$\chi^2_{red}(\alpha_1, \ldots \alpha_M) = \frac{1}{N-M} \sum_{i=1}^{N} \frac{\left(I_i^{exp} - I^{mod}(q_i; \alpha_1, \ldots \alpha_M)\right)^2}{\sigma_i^2},$$

where N is the number of experimental data points I_i^{exp}, q_i is a set of fixed control parameters e.g. detector positions, and σ_i is the error of the experimental data, while I^{mod} is the model prediction of the scattering at q_i. The model depends on the M parameters $\alpha_1, \ldots, \alpha_M$. The most likely set of control parameters assuming the model is true are determined by minimising χ^2_{red}. If the obtained reduced chi-square is close to unity it suggests that the model is a good description, and that the estimated parameter values are reliable, as the model curve will on average pass through a $2\sigma_i$ sized window about every data point I_i^{exp}. If the reduced chi-square is "large" the model is likely to be a wrong description of the data, and parameters obtained by the fits are meaningless. If, on the other hand, the reduced chi-square is less than unity, it suggests that the error bars are either systematically too large or that the model depends on too many parameters given the quality of the experimental data.

4.12 Maximum Entropy methods

A good introduction to Bayesian statistics and Maximum entropy (ME) has been written by Jaynes [86], while [87, 88] are reviews of scattering related applications of ME. The following is a heuristic introduction.

Given an experiment that involves a measurement on a distribution, and yields as experimental result for the mean a and variance σ^2 of the distribution, which distribution was measured? Clearly the question is ill-posed as no unique distribution can be specified based on the knowledge of the mean and variance, however, a unique distribution exists that assumes the least amount of extra information compared to the information we have. This is the maximum entropy distribution. From information theory [89] the relative entropy is defined as

$$H[P, Q] = -\sum_i P_i \log_2(P_i/Q_i) = -\int \mathrm{d}x P(x) \log_2 \left(\frac{P(x)}{Q(x)}\right).$$

In the context of information theory, this expression has the following interpretation: if a receiver has a prior information given by the frequency Q_i of symbols/letters received in earlier messages, and received a new message with symbol frequencies P_i, the relative entropy that the receiver has obtained is $H[P,Q]$, i.e. this is the number of bits of knowledge the receiver has after receiving the message. This is almost always different from the number of bits in the message itself. The relative entropy can be interpreted as the average of the information or "surprise", when we observe the i'th symbol as given by $-\log_2(P_i/Q_i)$. If P_i/Q_i is one it means that we are observing a particular symbol with the expected frequency, and this is not a surprise, nor will we receive any new information. However, if P_i/Q_i is large a particular symbol is observed more frequently than expected, and we will be very surprised by its occurrence, i.e. we have received a lot of new information.

Thus given the experiment which provides prior knowledge of the mean and variance, and assuming no prior knowledge about the shape of the distribution e.g. $Q(x) = 1$, the entropy is given by

$$H[P] = -\int \mathrm{d}x P(x)\log(P(x)) + \lambda_0\left(1 - \langle 1\rangle\right)$$

$$+\lambda_1\left(a - \langle x\rangle\right) + \lambda_2\left(\sigma - \left[\left\langle x^2\right\rangle - \langle x\rangle^2\right]\right),$$

where $\langle f(x)\rangle = \int \mathrm{d}x P(x) f(x)$ is the expectation value of the function $f(x)$. Here base e is used instead of base 2 in the logarithm, which makes no difference, as it corresponds to a redefinition of the unit of information from a number of bits (binary digits) to the number of base e digits. The three λ's are Lagrange multipliers. The Lagrange multipliers represent the constraints that the distribution should be normalised, and that the mean a and variance σ^2 correspond to the known values. The distribution which maximizes the entropy functional is given by the equation $\delta H[P]/\delta P = 0$ from which, it is easy to show that the solution is $P(x) = N\exp[-(x-a)^2/(2\sigma^2)]$, i.e. a Gaussian distribution.

Chapter 5

Monte Carlo Simulation

Computer simulation techniques can be graded on a scale from purely stochastic to purely deterministic algorithms. Deterministic algorithms, such as Molecular Dynamics (MD) simulate the trajectory of a system in phase space. This is done by solving the equations of motion numerically. MD simulations can be performed on non-equilibrium systems and simulate transport properties. It is possible to obtain time averages of all the properties of interests from a MD simulation. Assuming that the sampling of the system is ergodic, then ensemble averages are obtained. Typically MD simulations are done within the micro-canonical ensemble, but simulation of other ensembles are possible by modifying the MD algorithm. MD methods are limited by the small time steps required to perform an accurate numerical integration of the equations of motion, and objects with rigid constraints are computationally difficult to simulate.

At the other end of simulation techniques are stochastic algorithms, which are based on the application of (pseudo) random numbers. A Monte Carlo (MC) simulation allows canonical ensemble averages to be obtained for interesting properties. Whereas MD simulates the evolution of a system through the equations of motion, a MC simulation defines a purely fictitious dynamic, where each state of the system has a number of possible "neighbour states". The MC simulation is performed by allowing the active state to perform a random walk from neighbour to neighbour state. A neighbouring state to the active state is chosen randomly for each iteration of the MC algorithm. The energy of the neighbour state is calculated, and compared to the active state. The step to the neighbour state is accepted if the neighbour state has a lower energy, however, if the energy of the neighbour state is higher than the active state it is accepted with a probability $\exp[-\Delta E/(k_b T)]$, where $\Delta E > 0$ is the energy difference between the two states, k_b and T are the Boltzmann constant and the absolute temperature. The acceptance criterion is known as the Metropolis criterion [90]. The MC algorithm will perform a random walk, that visits a state ω with a frequency proportional to the Boltzmann probability associated with that state $\exp[-E[\omega]/(k_b T)]$. This is known as importance sampling, and requires only that the energy of an state can be calculated.

The choice of possible neighbour states of a particular state is to some extent arbitrary, however, the choice has to ensure an ergodic sampling of all configu-

rations, which is to say that any two states have to be connected by a number of neighbour steps. The choice also has to ensure an asymptotic convergence towards an unique equilibrium ensemble of states, and this requires a balance, such that the transitions into any state exactly equals the transitions out of that state, such that no state acts as an absorber. Detailed balance, i.e. the probability of choosing neighbour state B from an active state A must equal the probability of choosing neighbour state A from an active state B, is a sufficient requirement to ensure asymptotic convergence.

The choice of neighbour states do not have any physical meaning, but a clever design of neighbouring steps, for instance by taking rigid constraints into account when designing the neighbour class, allows the MC algorithm to roam the configuration space in relative few iterations, which makes a good sampling possible with a limited number of steps.

5.1 Overview of Simulations

We have performed MC simulations on a single diblock copolymer micelle, with the purpose of sampling the form factor as a function of a the number of tethered chains, the length of chains, and the radius of the core. The micelle was modelled as a core with a number of semi-flexible chains tethered to the core surface. Spherical cores and cylindrical cores with hemispherical end caps have been simulated. Chains were excluded from the core region, and chains interacted through excluded volume interactions implemented by placing hard spheres along the chains.

Because hard sphere interactions was used the energy of a particular state is either zero or infinite depending on whether chains overlap or not, as a result, the energy is independent of the temperature, which corresponds to the idealised case of an athermal solvent. To ensure ergodic sampling of the micellar corona, three MC moves were used; pivoting moves were used to modify individual chain configurations, while two surface moves were used to reorientate the chain and move it on the core surface. During the simulation a number of physical quantities was sampled such as the scattering contributions corresponding to the inter-chain scattering F, the inter-chain scattering H, and the corona form factor amplitude A_{cor}. We also sampled the single chain radius of gyration, the mean chain center-of-mass distance from the core, and the radial monomer profile.

5.2 Models of Chains Molecules

Polymers are string-like molecules consisting of many identical monomers bound by covalent bonds. The bonds between individual monomers have a certain torsional potentials, and the monomers can have side groups, which gives rise to local steric hindrance for rotations. These local interactions gives rise to a certain stiffness on length scales comparable to the monomer length scale [54]. We model a polymer chain by $n + 1$ vertices linked by n segments of length l_0. The angle between subsequent segments is fixed at a constant value θ, while the

dihedral angle w_i can take any value in the interval $[-\pi;\pi]$ for any segment, where $w_i = 0$ corresponds to a trans-configuration. This semi-flexible model provides a good meso-scopic description of polymers using an effective segment length and angle [91, 92].

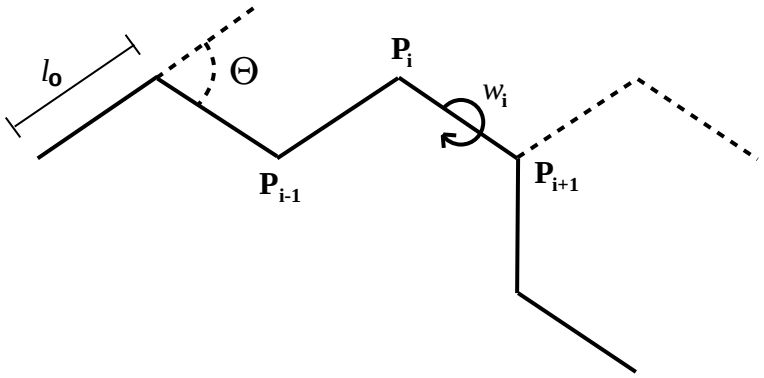

Figure 5.1: Illustration of a semi-flexible chain in trans-configuration, the tail of the chain has been pivoted 180° about the i'th segment.

A valence angle of $\theta = 44.4153^o$ was chosen, such that the Kuhn length $b = 6l_0$. In the long chain limit the radius of gyration of a flexible chain and semi-flexible chain coincide. The freely rotation chain model can be regarded as a discrete version of the continuous Kratky-Porod chain model, which is reached in the limit $L \to \infty$, $l_0 \to 0$, $\theta \to 0$ for fixed L/b.

Excluded volume interactions was simulated by placing hard spheres with radius ϵ at each vertex. The radius was chosen such that $\epsilon/b = 0.1$, which is known to reproduce the binary cluster integral of polystyrene in a good solvent [93].

5.3 Creating a chain

Defining the i'th segment vector by $\mathbf{r}_i = \mathbf{P}_{i+1} - \mathbf{P}_i$ where $\mathbf{P}_i$ is the position of the i'th vertex. We assume that the foot vertex $\mathbf{P}_1$ is given, along with the direction $\mathbf{r}_1$. To define a coordinate system, we need two vectors. We choose a random vector $\mathbf{R}$ not parallel to $\mathbf{r}_1$ is chosen. Then a vector orthogonal to $\mathbf{r}_1$ is constructed by

$$\mathbf{r}_\perp = \mathbf{R} - \left(\frac{\mathbf{R}\cdot\mathbf{r}_1}{|\mathbf{R}||\mathbf{r}_1|}\right)\mathbf{r}_1.$$

A fictitious zeroth segment vector can constructed using the orthogonal vector by

$$\mathbf{r}_0 = -l_0\cos\theta\frac{\mathbf{r}_1}{|\mathbf{r}_1|} + l_0\sin\theta\frac{\mathbf{r}_\perp}{|\mathbf{r}_\perp|}. \tag{5.1}$$

The zeroth and first segment vectors define a coordinate system from which all subsequent segments can be added, and the fictitious zeroth segment makes it possible to uniquely define the dihedral angle of the first segment. In general given the $i-2$ and $i-1$ segments the i'th segment can be constructed with

a specified segment length l_0, segment angle θ, and dihedral angle w_{i-1} of the previous segment as follows: Define two auxiliary vectors

$$\mathbf{n}_1 = \mathbf{r}_{i-2} \times \mathbf{r}_{i-1} \quad \text{and} \quad \mathbf{n}_2 = \mathbf{r}_{i-1} \times \mathbf{n}_1.$$

$\mathbf{n}_1$ is orthogonal to the plane spanned by the two segment vectors, while $\mathbf{n}_2$ lies within the plane, and points in the direction of a trans configuration. The three vectors $\{\mathbf{r}_{i-1}, \mathbf{n}_1, \mathbf{n}_2\}$ defines an orthogonal coordinate system. In this coordinate system the i'th segment can be constructed such that the previous segment has a torsion angle ω_{i-1} by

$$\mathbf{r}_i = -l_0 \cos\theta \frac{\mathbf{r}_{i-1}}{|\mathbf{r}_{i-1}|} + l_0 \sin\theta \left(\cos(\omega_{i-1}) \frac{\mathbf{n}_2}{|\mathbf{n}_2|} + \sin(\omega_{i-1}) \frac{\mathbf{n}_1}{|\mathbf{n}_1|} \right). \tag{5.2}$$

Here the dihedral angle is zero in the trans state, and the sign of the dihedral angle is defined in a right handed manner. Any chain configuration is completely specified by the knowledge of $\mathbf{r}_0$, $\mathbf{r}_1$, the fixed segment length and angle, and a table of dihedral angles w_i for $i \in \{1, \ldots, n-1\}$, while the chain position in space is given by the knowledge of any vertex for instance the foot vertex $\mathbf{P}_1$, which is fixed on the micelle surface.

This representation in terms of generalised coordinates suggests that an MD simulation based on propagating the system using the Euler-Lagrange equation [94] would be more effective than using Newtons second law and enforcing the constraints through a rattle or shake algorithm [95]. A hybrid MD/MC algorithm has been proposed that uses a generalised coordinates representation of a chain[96]. We have used a simple coordinate representation of all vertices as this facilitates the overlap check between different chains, and it is a natural choice when sampling the micellar scattering.

5.4 Creating a micelle

A micelle consists of a core and a number of tethered chains. The tethered chains are excluded from the core and are not allowed to overlap. Chains are grown simultaneously rather than by adding a single chain at a time. First all chain roots $(\mathbf{P}_0, \mathbf{P}_1, \mathbf{P}_2)$ are generated until all chains have a root. During this phase the $\mathbf{P}_1$ and $\mathbf{P}_2$ vertices are checked for overlap with other roots, and the second vertex $\mathbf{P}_2$ is checked for overlap with the core. If an overlap is detected the root is relocated. No checks are made for the zeroth segment as this is not a physical segment.

Chain construction starts when all roots have been placed and does not overlap. Chains are grown by adding a segment to the shortest chain until all chains have the required number of segments. Everytime a segment is added the end vertex is checked for overlap with all other chains. If an overlap is detected, the last 20 segments are removed. If this includes the root, then the root is relocated. During chain creation the dihedral angle is restricted to $[-60°; 60°]$ as this stretches the chains somewhat, and thus reduces the crowding at the surface. Chains are flexible enough, that they can be regrown around other chains after an overlap. While this procedure ensures that the initial micelle does not

overlap, it produces a strongly biased initial configuration. The configuration is equilibrated by performing MC steps until on average 200 moves per degree of freedom have been accepted. The equilibration was monitored by sampling the acceptance rate, which decays rapidly and stabilises when the corona reaches equilibrium. The equilibration was also monitored by sampling the radius of gyration and average chain center-of-mass distance from the core. These quantities are also seen to stabilise at the equilibrium values before the actual sampling starts. During the equilibration phase the acceptance and rejection frequency of the three MC moves was monitored, and the excursion of the moves was adjusted to obtain approximately 50% acceptance rate for the three moves.

The probability of choosing a move was chosen to be proportional to the number of degrees of freedom that is changed by an accepted move, and the number of degrees of freedom of the micellar corona. Thus an accepted surface move will modify two degrees of freedom, either two surface coordinates or two orientation angles. The pivot move (see next section) changes one degree of freedom, a single dihedral angle. The probabilities for the different types of moves was chosen as $P(\text{Surface rotation}) = P(\text{Surface translation}) \propto 2N$ and $P(\text{Pivot}) \propto (n-1)N$ where n is the number of segments, and N is the number of chains in the corona.

5.5 Pivot move

Numerous moves have previously been proposed for sampling the configuration space of an isolated chain both on a lattice and off-lattice. Some examples are reptation moves, concerted rotation moves, and biased moves such as chain removal and regrowth of the Rosenbluth type [97, 98, 99]. However, pivots moves used in the present work allows the semi-flexibility of the chains to be taken directly into account.

Pivot moves was originally introduced for chains on a lattice [100, 101]. A random site on the chain was chosen and the shortest half of the chain was transformed with an element from of the lattice symmetry group. This leads to a very large configurational change, however, the probability for overlap is considerable, and as a result many attempted moves are rejected, on the other hand when a move is accepted, it has a major effect on the chain configuration. Madras and Sokal have shown that the pivot algorithm is ergodic, and that it is the most effective move known for sampling self-avoiding random walks on a lattice [61, 101].

The idea of the lattice pivot move can easily be generalised to off-lattice semi-flexible chains [102]. For a chain in a micellar corona, a pivot move is performed by pivoting the tail of a chain around randomly chosen segment, as only the tail can be rotated due to the fact that the head of the chain is always tethered to the core surface. The result is that while only a single dihedral angle is changed, the chain configuration is very different, and after a few percent of the segments have been pivoted an essentially new configuration is reached.

Pivoting the chain about a segment i with an angle ϕ is done by transforming all vertices P_j for $j \in \{i+2, \ldots, n\}$ according to

$$\mathbf{P}_j^{new} = \widetilde{Q}(\phi, \mathbf{P}_{i+1} - \mathbf{P}_i)(\mathbf{P}_j - \mathbf{P}_i) + \mathbf{P}_i.$$

The transformation matrix that performs a rotation ϕ around a direction given by the i'th segment is given by $\widetilde{Q}(\phi, \mathbf{r}) = U(\mathbf{r})^{-1} R_x(\phi) U(\mathbf{r})$, where $R_x(\phi)$ is a rotation matrix about the x axis, and $U(\mathbf{r})$ is the matrix of directional cosines, that relates the coordinate system with the x axis along the i'th segment to the lab frame. The directional cosines are given by

$$a_{11} = \frac{\mathbf{r}}{|\mathbf{r}|} \cdot e_x \quad a_{12} = \frac{\mathbf{r}}{|\mathbf{r}|} \cdot e_y \quad \text{and} \quad a_{13} = \frac{\mathbf{r}}{|\mathbf{r}|} \cdot e_z, \tag{5.3}$$

where e_x, e_y, and e_z are the unit vectors defining the x, y and z axis in the laboratory frame. The Matrix Q can be written [102]

$$\widetilde{Q} = S + A, \tag{5.4}$$

where the symmetric term is (denoting $\gamma = \cos\phi$)

$$S = \begin{pmatrix} a_{11}^2 + (1 - a_{11}^2)\gamma & a_{11}a_{12}(1-\gamma) & a_{11}a_{13}(1-\gamma) \\ a_{11}a_{12}(1-\gamma) & a_{12}^2 + (1 - a_{12}^2)\gamma & a_{12}a_{13}(1-\gamma) \\ a_{11}a_{13}(1-\gamma) & a_{12}a_{13}(1-\gamma) & a_{13}^2 + (1 - a_{13}^2)\gamma \end{pmatrix}, \tag{5.5}$$

and the antisymmetric term (denoting $\delta = \sin\phi$)

$$A = \begin{pmatrix} 0 & a_{13}\delta & -a_{12}\delta \\ -a_{13}\delta & 0 & a_{11}\delta \\ a_{12}\delta & -a_{11}\delta & 0 \end{pmatrix}. \tag{5.6}$$

In a polar representation of the chain the rotation is equivalent to $\omega_i = \omega_i + \phi$.

5.6 Surface moves

Two moves are required to move a chain, one reorientates the chain and another moves the chain foot point on the surface of core. The chain can be regarded as a rigid object where the zeroth segment is transformed as the rest of the chain. This ensures that the torsional angle of the first segment stays constant during surface moves. The reorientation move is made by pivoting the chain an random angle ϕ about the foot vertex around a random direction $\mathbf{r}$ as

$$\mathbf{P}_j^{new} = \widetilde{Q}(\phi, \mathbf{r})(\mathbf{P}_j - \mathbf{P}_1) + \mathbf{P}_1 \quad \text{for} \quad j \in \{0, \ldots, n\}.$$

For the special case of a spherical core the surface moves can be performed without the need for introducing a surface coordinate system. The surface move is performed by pivoting the entire chain about the core center around a random direction. Assuming that the center of the core is located at the origin, this move is given by

$$\mathbf{P}_j^{new} = \widetilde{Q}(\phi, \mathbf{r})\mathbf{P}_j.$$

However, general moves on a non-spherical core surfaces requires the introduction of a surface coordinate system and knowledge of the Jacobian, as moves are required to produce an uniform sampling of the micellar core surface.

For a class of core geometries the surface move can be vastly simplified by noting that the mapping from core surface onto the inscribed cylinder is area preserving. This is true for spherical cores and hemispherical end-capped cylinders. Thus a surface move can be regarded as a projection onto the inscribed cylinder, a move on the inscribed cylinder surface, and a projection back on the core surface. This defines a chain translation that moves the foot point to another position on the core surface. The problem of performing a surface move, that performs an uniform sampling of a complex surface, has then been reduced to the simple problem of making an uniform sampling from a cylinder surface.

A move on a cylinder surface can be composed of a rotation around the axis of the cylinder, and a step along the axis cylinder. If the step ends up above or below the cylinder it can be reflected back on the opposite side of the cylinder. The projection of such a move corresponds to a move that translates a chain to the opposite side of the north or south pole on the core surface.

5.7 Overlap

After a MC move the configuration must be checked for overlap. Three different types of overlap can occur; chain overlap with itself, chain overlap with another chain, and chain overlap with the core. Core overlap of a vertex (x, y, z) for a general rotationally summetric core shape can be checked by $x^2 + y^2 < R^2(z)$ where $R(z)$ a the core cross section at height z, which for a sphere is

$$R_{sphere}(z) = \sqrt{R_{co}^2 - z^2}.$$

Chain-chain overlap is done using the "zippering" algorithm [103]. Consider a situation where one vertex on one chain is being checked for overlap against any vertex on another chain. If the direct distance between the two vertices is d, and if the maximum direct distance between two vertices at the ends of an n segment long segment is $D(n)$, then the next vertex that has a possibility for overlap is located $\max\{n > 0 | d - D(n) - 2\epsilon > 0\}$ segments along the chain, where the direct end-to-end length of n chain segments is given by

$$D(n) = \begin{cases} l_0 \cos(\frac{\theta}{2})n & \text{semi-flexible} \\ l_0 n & \text{flexible} \end{cases}.$$

A naive algorithm for checking for overlaps within the same chain requires $O(n^2)$ checks, but the Zippering algorithm requires only about $n^{1.2}$ [103], which vastly reduces the number of distance comparisons necessary to check a number of chains for overlap. When checking for overlap between two vertices on the

same chain, a certain number of neighbour vertices are excluded from the comparison, to avoid introducing rigidity. When the hard-sphere radius ϵ is larger than the segment length, a number of neighbouring vertices will always be within the hard sphere, and the volume available to vertices just outside an excluded volume sphere is limited. The number of neighbours segments is chosen to allow the chain to perform a 180° degree turn with radius ϵ [91].

5.8 Sampling scattering

The scattering contributions could be sampled by sampling the configurationally averaged pair-distance distribution $4\pi R_k^2 P(R_k)$ for the k'th bin at radius R_k. Then calculating the scattering as

$$F(q) \approx \sum_k \Delta R_k 4\pi R_k^2 \frac{\sin(qR_k)}{qR_k} P(R_k),$$

where ΔR_k is the width of the k'th bin. However, this is not a very effective method, as it requires $O(N^2)$ operations per sample, where N is the number of chain vertices. A better option would be to sample the configurational average of the scattering given by $F(q) = \left\langle \sum_{i,j} \sin(qr_{ij})/(qr_{ij}) \right\rangle$ for all the distances r_{ij} between vertices i and j. This procedure requires $O(N^2 M)$ operations per sample, where M is the number of q values that are sampled. The scattering can also be obtained as

$$F(q) = \left\langle \left| \sum_j^N e^{-i\mathbf{q}\cdot\mathbf{R}_j^\alpha} \right|^2 \right\rangle_{\alpha o},$$

here both an orientational and configurational average are to be performed. And the orientational average has to be performed "by hand" i.e. by sampling the scattering along D different $\mathbf{q}$ directions. This requires $O(NDM)$ evaluations of a complex exponential function. The major difficult is how to evaluate the exponentials efficiently.

Frenkel et al. [104] have suggested to use $\mathbf{q}_{lkm} = \left(\frac{2\pi l}{L}, \frac{2\pi k}{L}, \frac{2\pi m}{L}\right)$ where L is the longest length scale that is interesting. As all $\mathbf{q}$ vectors are located on a cubic lattice, the exponentials can be calculated using Fast Fourier Transforms (FFT), which is a very efficient method for calculating exponentials on the form $\exp(i\alpha n)$ by exploiting recursive relations between different integers n. However, by virtue of the lattice the number of q vectors required by the FFT technique to sample scattering from q_{min} to q_{max} is $D = q_{max}/q_{min}$. This shows that if four decades of q values are to be sampled 10^4 FFT samples have to be performed, and most of these will be at high q values.

Inspired by the FFT technique, we have chosen a hybrid approach to calculating a few of the complex exponentials directly, and using symmetry properties to derive the rest. The goal is to locate q_n $n \in \{1, \ldots, M\}$ values approximately equidistant on a logarithmic scale between q_{min} and q_{max}.

The ideal distribution is

$$q_n^o = 10^{(\log q_{max} - \log q_{min})\frac{n}{M} + \log q_{min}}. \tag{5.7}$$

By tweaking the choice of q_n values slightly we can optimise the evaluation of the scattering contribution from the j'th vertex to the q_n'th scattering value along the q_e direction. Our goal is to evaluate

$$e^{-iq_n \mathbf{q}_e \mathbf{r}_j^\alpha} = e^{-i\gamma q_n} \quad \text{where} \quad \gamma = \mathbf{q}_e \cdot \mathbf{r}_j,$$

for all M values of q_n for all vertices, and for D different directions $\mathbf{q}_e$ to obtain the orientational average.

In the following we will concentrate on calculating the complex value of $\exp(-i\gamma q_n)$ in the case where $\exp(-i\gamma q_m)$ has already been calculated for all $m < n$. If q_m exists such that $q_n = 2q_m$ then $\exp(-i\gamma q_n) = \exp(-i\gamma q_m)^2$ (the double angle formula). Since we have previously evaluated $\exp(-i\gamma q_m)$, we only need to square that number. If q_m, q_p exists such that $q_n = q_m + q_p$ then $\exp(-i\alpha q_n) = \exp(-i\gamma q_m)\exp(-i\gamma q_p)$ (the addition formula). Since both exponentials have previously been evaluated, we only need to calculate the product of two known complex numbers. Thus by an advantageous choice of the q_n values, we can use symmetry properties of the exponentials to convert them into simple products of known complex numbers. The higher order symmetry properties require more algebraic operations, and do not provide a significant optimisation.

The actual distribution of q_n's are chosen as to minimise

$$E[q_1, \ldots, q_M] = k\left(\frac{M}{\ln(10)\,(\log q_{max} - \log q_{min})}\right)^2 \sum_{i=1}^{M} \frac{(q_i - q_i^0)^2}{(q_i^0)^2} \quad (5.8)$$

$$+\beta N_{calc} + \gamma N_{add} + \delta N_{double}, \quad (5.9)$$

where N_{calc},N_{add}, and N_{double} is the number of exponentials that require direct evaluation, or can be deduced using the addition formulae, or formulae for the double angle, respectively. Thus $M \equiv N_{calc} + N_{add} + N_{double}$. The weights β, γ, and δ are chosen to represent the duration of the respective numerical operation, and we have used $\beta = 1$ and $\gamma = \delta = 0.1$. The first term is a harmonic term, that determines how large deviations from a perfect logarithmic distribution should be allowed in order to speed up the evaluation. Since the distribution is on a logarithmic scale, we have to divide by the local length scale, which is given by the parenthesis and the denominator. The constant k should be chosen so small that the ordering $q_m < q_n$ when $m < n$ is ensured. We have used $k = 0.01$. This penalty functional is easily minimised by a simulated annealing quench with moves that shift q_n's, which require trigonometric evaluations into q_n's, that can be evaluated by simple algebraic operations on known numbers. If M is huge, care must be taken to avoid truncation errors in the evaluation. In our implementation only about 10% of the complex exponentials need to be evaluated directly.

5.9 Correction of positions

The repeated application of pivoting moves introduce numerical errors in the vertex positions, and as a result chains are periodically reconstructed using

the chain construction algorithm based on tabulated dihedral angles, which are updated after each accepted pivot move. The entire chain is also translated so the foot vertex is on the core surface, this avoids diffusive behaviour of chains away from the code surface due to truncation errors due to the repeated application of surface moves. The constructive chain correction algorithm is far more efficient than the iterative correction algorithm of Stellman and Gans[102]. While chain construction requires few evaluations per segment, the correction algorithm of Stellman and Gans requires the solution of a possible singular or ill-conditioned 3x3 matrix equation per segment.

After all the chains on a micelle have been corrected, the micellar corona is checked for any correction induced overlaps, and equilibrated until these have reached a state without overlap. However, this is very unlikely and has never been observed in practice. The maximal deviations of segment length, valence angle, and dihedral angle were monitored during the simulations, and found to be below 10^{-12}.

5.10 A practical remark

The simulator has been implemented in C++ [105]. C++ supports the Object Oriented Programming paradigm, which emphases code reuse, and the isolation of functionality in different modules with well defined interfaces. The simulator was implemented using a number of objects that provides different types of functionality.

Four objects was required for the micelle simulator. An object represented a single chain, and functionality such as pivot moves and chain corrections, another object represented the core, and implemented functionality for the core geometry, checking for core overlap, and foot vertex generation. A micelle object inherited the properties of an array of chain objects and a core object, and a MC object inherits all the properties of a micelle, and adds functions for sampling data and the basic MC algorithm.

The Monte Carlo algorithm only needs to know about the energy of configuration and when to sample and save data. A micelle consists of a core and some chains. But the micelle object does not need to know the core geometry nor how chains configurations are represented. However, the micelle object has to supply a neighbour move and a function that can calculate the energy to the Monte Carlo algorithm, and supply some way of creating a micelle. The chain object contains information about the chain configuration, the pivoting algorithm, and chain correction. The core object contains information about the core geometry, and routines for performing surface moves, creating foot vertices, and checking for vertex core overlaps. Thus when the Monte Carlo algorithm wants to select a new neighbour state, it calls a neighbour function supplied by the micelle object, this function selects if it should be a chain pivot move or a surface move. Pivots moves are performed by selecting an angle and a chain, and calling the pivot function supplied by that chain object. Surface moves are performed by randomly selecting a chain and calling a function in the core object that supplies a vector. This vector translates the foot vertex of the chain to another point on

the core surface, and the actual translation is performed by a function in the chain object.

Strict adherence to an object oriented approach allows a clean separation of functionality into different objects. This has an enormous advantage. If, for instance, a new core geometry has to be implemented, only the core object needs to be modified. If the micelle corona consists of chains of different length only the micelle object needs to be modified. Object Oriented Programming makes it very easy to modify the simulation code.

5.11 Possible improvements

5.11.1 Overlap checks

The overlap check use the zippering algorithm when testing for overlap between two different chains say chain A and B. Currently, this is implemented by comparing all vertices on chain A by zippering along the vertices of chain B. However, as the positions of each vertex, that is checked during the overlap check, is known, it is possible for a vertex on chain A and pair of vertices on chain B to calculate the closest possible separation between the intervening chain segment and the vertex on chain A. And the minimal separation distance between any site on chain B can be used as the contour length of the step along chain A. This double zippering algorithm would probably lead to a significant increase of efficiency of the overlap check for many chain systems especially for long chains.

5.11.2 Reptation

The pivoting algorithm would have a low acceptance rate for coronas with very large surface coverages, if the maximum excursion of the pivot angle was not dynamically adjusted during the equilibration phase to yield a 50% acceptance rate, the reason being that a small rotation about a segment close to the core can yield a very large excursion at the end of the chain. Reptation moves works by cutting the head off a chain and gluing it to the tail of the chain, that way chains can "reptate" through the voids between other chains. Reptation moves are very efficient for sampling configurations in polymer solutions at high concentrations. A naive reptation move in a micellar corona could be performed by cutting the head/tail of a chain, gluing it to the tail/head, and translating the new chain head such that it touched the micellar surface. Since the head environment is different from the tail environment the criterion of microscopic reversibility will not be fulfilled as head to tail moves will be accepted with a larger probability than tail to head moves. However, by cutting the tail of one chain and the head of another chain, and cross transplanting the head to the tail of the other chain, and tail to the head of the first chain, and then translating the two chains such that they are still tethered to the chain a reptation move is made that is probably microscopic reversible as the operation is completely head/tail symmetric. However, it remains to be seen whether such a move can be formulated for semi-flexible chains.

Chapter 6

Summary of articles

Small-angle scattering is an ideal technique for obtaining information about macro-molecular structures such as block copolymer micelles, however, expressions for form factors and structure factors are required for a reliable interpretation of the scattering data obtained from scattering experiments. The topic of the first three articles is the formulation of an expression for the form factor of a micelle with a spherical core. The main difficulty is howto include the effects of excluded volume interactions on the corona form factor. The fourth paper introduces a general formalism for the form and structure factors of general polymer structures, such as star polymers with arms of block copolymers, and micelles with arbitrary core geometries. In the formalism it is assumed that the different subunits do not interact with each other, however, a method of how to include excluded volume effects at the level of a linear polymer is presented.

A diblock copolymer micelle consists of a dense core surrounded by the dissolved chains forming a diffuse corona. The structure of the micellar corona depends on the contour length of the tethered chains L, the number of chains N, and on the core radius R_{co}. From these three quantities three dimensionless numbers can be derived that quantify the structure of the micellar corona: N the number of chains, $\eta = R_g/R_{co}$ the effect of surface curvature on the corona structure, and σ the reduced surface coverage. The reduced surface coverage is defined as $\sigma = N\pi R_{go}^2/[4\pi(R_{co} + R_{go})^2]$, here R_{go} is the unperturbed radius of gyration, as opposed to R_g, which is the actual radius of gyration. In the expression it was assumed that the center-of-mass of a chain is displaced by approximately a distance R_{go} from the core surface. As a result, the effective core area is $4\pi(R_{co} + R_{go})^2$, and the cross sectional area of the chains is πR_{go}^2 .

The quantity σ is expected to be the corona analog of the reduced concentration $c/c^* = 4\pi R_{go}^3\rho_m/3$, where ρ_m is the number density of polymers. For a polymer solution $c/c^* \ll 1$ signifies a dilute solution. In which polymers behave as a gas of hard spheres with radius R_g. The configuration of chains depend only on the chain entropy, which favours random-walk configurations, and interactions within the same chain. Entanglement between different polymers are energetically unfavourable as it reduces the configurational degrees of freedom, i.e. the entropy. For $c/c^* \gg 1$ (and still not a melt) the solution is in the semi-dilute regime, which is particular to chain molecules and is charac-

terised by the entanglement of chains. Thus a semi-dilute solution of polymers consists of a transient network of intermeshed chains. The characteristic size of a dilute solution, the radius of gyration, is replaced by the correlation length ξ. In a semi-dilute network a single chain can interact with many neighbouring chains, and the correlation length is the length scale on which connectivity information persists [21]. On length scales smaller than the correlation length interactions are predominantly excluded volume interactions between sites on the same chain, and above the correlation length no information about chain connectivity persists.

The corona of a micelle consists of polymers, but these are tethered by one end to the micellar core, and if the micellar core is crystalline or glassy the tethering points will be fixed on the core surface. For $\sigma \ll 1$ chains in the corona are far from each other, and interactions between different chains are rare. As a result excluded volume interactions between sites on the same chain and core expulsion influence the configuration, and the corona will be in the mushroom regime. This is similar to the situation of a dilute polymer solution where $c/c^* \ll 1$. For $\sigma \gg 1$ the chains form a polymeric brush where chains are strongly stretched away from the surface, i.e. the corona will be in the brush regime. No analogy exists for an ordinary polymer solution, as the ordering is induced by the presence of a surface. A broad crossover exists between dilute and semi-dilute solute behaviour, and a similar broad crossover exists between the mushroom and brush regimes.

It was shown in the theory chapter that the normalised scattering $[F_{micelle}(q = 0) = 1]$ for a micelle with a spherical core is given by

$$F_{micelle}(q) = (\beta_{ch} + \beta_{co})^{-2} \left(\beta_{ch}^2 F_{cor} + \beta_{co}^2 \Phi^2 + 2\beta_{ch}\beta_{co} A_{cor}\Phi\right). \tag{6.1}$$

$F_{cor}(q)$ is the corona form factor, $\Phi^2(q)$ the core form factor, $A_{cor}(q)\Phi(q)$ is a corona-core interference function, and β_{ch} and β_{co} is the total excess scattering lengths of the corona and core, respectively. As the core is assumed to be spherical and homogeneous the form factor amplitude is $\Phi(qR_{co}) = 3[\sin(qR_{co}) - qR_{co}\cos(qR_{co})]/(qR_{co})^3$ [78]. The core form factor contains information about the core radius, however, this information is also present in the corona form factor amplitude $A_{cor}(q)$, and as a result the three first papers focus on the corona form factor and form factor amplitude.

In the theory section it was shown that the correlations of a polymer solution can be separated into intra-chain correlations and inter-chain correlations. An analogous separation can be performed on the corona form factor, and as shown in the theory section, this yields the corona form factor expressed through the intra-chain scattering F_c and inter-chain scattering H weighted as

$$F_{cor}(q) = \frac{1}{N}F_c + \frac{N-1}{N}H. \tag{6.2}$$

The characteristic length scale of intra-chain correlations is comparable to the radius of gyration, which is typically smaller than the inter-chain correlations. The characteristic length scale of inter-chain correlations is comparable

with the radius of the core. Typically the intra-chain scattering contribution will dominate at large q values, while the inter chain scattering contribution will dominate at low q values, due to the different characteristic scales of the correlations.

The corona form factor can also be separated into the contributions from configurationally averaged density and from density fluctuation correlations. The scattering contribution due to the average density is the corona form factor amplitude $A_{cor}(q) = \int_0^\infty \mathrm{d}r 4\pi r^2 \frac{\sin(qr)}{qr}\rho(r)$, where $\rho(r)$ denotes the radial profile of the corona. The scattering contribution due to density fluctuation correlations is denoted $F_{fluc}(q)$. Using this separation, the scattering corona scattering can be expressed as

$$F_{sol.prof}(q) = \frac{1}{N}F_{fluc} + \frac{N - F_{fluc}(q=0)}{N}A_{cor}^2. \tag{6.3}$$

Here the first term is denoted fluctuation scattering, while the second is denoted profile scattering as it only depends on the radial profile. The peculiar weighting between the two terms is due to the fact that the fluctuation scattering is not normalised in the forward direction. Provided an exact expression for the scattering due to density fluctuations $F_{sol.prof}(q) \equiv F_{cor}(q)$. However, at present no analytical expression is available for the fluctuation scattering contribution in the case of micellar corona, and as a result it has been approximated by an RPA expression $F_{fluc}(q) = F_c(q)/[1 + \nu F_c(q)]$, which describe the fluctuation scattering of a dilute/semi-dilute polymer solution. The excluded volume parameter ν is related to the apparent second virial coefficient of the solution as $\nu = 2A_2(\sigma)\sigma$. The expression $F_{sol.prof}(q)$ has the interpretation of the scattering one would expect from a dilute/semi-dilute polymer solution with a radial monomer profile $\rho(r)$, and it is denoted solution profile scattering.

The fluctuation scattering will dominate the scattering at large q values, as density fluctuations correlations are expected to be short ranged, while the profile scattering will dominate at small q values. All the contributions to the corona scattering are shown in figure 6.1. The profile scattering ($\propto A_{cor}^2$), and the inter-chain scattering $H(q)$ dominates at small q values, but they are rapidly decaying functions. The intra-chain/fluctuation scattering contribution dominates at high q values as expected. The inter-chain scattering oscillates about zero, the absolute value is plotted and each sign change leads to an inverted peak. The corona form factor is the sum of intra-chain and inter-chain scattering, and as a result the minima/maxima of the corona form factor correspond to minima/maxima of the inter-chain scattering. The minima/maxima of the corona form factor correspond to minima/maxima of the profile scattering, and the height of the minima can be seen to be given by the fluctuation scattering

Single chain properties such as radius of gyration, the chain length, and the Kuhn length can be obtained from the intra-chain scattering $F_c(q)$. The Hausdorff dimension d_H of the chains can also be determined, and carry information about the chain connectivity statistics. The interpretation of the inter-chain scattering $H(q)$ is more difficult, as it has a very complex q dependence, but it depends on the corona profile, as well as interactions between different chains which introduce a "correlation hole" [20, 21]. The profile scattering contribution

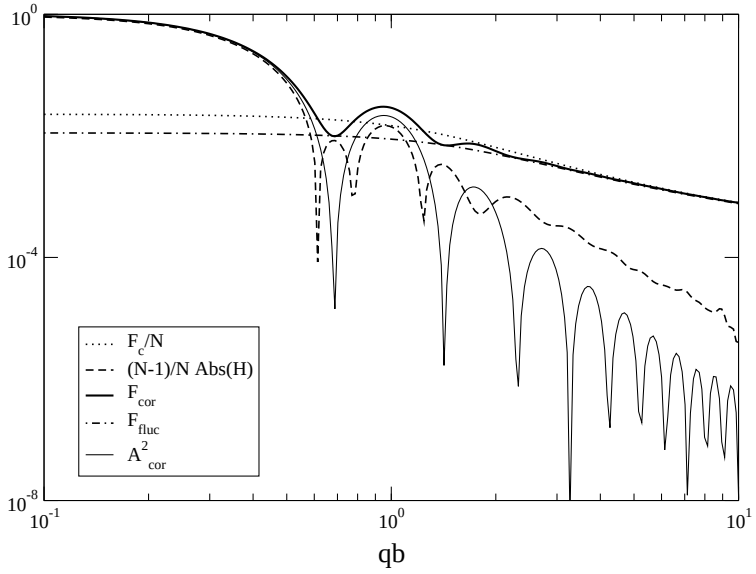

Figure 6.1: The contributions to the corona form factor appropriately scaled for the standard micelle $N = 44$, $L = 8.33b$ and $R_{co} = 3.33b$.

($\propto A_{cor}(q)^2$) is simply the scattering one would obtain from a core-shell model of the corona, and it only depends on the radial profile, hence the radial profile can be obtained from this term. The fluctuation scattering is caused by chain connectivity, chain-chain interactions, and core expulsion, and carries thermodynamic information such as the osmotic compressibility and apparent second virial coefficient of the corona.

A comparison of eq. (6.2) and eq. (6.3) shows that the scattering due to interaction-induced correlations between different chains have been shifted from the inter-chain scattering contribution into the intra-chain scattering, thus producing the fluctuation scattering term, while leaving the profile scattering contribution.

6.1 Article I

The intra-chain, inter-chain, and form factor amplitude (F_c, H, and A_{cor}, respectively) scattering contributions can be obtained directly from computer simulations of the micellar corona as shown in the chapter on Monte Carlo (MC) simulations. Computer simulations allow the partial scattering contributions, as well as the single chain radius of gyration, and the radial profile $\rho(r)$ to be systematically investigated as function of the parameters chain length, number of chains, and core radius denoted L, N, and R_{co}, respectively. Simulations can also be performed with and without excluded volume interactions for different models of chains, such as flexible and semi-flexible chains. A standard micelle

was chosen having $N = 44, L = 8.33b$, and $R_{co} = 3.33b$, where the Kuhn length b is used as length scale. Each of these three parameters was varied in turn, while keeping the remaining two fixed at their reference values. The range of variation was chosen to correspond to a range of σ values from 0.01 to about five. The radius of gyration directly depends on the chain length, but it has only an indirect dependence on the number of chains or the core radius due to the effects of chain stretching. The surface curvature $\eta = R_g(L)/R_{co}$ is essentially fixed when the number of chains is varied, as chain stretching is negligible in the simulated range.

Article I contains a qualitative discussion on how the corona form factor and form factor amplitude depend on these three parameters with and without excluded volume interactions. From the MC simulations it is seen that intra-chain scattering is a slowly decaying non-oscillatory function, while both the inter-chain scattering and corona form factor amplitude are rapidly decaying and oscillating functions. Varying the number of chains has a large impact on the corona form factor, as oscillations become apparent as the number of chains is increased. This is caused by the number of chains dependent weighting between the oscillatory intra-chain scattering contribution and the non-oscillating single chain contribution. However, the phase of the oscillations of the corona form factor and form factor amplitude is essentially unchanged, when varying the number of chains. This is consistent with the observation that the corona width is essentially unchanged, when the number of chains is varied.

Increasing the chain length simultaneously increases the width of the corona, i.e. shifts the corona away from the core center, this results in a shift towards smaller q values of the corona form factor amplitude oscillations. Decreasing the core radius shifts the corona closer to the core, and a corresponding shift of the form factor amplitude oscillations towards larger q values are observed. This behaviour of the oscillations can be understood by the definition of the corona form factor amplitude as the Fourier transform of the radial profile. It is also apparent that the oscillations of the corona form factor are reduced as the surface coverage is increased. This is a curvature effect that occurs when $\eta \simeq 1$.

Figure 6.2 shows the scaled contributions to the corona form factor from the intra-chain and inter-chain scattering, and it is apparent that the oscillatory behaviour is replace by a negative power law-like behaviour, while a single secondary peak remains for simulations with a large number of chains. A broadening of the second secondary peak of the form factor amplitude is observed for micelles with a large number of chains attached, while a broadening of the first secondary peak is observed for micelles with large core radius or long chains. This broadening is probably due to the different profile shapes obtained for a large number of chains or a large curvature η.

Article I also compares the corona form factor and form factor amplitude from simulation with and without excluded volume interactions but with core expulsion. For simulations without interactions the inter-chain scattering is related to the corona form factor amplitude as $H(q) = A_{cor}(q)^2$. For low surface coverages no difference is observed between simulations with and without excluded volume interactions as expected, however, at high surface coverages a

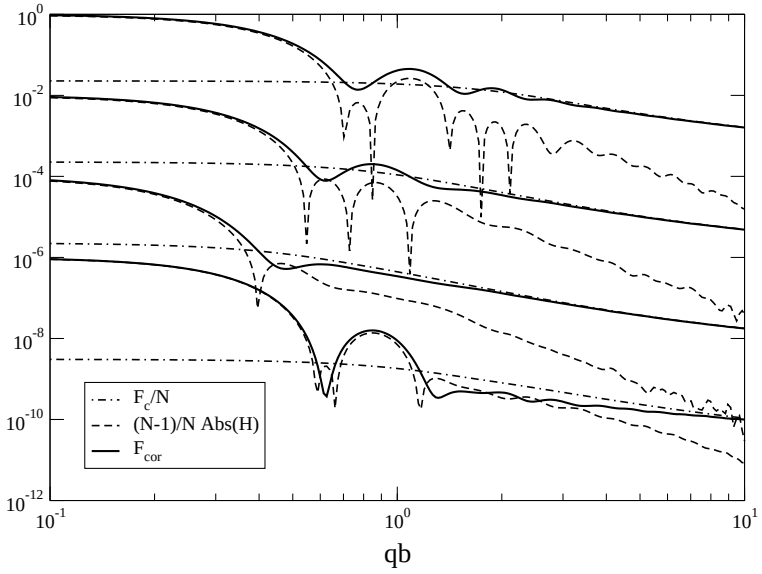

Figure 6.2: Scaled F_c and H contributions to F_{cor} for simulations varying chain length $L = 4b$,13.67b and 38.17b (from top to bottom), the simulation with $N = 327$ is shown for comparison. The inter-chain scattering H changes sign and the absolute value is plotted, and each inverted peak corresponds to a sign change, and the powerlaw tail has a negative sign.

clear decrease in the corona form factor can be seen for simulations with interactions. A shift of the form factor amplitude oscillations towards smaller q values is observed for simulations with excluded volume interactions compared to simulations without excluded volume interactions for large surface coverages. This is consistent with a stretching of the corona away from the core due to excluded interactions. As the chain length of the standard configuration is short, no excluded volume effects are observed on the intra-chain scattering except for the longest chains where a different power law behaviour are observed at high q values for the corona form factor, where the intra-chain scattering dominates. This is caused by the excluded volume interactions modifying the $(qR_g)^{-d_H}$ behaviour from $d_H = 2$ consistent with a random walk to $d_H = 1.70$ consistent with an excluded volume chain.

The model due to Pedersen and Gerstenberg [106, 107] provides expressions for F_c, S_{cc}, and A_{cor} as

$$F_c(q, Rg) = F_{Debye}(qR_g),$$

$$A_{cor}(q) = \frac{\sin[q(R_{co} + dR_g)]}{q(R_{co} + dR_g)} A_c(qR_g),$$

and

$$H(q) = A_{cor}^2(q).$$

Here the form factor amplitude of a flexible non-interacting chain is $A_c(qR_g) = [\exp(-x) - 1]/x$ with the abbreviation $x = (qR_g)^2$ [108]. This model includes the effects of connectivity in the scattering, but neglects chain expulsion from the core region, however, this can be emulated by artificially shifting the chains away from the core surface. The shift is controlled by the d parameter. Comparing eq. (6.2) and eq. (6.3) with the Pedersen-Gerstenberg model expressions shows that $F_{fluc}(q) = F_c(qR_g)$ and $\nu = 0$, as a result the $A_2(\sigma) = 0$, which is consistent with the fact that chain-chain interactions are neglected in this model.

A modification to the model due to Pedersen and Gerstenberg is presented in article I, where the chains are shifted away from the micellar core, but connected to the core surface by a rigid radially pointing rod.

The main topic of article I is to explore to what extend the two models can be used to analyse the scattering data from the MC simulations, which include both the effects of excluded volume interactions as well as semi-flexibility. Comparing the model due to Pedersen and Gerstenberg to the modified model shows that the modified model provides more accurate estimates of the chain center-of-mass distance from the core radius, while the Pedersen-Gerstenberg model provides a more accurate estimate of the radius of gyration. The chain center-of-mass distance is estimated by fitting the radial profile, and the addition of a rod can be seen to provides better fits of the corona form factor amplitude. This is attributed to the improvement of the radial profile due to the addition of a rod section.

The conclusion is that for $\sigma < 1$ the Pedersen-Gerstenberg model and the modified model provide accurate estimates for the radius of gyration and core radius, however, at larger surface coverages larger deviations becomes apparent between parameter values estimated by fits and the true values sampled during the simulations. While large deviations exist for $\sigma > 1$ the fits still provides reasonable results.

6.2 Article II

Article II presents a self-consistent analysis of the corona form factor $F_{cor}(q)$ and the solution profile scattering $F_{sol.prof}(q)$. All terms in the corona form factor and solution profile scattering are obtained from the MC simulations, when the RPA expression is used for the fluctuation scattering $F_{fluc}(q)$. Hence, the corona form factor and solution profile scattering can be compared without introducing any model expressions for intra-chain scattering and radial profile, and this comparison provides a way of investigating the validity of the RPA approximation for the fluctuation scattering.

The intra-chain, inter-chain and corona form factor amplitude F_c, H, and A_{cor} are known from simulations. The excluded volume parameter can be obtained by letting $F_{cor}(q) = F_{sol.prof}(q)$, and since $A_{cor}(q)$ oscillates about zero,

a value q_0 can be chosen, such that $A_{cor}(q_0) = 0$. Then the excluded volume parameter is

$$\nu = \frac{(N-1)H(q_0)}{F_c(q_0)\left[F_c(q_0) + (N-1)H(q_0)\right]}. \tag{6.4}$$

Data are sampled at discrete q values, and a linear interpolation was used for finding the smallest value q_0 where $A_{cor}(q_0) = 0$, as well as estimating values $H(q_0)$ and $F_c(q_0)$. Error bars on ν was estimated by calculating the variance of the ensemble of ν values consistent with the error bars on the scattering data [82]. The corona form factor amplitude has several minima in general, and the smallest q_0 value is chosen as the inter-chain scattering typically has the smallest error bar at low q values.

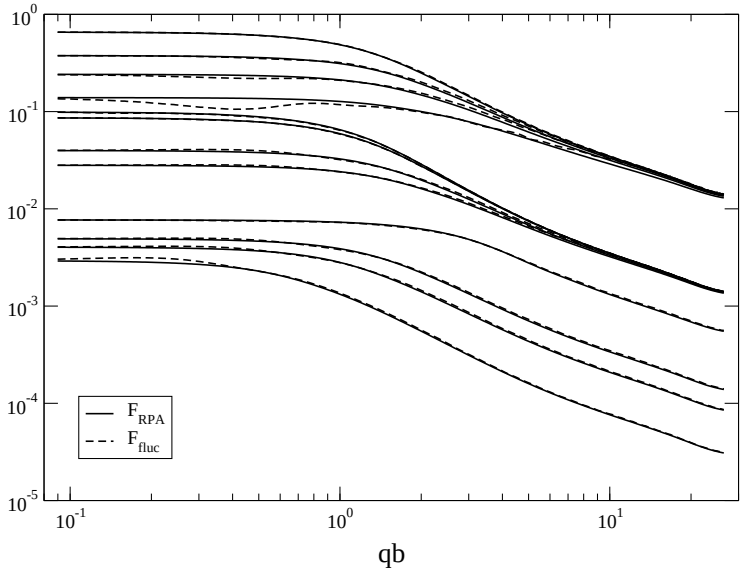

Figure 6.3: Comparison between F_{fluc} as obtained from simulations, and $F_{RPA} = F_c/(1 + \nu F_c)$ using the intra-chain scattering F_c from computer simulations. The excluded volume parameter ν are obtained from eq. (6.4). Curves are from top to bottom simulations varying number of chains $N = 3, 66, 131, 327$, varying core radius $R_{co} = 27.78b, 9.44b, 2.53b, 1.48b$ (shifted down one decades), and varying chain length $L = 2b, 8.33b, 13.67b, 38.17b$ (shifted down two decades).

Based on the excluded volume parameter, the fluctuation scattering contribution F_{fluc} can be obtained from simulations and compared with the RPA approximation using simulation data for the intra-chain scattering F_c. This is shown in figure 6.3, and there is an excellent agreement between the two expressions for the fluctuation scattering.

A similar excellent agreement is is obtained between the corona form factor

and the solution profile scattering for the simulation scattering as shown in figures 6.4, 6.5, and 6.6. This validates our approximation of using an RPA expression for the fluctuation scattering contribution. From the figures 6.4, 6.5, and 6.6 it can be seen that the fluctuation scattering F_{fluc} defines the depths of the minima of the solution profile scattering, and it can also be seen that the profile scattering dominates the forward scattering as expected. The forward scattering due to density fluctuation decreases with increasing surface coverage consistent with the concentration dependence of the scattering from an ordinary polymer solution.

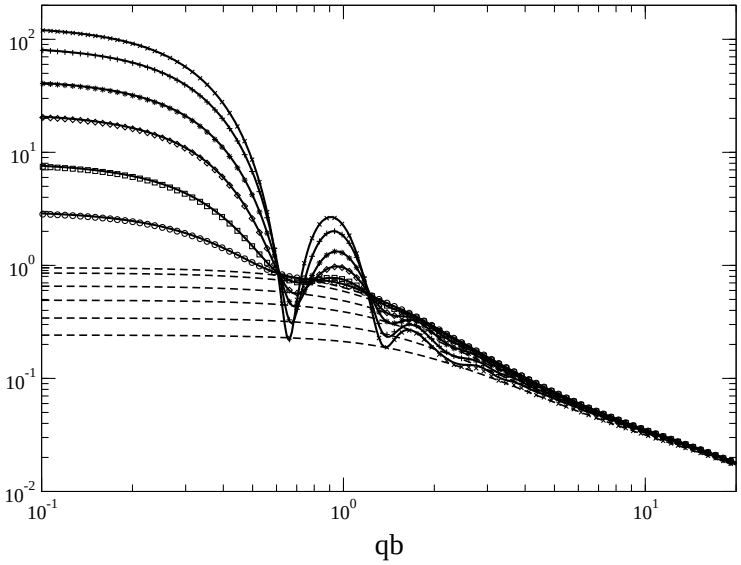

Figure 6.4: F_{cor} (thick lines), $F_{sol.prof}$ (symbols), and F_{fluc} (thin dashed line) varying number of chains $N = 3, 8, 22, 44, 87$, and 131, corresponding to $\sigma = 0.05, 0.13, 0.36, 0.72, 1.43$ and 2.15 (circle, box, diamond, star, plus and cross from bottom to top). The curves are normalised to coincide at large q values.

This is the reason why the corona form factor was seen to decrease in article I, when comparing simulations with and without interactions. Without excluded volume interactions $F_{fluc}(q) = F_c(qR_g)$ and $H(q) = A^2_{cor}(q)$, while in the presence of excluded volume interactions the fluctuation scattering contribution decreases and the inter-chain scattering is modified due to the presense of the "correlation hole"..

For an ordinary polymer solution it is predicted that the excluded volume parameter has a universal dependence on the reduced concentration as $\nu \propto (c/c^*)f(c/c^*)$, where $f(x)$ is some function, that is constant for small x [73]. Plotting the excluded volume parameter ν against σ as in figure 6.7 shows that the data points falls approximately on a power law relation $\nu(\sigma) = \alpha\sigma^\beta$ with $\alpha = 1.35 \pm 0.02$ and $\beta = 0.95 \pm 0.02$. That excluded volume parameters

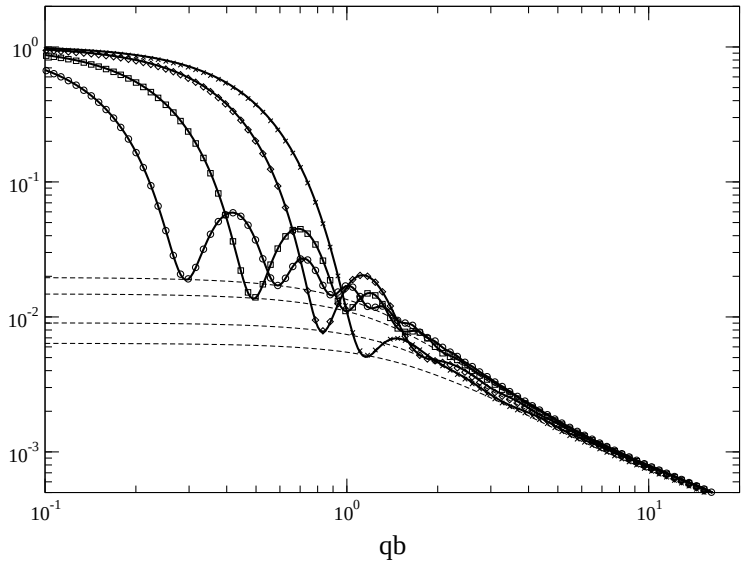

Figure 6.5: F_{cor} (thick lines), $F_{sol.prof}$ (symbols), and F_{fluc} (thin dashed line) varying core radius $R_{co} = 1.48b, 2.53b, 4.94b$, and $9.44b$, corresponding to $\sigma = 0.13, 0.36, 1.07$, and 2.10 (circle, box, diamond, and cross from bottom to top).

from simulations varying the number of chains, chain length and core radius collapses on a common curve, shows that the reduced surface coverage σ is the characteristic reduced parameter which describes the corona interactions. Note the grafting density $N/(4\pi R_{co}^2)$ is expected to be characteristic parameter in the brush regime. The deviations observed at large and small coverages are attributed to a weak dependency on the number of chains and surface curvature. Deviations are also observed for simulations with only two and four statistically independent segments.

As shown in the theory chapter a very simple relation exists between the fluctuation scattering and the osmotic compressibility. The compressibility κ fulfils $\kappa = F_{fluc}^{-1}(q = 0) = 1 + \nu$, and thus the deviations of ν at low surface coverages are dominated by one. The result is a universal behaviour of the compressibility for surface coverages, except for large surface coverages where deviations are apparent. These are attributed to the effects of the number of chains and surface curvature on the corona structure.

The solution profile scattering expression $F_{sol.prof}$ using the RPA expression for the fluctuation scattering contribution has the interpretation of being the scattering from a dilute/semi-dilute solution with a radial profile. The self-consistent analysis shows that the solution profile expression provides an excellent description of the corona form factor. On the basis of the agreement between the solution profile scattering and the simulated scattering is we conclude that the corona of a micelle can be regarded as a polymer solution with a certain

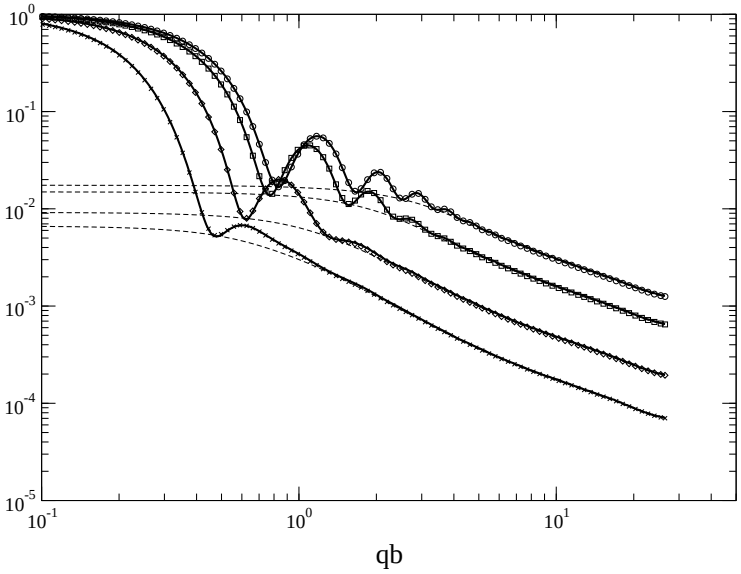

Figure 6.6: F_{cor} (thick lines), $F_{sol.prof}$ (symbols), and F_{fluc} (thin dashed line) varying chain length $L = 2b, 4b, 13.67b$, and $38.17b$, corresponding to $\sigma = 0.16, 0.35, 1.11$, and 2.35 using (circle, box, diamond, and cross from top to bottom).

radial profile. As the corona width is comparable to the radius of gyration the corona is quasi-two dimensional.

6.3 Article III

While the self-consistent analysis validates that the solution profile expression reproducing the simulated scattering, it does not confirm that the solution profile expression can be used for estimating parameters for physical parameters of interest when analysing experimental data. Hence, the aim of the article III is to formulate expressions for F_{fluc} and A_{cor} which can be used to extract physical parameters, such as the radius of gyration, the excluded volume parameter ν, and the radial profile for a micelle by fitting experimental data. For $F_{fluc}(q)$ the following equations was used

$$F_{fluc}(qR_g) = \frac{F_{Daniels}\left(\frac{q^2R_g^2}{e(L/b)}\right)}{1 + \nu F_{Debye}(q^2R_g^2)}, \tag{6.5}$$

$$F_{Daniels}(x) = F_{Debye}(x) + \frac{b}{15L}\left(4 + 7x^{-1} - (11 + 7x^{-1})e^{-x}\right),$$

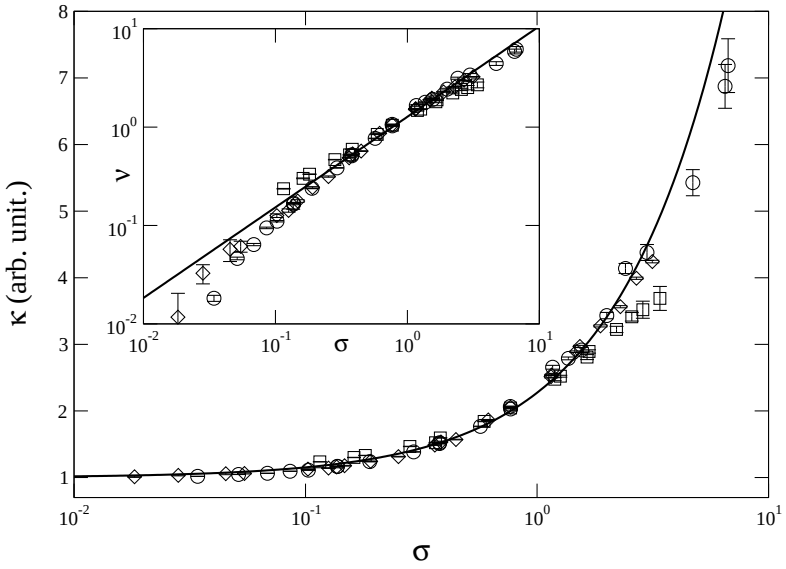

Figure 6.7: The osmotic compressibility κ plotted against reduced surface coverage for simulations varying number of chains (circle), varying chain length (box), and varying core radius (diamond). The inset shows the excluded volume parameter ν plotted against reduced surface coverage. The line in the inset is the power law $\nu(\sigma) = 1.35\sigma^{0.95}$ and the corresponding osmotic compressibility is shown as the line on the figure.

$$F_{Debye}(x) = \frac{2[x - 1 + \exp(-x)]}{x^2},$$

and

$$e(n) = 1 - \frac{3}{2n} + \frac{3}{2n^2} - \frac{3}{4n^3}\left(1 - e^{-2n}\right).$$

The equation is based on the RPA expression, but uses a chain form factor based on the Daniels distribution in the denominator, while using the Debye form factor in the numerator. This expression has been shown to provide a quite accurate description of the scattering from a semi-dilute solution of semi-flexible polymers [92]. The radius of gyration in the Daniels form factor is corrected by the Kratky-Porod expansion factor due to semi-flexibility, which was described in the theory section. The parameters are R_g, the radius of gyration, and ν. The excluded volume parameter, the ratio b/L was fixed at the value of the simulation, in order to reduce the number of fit parameters.

The corona form factor amplitude is the Fourier transform of the radial profile, and three radial profiles was used. The first is a Box with a Gaussian tail (abbreviated BoxGauss) and given by

$$\varphi_{BoxGauss}(r) = \begin{cases} 0 & r < R_{co} \\ B & R_{co} \leq r < R_{ch} \\ B \exp\left[-(r - R_{ch})^2/(2s^2)\right] & R_{ch} \leq r \end{cases} .$$

The last two profiles are two Maximum Entropy profiles where knowledge of the first two (abbreviated the ME2 profile) or three momenta (abbreviated the ME3 profile) was assumed, respectively. The radial profile is given by

$$\varphi_{ME}(r) = \begin{cases} 0 & r < R_{co} \\ B \exp\left[-\sum_{n=1}^{m} a_n (r - R_{co})^n\right] & r \geq R_{co} \end{cases} ,$$

where B is a normalisation constant. For both profiles it is assumed that no chains enter the core region. While the BoxGauss profile is an arbitrarily chosen empirical profile, the maximum entropy profiles are less arbitrary. As argued in the theory section, a maximum entropy profile is the least biased profile consistent with the requirements that chains do not enter the core region, that the profile is normalised, and that we posess knowledge of first m moments. Expressions for $A_{cor}(q)$ corresponding to the BoxGauss and ME2 profiles ($m = 2$) are given in the third article, while the form factor amplitude corresponding to the ME3 profile ($m = 3$) is obtained by numerical integration.

The simulation results for $F_{cor}(q)$ and $A_{cor}(q)$ were simultaneously fitted by the corresponding expressions for $F_{sol.prof}(q)$ and $A_{cor}(q)$, where the corona form factor amplitude were derived from the BoxGauss, ME2, and ME3 radial profiles. The radius of gyration, the excluded volume parameter, and the two or three parameters required by the radial profile were fitted. For $\sigma < 1$ all fits provides very similar estimates of the fit parameters for the three profiles, and the profiles estimated by the fits are in good agreement with each other and the simulated data. For $\sigma > 1$ the fits using the ME3 profile provides significantly better fits compared to the BoxGauss and ME2 profiles. This improvement of the corona scattering fits is directly related to the improvement of the fits of the form factor amplitude. Excellent agreement was also obtained comparing the radius of gyration and radial profiles obtained from simulations to those estimated by the fits. The $\nu(\sigma)$ dependence obtained from fitting ν is similar to that obtained from the self-consistent analysis, however, with slightly modified constant and exponent: $\alpha = 1.42 \pm 0.03$ and $\beta = 1.04 \pm 0.02$. This difference is attributed to systematic effects caused by the expressions used for the fits.

Article II and III demonstrate that the expression for the solution profile scattering provides an accurate description of the micellar corona scattering, and that the expression can be used to obtain reliable estimates of the physical parameters: the single chain radius of gyration, the excluded volume parameter, and the radial profile. From the excluded volume coefficient thermodynamic information about the corona can be obtained from scattering experiments, just as for a polymer solution. The difference is that for a polymer solution all the observed scattering is due to F_{fluc}. Tethering chains to the core has the effect of creating an additional $A^2_{cor}(q)$ scattering contribution due to the radial profile of the polymer layer as it is confined to the micellar surface, and this scattering

dominates in the forward direction where the value $F_{fluc}(q = 0)$ is of particular interest.

6.4 Article IV

Article IV presents a formalism for calculating the form factor and inter-particle structure factor of various structures, such as triblock copolymers stars, and micelles with arbitrary core geometries. The article proves that the form factor of a composite particle consisting of non-interacting subunits can be written as

$$F(q) = \left(\sum_i \beta_i \right)^{-2} \left\{ \sum_i \beta_i^2 F_i + 2 \sum_{j<k} \beta_j \beta_k A_j \left(\prod_{i=1}^{n_{jk}} \Psi_{jk}^i \right) A_k \right\}.$$

The particle is considered as consisting of a number of non-interacting subunits referred to by the indices i,j and k. Each subunit has a reference point, which could be the center of a micellar core, the end of a chain, or the boundary between two adjacent blocks on a copolymer. β_i denotes the total excess scattering length of the i'th subunit, while F_i is the Fourier transform of the site-site correlation function, i.e. the form factor of the i'th subunit. A_i is the Fourier transform of the site-to-reference point distribution, i.e. the form factor amplitude. For any subunit j and k it is assumed that there exists a unique path of n_{jk} steps along reference points of other subunits connecting reference points subunit j and k. This could for instance be the block boundaries along a 5-block copolymer. The Fourier transform of the distance distribution of the i'th step between the j and k subunits is denoted Ψ_{jk}^i, i.e. it is a phase factor.

This expression has the following interpretation. The distance between two sites on two different subunits j and k can be written as the a sum of a number of steps, corresponding to site-to-reference point step, and a numner of reference-to-reference point steps until the second subunit is reached, and finally a step from the reference point of the second subunit to the second site.

Similarly the pair-distance distribution between two different sites on two different subunits can be factorised into the convolution of distributions representing the site-to-reference point step (yielding form factor amplitude A_j), a product of the distributions representing the reference-to-reference point steps (yielding phase factors Ψ_{jk}^i), and a step from the reference point to a site in subunit k (yielding A_k). This is due to the fact that the Fourier transform of a convolution is simply the product of the Fourier transforms. This is only true if the configurational average of the pair-distance distribution can be regarded as the product of configurational averages of the individual steps, which is only true if the subunits are non-interacting. Hence, this expression is valid for any acyclic structures of subunits, where the interactions between different subunits are negligible, while interactions within the subunit can be incorporated in the expressions for F_i and A_i. Hence, all connectivity information about the structure is included, even though interactions between subunits are neglected. In article IV it is shown how to include excluded volume interactions on the level of a linear chains of polymer subunits, such as a block copolymer.

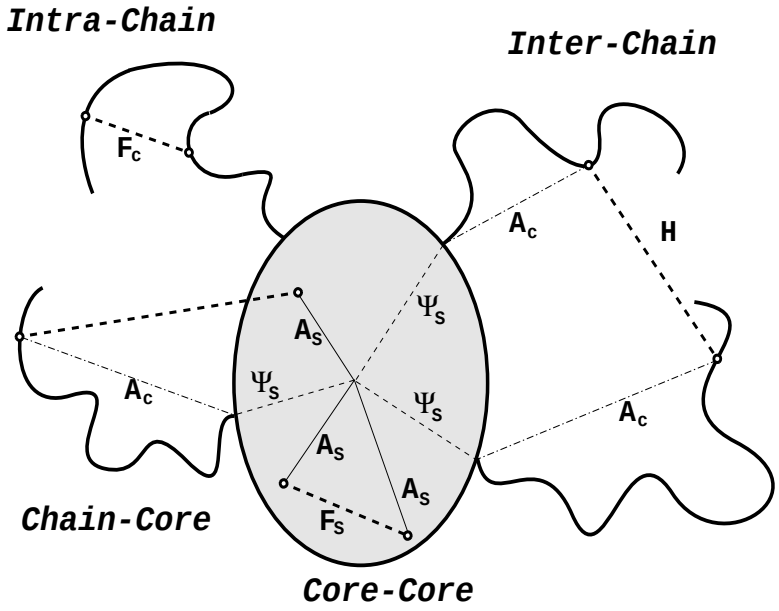

Figure 6.8: Illustration of possible the site-site correlations of a micellar structure.

An example: assuming the particle is a micelle which consists of two subunits chains in the corona (index "c") and a core (index "s"). No assumptions are made about the core geometry. Then the possible site-site correlation functions are intra-chain correlations, inter-chain correlations, chain-core correlations and core-core correlations, as shown in figure 6.8.

The intra-chain scattering F_c can be calculated from the pair-distance distribution within a chain, while the core form factor F_s can be calculated from the pair-distance distribution between sites within the core. The distance between two sites within the core can be written as two steps: a vector from one site to the center, and a step from the center to the second site, as shown in figure 6.8. Thus the pair-distance distribution can be written as the convolution of two identical step probability distributions $P_s(\mathbf{r})$ describing the probability for a site at position $\mathbf{r}$ relative to the center being within the core for a fixed core orientation. Denoting by $A_s(\mathbf{q})$ the Fourier transformation of the distribution $P_s(\mathbf{r})$, the pair-distance distribution is simply for core form factor $F_s(\mathbf{q}) = A_s^2(\mathbf{q})$ by virtue of the Fourier theorem for convolutions.

The vector distance between a particular site on a chain and another site in the core can be written as the sum of three steps: a vector from the site to the tethering point of the chain, a vector from the tethering point to the core center, and a vector from the core center to the site in the core. Thus the pair-distance distribution can be written as the convolution of the probability distributions of the three steps, and the Fourier transform of this convolution yields the product of the Fourier transforms of the probability distributions. The step from a site on a chain to the tethering point is the form factor amplitude of the chain yields a factor $A_c(q)$, the step from a site on the core surface to the core center yields a factor $\Psi_s(\mathbf{q})$, and the step from the core center to the site in

the core yields $A_s(\mathbf{q})$. Thus the chain-core scattering contribution has the form $A_c(q)\Psi_s(\mathbf{q})A_s(\mathbf{q})$, where $\Psi_s(\mathbf{q})$ is the core surface phase factor.

The distance between two particular sites on two different chains can be written as the sum of four steps: a step from the site to the tethering point, from tethering point to the core center, from the core center to another tethering point, and from the tethering point to the site on that chain. Thus the inter-chain scattering has the form $A_c(q)\Psi_s(\mathbf{q})\Psi_s(\mathbf{q})A_c(q)$, as illustrated on figure 6.8.

Weighting the contributions with the proper total scattering lengths and taking care of the weighing between intra- and inter-chain correlations the form factor of a micelle with an arbitrary core geometry and non-interacting chains is

$$F_{mic}(q) = (\beta_c + \beta_s)^{-2} \left\langle \beta_s^2 A_s^2(\mathbf{q}) + \frac{\beta_c^2}{N} F_c(q) \right.$$

$$\left. + \beta_c^2 \frac{(N-1)}{N} A_c^2(q)\Psi_s^2(\mathbf{q}) + 2\beta_c\beta_s A_c(q)\Psi_s(\mathbf{q})A_s(\mathbf{q}) \right\rangle_o . \tag{6.6}$$

The terms are the core form factor, the intra-chain scattering, the inter-chain scattering, and the chain-core interference function. The intra-chain scattering is proportional to the number of chains N, while the inter-chain scattering is proportional to the number of pairs of chains $N(N-1)$, while the total is N^2. This explains the weighting between intra-chain and inter-chain scattering contributions, an orientational average has to be performed on the product of Fourier transforms as the core surface is rigidly attached to the core.

In the special case of a spherical core, the probability of a vector $\mathbf{r}$ is within the core is $P_s(\mathbf{r}) = \Theta(|\mathbf{r}| - R_{co})/(4\pi R_{co}^3/3)$, where $\Theta(x)$ is the step function ($\Theta(x) = 1$ for $x \geq 0$ and $\Theta(x) = 0$ for $x < 0$). The probability for a vector $\mathbf{r}$ to be located on the core surface is $P_{surf}(\mathbf{r}) = \delta(|\mathbf{r}| - R_{co})/(4\pi R_{co}^2)$. From these simple distributions the surface phase factor and core form factor amplitude are given by

$$\Psi_s(q) = \int_0^\infty \mathrm{d}\mathbf{r} 4\pi r^2 \sin(qr)/(qr) P_{surf}(r) = \sin(qR_{co})/(qR_{co})$$

and

$$A_s(q) = \int_0^\infty \mathrm{d}\mathbf{r} 4\pi r^2 \sin(qr)/(qr) P_s(r) = \Phi(qR_{co}).$$

Thus the micellar form factor eq. (6.6) becomes

$$F_{mic}(q) = (\beta_c + \beta_s)^{-2} \left(\beta_s^2 \Phi^2(qR_{co}) + \frac{\beta_c^2}{N} F_c(q) \right.$$

$$\left. + \beta_c^2 \frac{(N-1)}{N} A_c^2(q) \left(\frac{\sin(qR_{co})}{qR_{co}} \right)^2 + 2\beta_c\beta_s A_c(q) \frac{\sin(qR_{co})}{qR_{co}} \Phi(qR_{co}) \right) .$$

This expression reduces to the expression for the micellar scattering presented at the start of this chapter (eq. 6.1) using the abbreviations of the

Pedersen-Gerstenberg model with $d = 0$, and comparing eqs. (6.6, 6.2 and 6.3) suggests that solution profile form factor for a micelle with an arbitrary core geometry is

$$F_{mic}(q) = (\beta_c + \beta_s)^{-2} \left\langle \beta_s^2 A_s^2(\mathbf{q}) + \frac{\beta_c^2}{N} F_{fluc}(q) \right.$$

$$\left. + \beta_c^2 \frac{[N - F_{fluc}(q=0)]}{N} A_{cor}^2(\mathbf{q}) + 2\beta_c\beta_s A_{cor}(\mathbf{q}) A_s(\mathbf{q}) \right\rangle_o , \qquad (6.7)$$

The rationale behind the derivation of the form factor can be used to derive an expression for the inter-particle structure factor. The vector between two sites on two subunits on two different aggregates can be regarded as consisting of a number of steps from the site to the reference point of that subunit, steps along a path from reference-to-reference points until the aggregate centre is reached. Then a step from the center of one aggregate to the center of another aggregate, followed by a path from that center along reference points of subunits until the second subunit is reached, and a step to the final site on that subunit. The intermolecular structure factor is

$$H_{ss}(q) = \left(\sum_i \beta_i \right)^{-2} \left\{ \sum_k \beta_k A_k \left(\prod_{i=1}^{n_{ck}} \Psi_{c,k}^i \right) \right\}^2 (S_{cc}(q) - 1) ,$$

Here index "c" denotes the center of the aggregate, and $S_{cc}(q)$ is the center-to-center structure factor. The term in the bracked is the form factor amplitude A of the entire particle. The scattering from a solution of aggregates is the sum of intra-molecular and inter-molecular scattering given by

$$P(q) = F(q) + H_{ss}(q) = F(q) S_{app}(q),$$

where the effective structure factor is given by

$$S_{app}(q) = \frac{H_{ss}(q)}{F(q)} + 1.$$

In the special case, where aggregates consist of a spherical symmetric aggregate with a form factor amplitude $A(q)$ then $H_{ss}(q) = A(q)^2 (S_{cc}(q) - 1)$ and $F(q) = A^2(qr)$, which leads to $S_{app}(q) = S_{cc}(q)$. Thus the apparent structure factor corresponds to the center-to-center structure factor for spherically symmetric scatterers. This is a well known result for monodisperse suspension of spherical scatterers [109].

The inter-molecular structure factor for a solution of non-interacting micelles can easily be shown to be

$$H_{mic}(q) = (\beta_c + \beta_s)^{-2} \left(\langle \beta_s A_s(\mathbf{q}) + \beta_c A_{cor}(\mathbf{q}) \rangle_o \right)^2 (S_{cc}(q) - 1) .$$

The corona form factor amplitude is given by a generalised core-shell model expression $A_{cor}(\mathbf{q}) = \int_{R_{co}}^{\infty} \mathrm{d}r A(r) \Psi_s(\mathbf{q}, r) \rho(r)$, where $\rho(r)$ is the area density of scatterers in the r sized shell, and $A(r)$ is the area of that shell. It remains to validate these generalisations of the micellar scattering.

Chapter 7

Article I

JOURNAL OF CHEMICAL PHYSICS VOLUME 112, NUMBER 21 1 JUNE 2000

A Monte Carlo study on the effect of excluded volume interactions on the scattering from block copolymer micelles

Carsten Svaneborg and Jan Skov Pedersen
Condensed Matter Physics and Chemistry Department, Risø National Laboratory, DK-4000 Roskilde, Denmark

(Received 26 January 2000; accepted 10 March 2000)

Effects of excluded volume interaction on the form factor of a block copolymer micelle model have been investigated by performing Monte Carlo simulations. The micelles are modeled as a corona of semi-flexible chains tethered to a spherical core. Simulated form factors are analyzed using the model proposed by Pedersen and Gerstenberg. A slightly modified model is presented, in which chains consists of a radially pointing rigid rod, onto which a Gaussian chain is attached. The straight section emulates chain stretching near the micelle core. Both models are fitted to the simulation data using two parameters, that describes the individual chains: the radius of gyration, and the average center-of-mass distance to the micelle core. Based on a comparison between parameters obtained from fits, and those obtained directly from the simulation, it is concluded that the models provide good estimates for the radius of gyration and the chain center-of-mass distance for a low surface coverage, while systematic deviations are observed for high surface coverage, where chains begin to overlap, and excluded volume interactions becomes significant. © *2000 American Institute of Physics.* [S0021-9606(00)51321-X]

I. INTRODUCTION

When diblock copolymers are put into a selective solvent, that is, a good solvent for one block, and a poor solvent for the other, the copolymers spontaneously self-assemble into aggregates. These micellar aggregates have a dense core and a corona of solvated polymers chains. Different morphologies will self-assemble upon variation of the concentration, solvent or the relative length of the two blocks. These morphologies include micelles with spherical, elliptical or cylindrical cores. At high volume fractions the aggregates might order into structures such as: crystals structures of spherical micelles, hexagonal rod structures of cylindrical micelles, or the micellar aggregates can coalesce forming a number of continuous structures as for instance a lamellae structure.[1,2] These colloidal polymer solutions are examples of complex fluids, which exhibit novel and interesting physical phenomena.[3–6]

Light scattering, small angle neutron or x-ray scattering (LS, SANS and SAXS, respectively) are powerful techniques for obtaining structural information about colloidal solutions.[7] SANS combined with contrast variation techniques is an especially powerful technique, as it allows for the separation of the contributions from the various colloid constituents. However, it is very difficult or even impossible to invert the measured scattering intensities and deduce the constituents structure directly, since all phase information is lost in the measurement process. Instead, structures must be inferred by fitting models to the experimental data.[8] This necessitates the development of analytical models, or semi-analytical models as one obtains by parameterization of results from computer simulations, to allow for a detailed interpretation of the experimental data. Furthermore computer simulations allows ''computer experiments'' to be performed, which emulates an experiment, but an experiment carried out on a well-defined model system. The simulation results can then be analyzed as real experimental data, and from the analysis correlations between scattering data and structural properties of the simulated model can be deduced, and limits of validity can be established for particular models.

The aim of the present work is to investigate the effects of inter-chain as well as intra-chain excluded volume interactions on the scattering form factor of micelles with a spherical core, and to examine to what extent the model proposed by Pedersen and Gerstenberg[9] can be applied. This analytical model accurately describes the scattering from micelles having chains that do not interact among themselves and with the core. Core expulsion can be emulated in this model by lifting the chains away from the core surface. We present a modified model, which improves the Pedersen Gerstenberg model, when chains are excluded from the core. In this model the chain section is joined to the core surface by means of a rigid radially pointing rod. We also suggest improvements of the models that, to some extent, include effects of excluded volume interactions. We have used Monte Carlo simulations as a tool to investigate the excluded volume effects, and modeled the micelle as a number of semi-flexible chains tethered to a spherical core. These chains interact among themselves and with the core via excluded volume interactions. We have also made a number of simulations with core expulsion, but without chain interactions. This allows us to gauge the effects of excluded volume effects on the scattering from the polymer corona.

To our knowledge, no study has previously been made that focuses on the form factor of micelles with chains with excluded volume interactions. Previous studies of the struc-

ture of chains tethered to micelles have predominantly focused on determining the radial density profile,[10–12] or the conformational properties of chains in the core.[13] However, the radial density profile contains insufficient information for determining the full scattering function, because micelles are not centro-symmetric objects, as is assumed for core-shell models.[14] Absent from these models are the correlations due to the chain connectivity, and the lateral density fluctuations arising from the interactions between different chains. Similar arguments hold true for self-consistent field theories,[15] due to the large fluctuations about the most probable path at low surface coverage fractions. Core-shell models are not applicable to any of the simulations presented in this paper.

This paper is organized as follows: In Sec. II we present the two analytical models; in Sec. III we describe the Monte Carlo simulations, and define the parameters that we sample during a simulation. In Sec. IV we report the results, compare simulations with and without interactions, and discuss the models in the context of the simulations, and Sec. V contains a summary of our findings. An Appendix contains some practical information on how the partial scattering functions are sampled.

II. ANALYTICAL MODELS

Let q denote the length of the scattering vector, the normalized form factor [letting $F_{\text{micelle}}(q=0)=1$] of a block copolymer micelle with a spherical core can be written

$$F_{\text{micelle}}(q)=\frac{1}{(\rho_c+\rho_s)^2}[\rho_s^2\Phi^2(q)+\rho_c^2F_{ct}(q) +2\rho_c\rho_sS_{cs}(q)\Phi(q)]. \tag{1}$$

The form factor is comprised of three partial scattering contributions: a core–core contribution Φ^2, a chain–chain contribution F_{ct}, and a chain–core contribution $S_{cs}\Phi$ [for core-shell models $F_{ct}(q)=S_{cs}(q)^2$]. In this paper the partial scattering contributions are normalized to unity in the $q\to 0$ limit. The total chain and total core excess scattering lengths are denoted ρ_c and ρ_s, respectively, and they are defined as $\rho_c=NV_c(\rho_{\text{chain}}-\rho_{\text{solvent}})$ and $\rho_s=NV_s(\rho_{\text{core}}-\rho_{\text{solvent}})$, where V_c and V_s are the volume of a dissolved and core chain, respectively. A diblock copolymer micelle have implicitly been assumed, such that N denotes the aggregation number. Finally the scattering length density of a dissolved chain, a core chain, and the solvent is denoted ρ_{chain}, ρ_{core} and ρ_{solvent}, respectively. The total chain scattering function can be subdivided into two contributions: intra-chain correlations denoted F_c, which arises from self-correlations within each chain, and is strongly influenced by chain connectivity, and inter-chain correlations denoted S_{cc}, which is an interference term, that describe correlations between different chains. When these partial contributions are normalized, the total chain scattering function becomes:

$$F_{ct}(q)=\frac{1}{N}F_c(q)+\frac{N-1}{N}S_{cc}(q). \tag{2}$$

The length scales of a single chain are: R_g the radius of gyration, b the Kuhn length, L is the contour length of the chain, and l_0 the step length. The radius of gyration measures the chain spatial extent. The Kuhn length measures the characteristic contour length of a semi-flexible chain, on which bond orientations are correlated; for a flexible chain the Kuhn and step lengths are equal. Scattering techniques probe correlations on various length scales, and we expect that the single chain scattering can be divided into three qualitative different regions: For qR_g less than unity (the Guinier region) the chains appear to be pointlike objects (Hausdorff dimension 0) and $F_c\approx 1$. In the range where qR_g are larger than unity and qb is less than unity, the random walk nature of the chains are probed. Since a random walk is a fractal object with Hausdorff dimension 2, we expect a scattering function that behaves as $F_c\propto(qR_g)^{-2}$. In the regime where qb is larger than unity, chains are probed on distances, where the bonds orientations are correlated and they exhibit rigid rod like correlations with a Hausdorff dimension of 1, and we expect a scattering function that behaves as $F_c\propto(qL)^{-1}$. The actual crossovers between these regions are very broad, making it difficult to accurately estimate R_g and b directly from location of the crossovers on a simulated $F_c(q)$ curve.

The characteristic scale of inter-chain correlations R_{ch} is comparable to the radius of the micelle. Because both the contributions to the total chain scattering function are normalized, inter-chain correlations will dominate the scattering for low q values, since the core radius usually is larger than the radius of gyration. Because the characteristic intra-chain distances are small, intra-chain scattering will dominate the total scattering at high q values.

If we assume the micelle core is a homogeneous sphere with radius R_{co}, the normalized form factor amplitude for the core is:[16]

$$\Phi(q,R_{co})=\frac{3[\sin(qR_{co})-qR_{co}\cos(qR_{co})]}{(qR_{co})^3}. \tag{3}$$

The remaining contributions to the micellar form factor are given by:[9]

$$F_c(q,R_g)=F_{\text{chain}}(q,R_g), \tag{4}$$

$$S_{cc}(q,R_g,R_{cm})=\psi^2_{\text{chain}}(q,R_g)\left[\frac{\sin(qR_{cm})}{qR_{cm}}\right]^2, \tag{5}$$

and

$$S_{cs}(q,R_g,R_{cm})=\psi_{\text{chain}}(q,R_g)\frac{\sin(qR_{cm})}{qR_{cm}}. \tag{6}$$

If we assume that excluded volume interactions are absent, and that chains are flexible, they are described by:

$$F_{\text{chain}}(q,R_g)=\frac{2(e^{-x}-1+x)}{x^2}, \tag{7}$$

and

$$\psi_{\text{chain}}(q,R_g)=\frac{1-e^{-x}}{x}, \tag{8}$$

where $x=(qR_g)^2$.

F_{chain} is the form factor of a flexible chain given by Debye,[17] and ψ_{chain} is the form factor amplitude of a flexible chain given by Hammouda.[18] R_{cm} is the chain center-of-mass (CM) radius, i.e., the distance from the core center to the CM of the individual chains. Core expulsion is mimicked by letting $R_{cm}=R_{co}+dR_g$ (with $d\approx 1$), which lifts chains away from the core surface. This has been shown by Monte Carlo simulations[9] to be a good approximation of core expulsion. We refer to this model as ''model 1'' in the remainder of this paper.

We have carried out a modification of model 1 by adding a radially pointing rod, of length $l=R_{cm}-R_{co}$ that joins the chain originating at the chain CM to the core surface (''model 2''). The rod section attempts to mimic the effect of chain stretching close to the micelle core surface. Let L be the total contour length of the rod and chain sections, and $\chi=l/L$ the fraction of polymer in the rod section. Then the partial scattering contributions are given by (suppressing function arguments for clarity):

$$F_c(q,R_g,R_{cm},l)=(1-\chi)^2F_{\text{chain}}+\chi^2F_{\text{rod}}+2\chi(\chi-1)\psi_{\text{chain}}\frac{\text{Si}(ql)}{ql}, \tag{9}$$

$$S_{cc}(q,R_g,R_{cm},l)=(1-\chi)^2\psi^2_{\text{chain}}\left[\frac{\sin(qR_{cm})}{qR_{cm}}\right]^2+\chi^2\varphi^2_{\text{rod}}+2\chi(1-\chi)\psi_{\text{chain}}\varphi_{\text{rod}}\frac{\sin(qR_{cm})}{qR_{cm}}, \tag{10}$$

$$S_{cs}(q,R_g,R_{cm},l)=(1-\chi)\psi_{\text{chain}}\frac{\sin(qR_{cm})}{qR_{cm}}+\chi\varphi_{\text{rod}}. \tag{11}$$

The individual rods are described by the form factor of an infinite thin rod,[19] and the form factor amplitude of a rod, respectively:

$$F_{\text{rod}}(q,l)=\frac{2}{lq}\text{Si}(ql)-\frac{4}{(lq)^2}\sin^2\left[\frac{lq}{2}\right], \tag{12}$$

and

$$\varphi_{\text{rod}}(q,l,R_{cm},R_{co})=\frac{1}{ql}[\text{Si}(qR_{cm})-\text{Si}(qR_{co})], \tag{13}$$

with $\text{Si}(x)=\int_0^x(t^{-1}\sin t)\,dt$.

The rod section will usually be short ($l\sim R_g$) compared to the contour length of the chain section, and thus give only a small correction to the total chain scattering. However, the addition of the nonoscillatory rod term to the oscillatory chain term in scattering expression Eq. (11) is more pronounced, as it influences both the phase and amplitude of the oscillations. The equations defining model 1 and 2, Eqs. (4)–(6) and Eqs. (9)–(11), are purely due to the geometrical assumptions: The chain CMs are evenly distributed on a sphere with radius R_{cm}, and that chains are tethered to the end of a rod; whereas the objects that scatter radiation are described by the form factor and form factor amplitudes, Eqs. (7), (8), (12), and (13). Neither model 1 nor model 2 accounts for chain–chain interactions in the corona, both models, however, take chain connectivity explicitly into account, and they mimic the chain exclusion from the core by raising the chain CM above the core surface. Since chains are described by the Debye and Hammouda expressions, finite length effects and effects due semi-flexibility are not included. In the $R_{cm}\to 0$ limit model 1 reduces to the expression for a star polymer.[20]

III. MONTE CARLO SIMULATION

In the simulation we model the micelle as a spherical core, having N semi-flexible chains tethered to the surface. Each chain in turn consists of n bonds (or $n+1$ vertices) of length l_0. The valence angle between subsequent bonds is fixed at 135.585 degrees, while the dihedral angle is free. This results in a Kuhn length $b=6l_0$, such that the radius of gyration of a flexible and semi-flexible chain coincides in the long chain limit.

We introduce excluded volume interactions by placing hard spheres along each of the chains, and a large hard sphere at the core center. We have 6 vertices per Kuhn length of chain, which corresponds to one sphere at each vertex. We have chosen the hard-sphere radius $\rho=0.1b$, a choice which reproduces the binary cluster integral of polystyrene in a good solvent.[21]

Each of the tethered chains on the micelle is initially generated by growing it from a root. A root consists two bonds, the first bond originating at the micelle core surface and a virtual zeroth bond ending on the surface, each of the two bonds point in a random direction. The two root bonds and their cross product defines a coordinate system, which can be used as a basis for adding a new bonds with a given valence and dihedral angle, and this procedure is easily iterated.

The micellar corona is generated by creating roots until all chains have roots, then bonds are successively added to the shortest chain, until all chains have the desired number of bonds. Every time a root is created or a bond is added, it is checked for overlap with the existing chains and the core. If an overlap is detected then 20 bonds are removed from the chain. If this includes removing the root, then a new root is generated at a different location. A micelle with a dense corona is difficult to generate, therefore we artificially reduce the chance for overlap during the creation of the initial micelle configuration, by limiting the range of the dihedral angle to the interval $[-60°,60°]$. This tends to stretch the chains, thereby reducing the probability for overlap, while the micelle is grown.

During the Monte Carlo (MC) simulation we update chains using the pivot algorithm of Stellman and Gans.[22] The chain vertices are periodically corrected for numerical errors introduced by the repeated multiplication of rotation matrices during the pivot moves; our correction algorithm is similar to that used by Stellman and Gans. Furthermore, we use two types of surface updates; the first type moves the chain on the core surface by pivoting the entire chain about core center. The second type reorientates the chain by pivoting it about the tether vertex. The zeroth bond is not used when collecting data, nor is it used when checking for chain over-

lap; however, it is pivoted with the rest of the chain, and this ensures that the first two bonds define a local coordinate system for the chain, that is, rotated along with all the MC moves, which provides a constant basis from which to run the Stellman and Gans correction algorithm.

After each chain update, we check for core overlap, intra-chain overlap, and inter-chain overlap. An update is rejected if it overlaps. Both types of chain checks are performed using the ''zippering method.''[23] The inter-chain check is performed in an order where chains that previously overlapped with the updated chain are checked first. This is a heuristic attempt to check chains more prone to overlap before others, which on average reduces the time spent on checking for inter-chain overlap.

After a micelle is grown it is equilibrated for 200 times the total number of degrees of freedom of accepted MC moves to avoid sampling the initially biased configuration. A simulation consists of 50 or 100 blocks, each block is the configuration average of 100 samples, and 1000 MC updates is performed between each sampling. Error bars are estimated from the fluctuations of block averages.

Let $\mathbf{r}_{ik}$ be the position of the kth vertex on the ith chain relative to the core center. In the following i,j denote chain indices with a $1,\ldots,N$ range, and k,l denote vertex indices with a $1,\ldots,n+1$ range. During a simulation, we sample the average chain CM radius R_{cm}, and the square radius of gyration R_g^2 of the individual chains. These are defined as:

$$R_{cm}=\left\langle \frac{1}{N}\sum_i |\mathbf{R}_{cm,i}| \right\rangle \quad \text{with} \quad \mathbf{R}_{cm,i}=\frac{1}{n+1}\sum_k \mathbf{r}_{ik}, \tag{14}$$

and

$$R_g^2=\left\langle \frac{1}{(n+1)N}\sum_i \sum_k (\mathbf{R}_{cm,i}-\mathbf{r}_{ik})^2 \right\rangle. \tag{15}$$

We also sample the partial scattering contributions, corresponding to the chain self-correlation $F_c(q)$, the chain–chain correlation function $S_{cc}(q)$, and the chain–core correlation function $S_{cs}(q)$; these are, respectively, given by:

$$F_c(q)=\left\langle \frac{1}{(n+1)^2N}\sum_i \left(\sum_k e^{-i\mathbf{q}\mathbf{r}_{ik}}\right)\left(\sum_l e^{i\mathbf{q}\mathbf{r}_{il}}\right)\right\rangle, \tag{16}$$

$$S_{cc}(q)=\left\langle \frac{1}{N(N-1)(n+1)^2}\sum_i \left(\sum_k e^{-i\mathbf{q}\mathbf{r}_{ik}}\right) \times\left(\sum_{j\neq i}\sum_l e^{i\mathbf{q}\mathbf{r}_{jl}}\right)\right\rangle, \tag{17}$$

and

$$S_{cs}(q)=\left\langle \mathrm{Re}\left(\frac{1}{(n+1)N}\sum_i \sum_k e^{i\mathbf{q}\mathbf{r}_{ik}}\right)\right\rangle. \tag{18}$$

A practical description of how these quantities are evaluated during a simulation is presented in the Appendix. The averages consist of both an orientational average, and a conformal average over nonoverlapping conformations. These are performed by averaging the partial scattering contributions over 13 different directions for each configuration sample. The partial scattering contributions are all normalized to unity in the $q\to 0$ limit. Note that the core form factor amplitude has been taken out of the chain–core scattering contribution, which allows data obtained from the MC simulation to be compared to the corresponding expressions in the analytical models.

IV. RESULTS AND DISCUSSION

In order to describe the dependence of the various properties on surface coverage, we define a dimensionless measure of surface coverage as the ratio between the area of a single chain, defined by the radius of gyration R_0 of a unperturbed semi-flexible chain with a finite number of steps[24] and the surface area available per chain at a distance $R_{co}+R_0$ from the core center:

$$\sigma=\frac{N\pi R_0^2}{4\pi(R_{co}+R_0)^2}. \tag{19}$$

Our surface fraction is analogous to the dimensionless c/c^* concentration in semi-dilute solutions, where c^* is the concentration at which the individual polymers begin to overlap. At a surface coverage much less than one, chains are separated and their conformation mainly influenced by core expulsion and expansion due to excluded volume effects within each chain. We expect that as the surface coverage reaches unity, polymers begin to overlap and the interaction between different chains becomes more pronounced. Curvature is another effect which influences the properties of the micellar corona. When chains are tethered to a flat surface, they will approximately be uniformly stretched away from the surface (the Alexander–de Gennes approximation) in order to balance the elastic stretching energy and excluded volume interaction between monomers.[12] However, chains tethered to a sphere (or any convex surface) will gain a relatively larger accessible volume at constant surface coverage, as they stretch away from the surface with a large curvature (i.e., small core), compared to chains tethered to surface with low curvature (i.e., large core). We use the dimensionless ratio η between the radius of gyration and the core radius as a measure of curvature effects. When this ratio is small, chains behave as they are tethered to a flat interface. If the ratio is large, i.e., chains have a large radius of gyration compared to core radius, the micelle becomes more like a star polymer. These proposed measures of surface coverage and curvature will fail, if chains are stretched away from the core to such an extent that the chains can no longer be considered to be isotropic, i.e., when the chains form a brush, or if the chains are so short that their radius of gyration and contour lengths are comparable.

We have defined a reference micelle having $N=44$ chains, core radius $R_{co}=3.33b$, and contour length $L/b=8.32$ corresponding to $n=50$ bonds. We have performed simulations, varying each of the three parameters in turn, while keeping the remaining two parameters fixed at their reference values. Eighteen simulations have been performed with the number of chains ranging from 1 to 360, corresponding to a surface coverage in the range from 0.01 to 4.9.

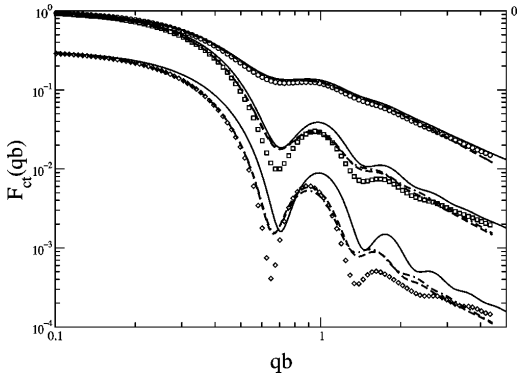

FIG. 1. Total chain scattering functions when varying the number of chains. The simulations with $N=6$ (circles), $N=44$ (boxes), and $N=160$ (diamonds, shifted down half a decade) correspond to surface densities $\sigma=0.09$, 0.67, and 2.44, respectively. Curves are simulation results without excluded volume interactions (full), model 1 (dash-dotted), and model 2 (dashed) fits.

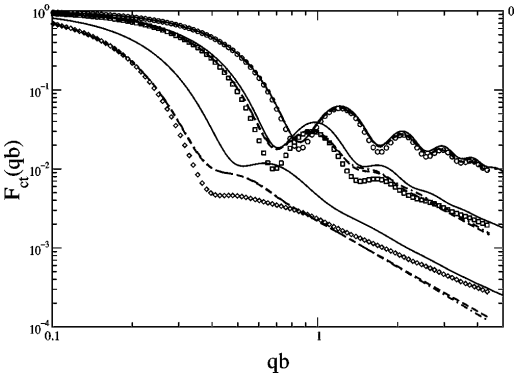

FIG. 3. Total chain scattering function when varying the chain length. The simulations with $L=1b$ (circles), $L=8.32b$ (squares), and $L=60.67b$ (diamonds) correspond to surface densities $\sigma=0.11$, 0.67, and 2.59, respectively. Curves are simulation results without excluded volume interactions (full), model 1 (dash-dotted) and model 2 (dashed) fits.

16 simulations varying core radius in the range $1.24b-22.11b$, corresponding to a surface coverage from 0.02 to 2.4, and 11 simulations varying contour lengths in the range $1.5b-60.67b$ corresponding to a surface coverage in the range from 0.1 to 2.6.

Simulation results for the total chain scattering are shown in Figs. 1–3, for low ($\sigma\approx0.1$), medium ($\sigma=0.67$) and high ($\sigma\approx2.4$) surface coverage. The medium results correspond to the reference micelle, which is shown in all figures as a common basis for comparison. The total chain scattering from simulations carried out with core expulsion, but without excluded volume interactions, is also shown on the figures. These are termed noninteraction simulations in the remainder of the paper. Scattering from these simulations is independent of the number of chains, except for the weighting between the inter- and intra-chain scattering contributions to the total chain scattering. These simulation results are well described by both the analytical models from Sec. II (these fits are not shown in the figures). Comparing noninteracting simulations to simulations with interactions allows us to identify features in the observed scattering which are due to excluded volume effects.

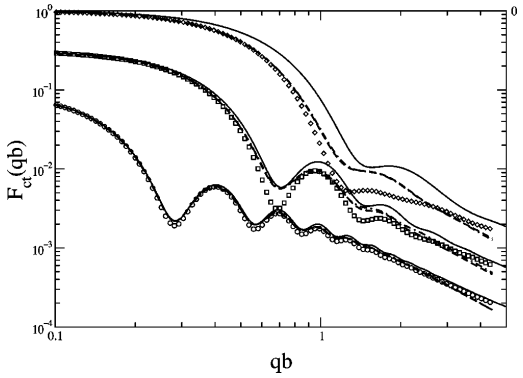

FIG. 2. Total chain scattering function when varying the core radius. For simulations with $R_{co}=9.89b$ (circles, shifted down a decade), $R_{co}=3.33b$ (squares, shifted down half a decade), and $R_{co}=1.24b$ (diamonds) corresponding to surface densities $\sigma=0.11$, 0.67, and 2.43, respectively. Curves are simulation results without excluded volume interactions (full), model 1 (dash-dotted) and model 2 (dashed) fits.

A qualitative examination of the simulation results shown in Fig. 1 reveals that the total chain scattering has a very nontrivial dependence on the number of chains for simulations with excluded volume interactions compared to the noninteracting simulations. The general behavior observed is one where the scattering intensity at high q values drops, while oscillations become more pronounced, as we increase the number of chains. This is a direct consequence of weighting of intra-chain and the oscillatory contribution from inter-chain correlations in Eq. (2), and is clearly observed on the noninteraction simulations. Simultaneously, the excluded volume interactions causes the first minima to grow progressively more narrow, while the higher order oscillations appear to be attenuated, when compared to the noninteraction simulations. The noninteracting simulations are well described by both models, and since the inter-chain contribution in both models is always positive, the minima in the total chain scattering correspond to the zero points of the inter-chain contribution; thus the depth of the minima is defined by the intra-chain contribution. The fact that the minima of the simulations with excluded volume interactions are below those of the simulations without interactions leads us to conclude that the inter-chain contribution is negative at the first minima, and at the higher order oscillations, since the intra-chain contribution is only slightly affected by the increase in the number of chains.

By examining the pair distance distribution corresponding to the inter-chain correlations $S_{cc}(q)$ for: (i) simulations without core expulsion and excluded volume effects (not shown, but described by model 1); (ii) simulations with core expulsion but without interactions between different chains;

and (iii) full interacting chains, we observe that the intra-chain interaction introduces a correlation hole in the short range part of the pair-distance distribution. At low surface coverage, chain overlap is negligible, and effects of the hole are absent from the observed scattering. However, as the surface coverage increases, and chains begin to overlap, and the shape of the correlation hole becomes clearly defined. This is consistent with the correlation hole associated with semi-dilute polymer solutions and polymer melts.[25]

Figure 1 shows an inward shift of the first secondary peak as the number of chains increases, when comparing simulations with and without excluded volume interactions. This is consistent with the expectation that an increase in chain interactions forces the chain CM away from the core. A very slight decrease in scattering at high q values is observed for the low surface coverage simulation, which is due to the slight increase in the radius of gyration due to intra-chain excluded volume interactions. The decrease of scattering at high q values for higher surface coverage is caused by the negative inter-chain scattering contribution, which decays slower than the noninteraction simulation results.

A qualitative pairwise comparison between Figs. 2 and 3 shows curves that appear to be identical except for a scale factor. This is to be expected since the simulations shown in the two figures have nearly identical surface coverage, curvature measure $\eta = R_g / R_{co}$, and number of chains, and these are the dimensionless quantities that describe the corona. Thus we expect the two scattering contributions to follow a scaling behavior of the form:

$$S(q) = f_{\sigma,\eta,N}(qR_g). \tag{20}$$

The curves shown in Fig. 2 coincide at high q values, where the intra-chain scattering contribution dominates. This is to be expected, since the radius of gyration is only perturbed by the reduction of the core radius. However, the reduction of the core radius moves the chains CM closer to the core center, which corresponds to a shift of the oscillations toward larger q values as observed. In Fig. 3 the large change in the radius of gyration associated with the increase in the chain length is clear from the decrease of scattering in the high q range. However, as the chains become longer, the chain CM move away from the core, which corresponds to a shift of the oscillations toward lower q values, which is also observed. In Fig. 3 we observe a clear difference in the decay of the intra-chain contribution for the longest chains. The decay is given by $(qR_g)^{-1/\nu}$, where ν is the critical length exponent, which is $\nu = 0.5$ for a random walk, and $\nu = 0.588$ for a self-avoiding random walk.[14] For simulations with short chains this decay is not observed due to finite size effects.

For the simulations shown in Figs. 2 and 3, the amplitude of oscillations due to the inter-chain scattering contribution is observed to decrease with increasing surface coverage and decreasing core radius, i.e., for increased curvature. For the noninteracting simulations, this is due to the fact that intra-chain correlations dominate the inter-chain correlations in the q range, where oscillations would be observed, and as a result oscillations appear to be attenuated. This is also true for the noninteracting simulations, however, the intra-chain term is strongly affected by the effects of the correlation hole due to the increased curvature and surface coverage.

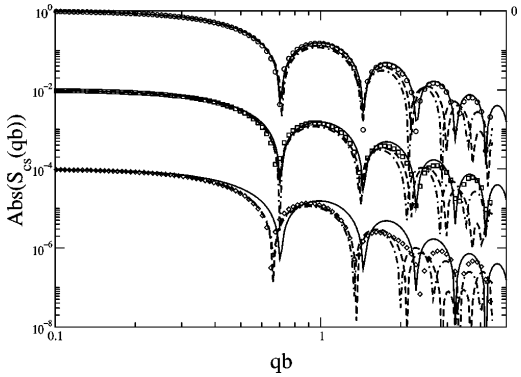

FIG. 4. Chain–core scattering when varying the number of chains for the simulations shown in Fig. 1. The medium and high surface coverage curves have been shifted down two and four decades, respectively. Curves are simulation results without excluded volume interactions (full), model 1 (dash-dotted) and model 2 (dashed) fits.

Figures 4–6 show the logarithm of the absolute value of the chain–core scattering, a term that only depends on the radial density distribution of chains. This term oscillates around zero, and for each sign change the logarithm gives rise to an inverted peak. A qualitative comparison between the chain–core scattering shown in the figures reveals that the frequency of the oscillations depends strongly on the chain length and core radius, but they are only slightly perturbed by a variation in the number of chains. The noninteracting simulations are well represented by both models, where the oscillatory behavior originates in the dependence on the chain CM radius. This explains why increasing the number of chains only slightly effects the oscillations, compared to simulations where the core radius or radius of gy-

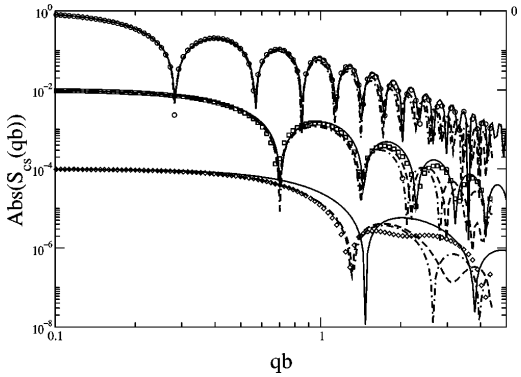

FIG. 5. Chain–core scattering when varying the core radius for the simulations shown in Fig. 2. The medium and high surface coverage curves have been shifted down two and four decades, respectively. Curves are simulation results without excluded volume interactions (full), model 1 (dash-dotted) and model 2 (dashed) fits.

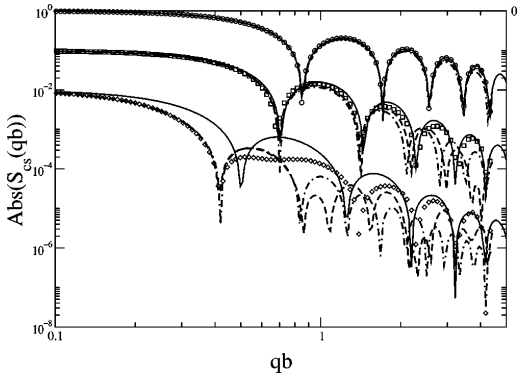

FIG. 6. Chain–core scattering when varying the chain length for the simulations shown in Fig. 3. The medium and high surface coverage curves have been shifted down one and two decades, respectively. Curves are simulation results without excluded volume interactions (full), model 1 (dash-dotted) and model 2 (dashed) fits.

ration of the chains changes. In the latter cases the chains CM moves closer or further away from the core, and this corresponds to the observed shift of the oscillations toward larger or smaller q values; whereas an increase in the number of chains only perturbs the radius of gyration slightly and we only observe a slight shift of the oscillations shown in Fig. 4.

We have fitted the model expressions for $F_{ct}(q,R_g,R_{cm})$ and $S_{cs}(q,R_g,R_{cm})$ simultaneously to the corresponding data obtained from the simulation. We have used R_g and R_{cm} as fit parameters and fixed the number of chains N, and core radius R_{co} at the values used in the simulation. The total contour length is fixed at $L=nl_0$. The contour length along with R_{cm} defines the weighting between the scattering from the rod and chain sections for model 2 fits.

Figures 1–3 show model 1 and 2 fitted to the total chain scattering for simulations with excluded volume interactions. It is apparent that both models show systematic deviations at high q values. At large q values the intra-chain scattering term $F_c(q)$ dominates the total chain scattering $F_{ct}(q)$, and both models use the Debye expression for the chain self-correlation function. However, the simulated chains are semi-flexible and have a finite number of bonds, and this influences the self-correlation function at high q, where a crossover to rigid rodlike scattering is expected. As a result of this observation, we have limited the fit range to $qb<4.5$, where the Debye expression works reasonably well. Note that both models fit the noninteracting simulation data in this range.

The fits are in very good agreement with the simulation data for surface densities $\sigma\sim 0.1$, but as the surface coverage increases toward unity, the minima become deeper, and both models fail to account for this since they fail to reproduce the negative inter-chain scattering contribution due to the correlation hole. However, both models are able to reproduce the correct oscillatory behavior, and can account for the height of the first oscillation. The difference between models 1 and 2 on the total chain scattering is marginal, and only shows up as a slightly more accurate fit to the first oscillation for model 2.

Model 1 and model 2 fits to the simulated the chain–core scattering are shown in Figs. 4–6. For surface coverages less than unity, the fits are in good agreement with the simulation results except for some phase and amplitude deviations at high q values. The amplitude deviations are caused by the failure of the Gaussian chain form factor amplitude in representing the simulated chains, analogous to the situation for the intra-chain scattering contribution. The addition of a rod section to model 1 yielding model 2 has visibly improved both amplitude and phase matching. The rod term has the effect of shifting the zero points of the chain–core scattering contribution of model 2 given by Eq. (11), which explains the improved phase and amplitude matching. For high surface densities the second secondary peak in Fig. 4 is broadened, while the first secondary peaks in Figs. 5 and 6 are broadened. Neither model reproduces this broadening, which we believe is due to the high monomer density close to the surface.

When comparing values for R_g and R_{cm} obtained from simulations with those obtained from the fits, we need to make some corrections for model 2. The two fit parameters describe the Gaussian chain part of the chain, and not the rod section. The rod section decreases the chain CM radius, while it increases the radius of gyration. These corrections can be calculated analytically, and are given by:

$$(R_{cm})_{\mathrm{corr}}=R_{cm}-\frac{l^2}{2L}, \tag{21}$$

and

$$(R_g^2)_{\mathrm{corr}}=R_g^2\left(3\frac{l(L-l)}{L^2}+\frac{(L-l)^2}{L^2}\right)+l^2\left(\frac{l^2}{12L^2}+\frac{l(L-l)}{3L^2}\right). \tag{22}$$

The correction of the total CM radius is the weighted average between the rod and chain CM, while the correction to the radius of gyration was obtained by expanding Eq. (9). Note again that $l=R_{cm}-R_{co}$ is the length of the rod section, which connects the core surface to the chain segment starting a distance R_{cm} from the core, while L is the total length of the rod and chain section. In the $l\to 0$ limit the rod section and associated corrections vanish, while in the $l\to L$ limit the chain segment vanishes. In the limit where the chain section vanishes, R_{cm} moves inward by $L/2$, which is the location of the rod CM, and the radius of gyration correction reduces to $L^2/12$, which is the radius of gyration of a rigid rod of length L.

Figures 7–9 show a comparison between R_g and R_{cm} obtained from the fits shown in Figs. 1–6 and the values obtained directly from the simulation. All figures show the onset of chain interactions effects at $\sigma\sim 1$. For the two simulations where a minimal surface coverage limit is well defined, i.e., $N=1$ and $R_{co}=22b$, both simulations show that $d=R_{cm}-R_{co}=1.085R_g$. The simulation results shown in Fig. 9 display a qualitatively different behavior compared to

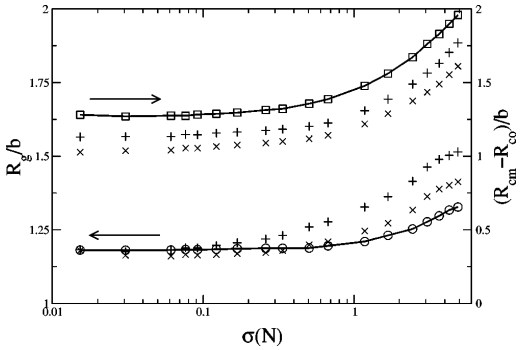

FIG. 7. Plot of radius of gyration (bottom curve against the left axis) and the chain CM radius (top curve against the right axis) when varying the number of chains. Symbols: Radius of gyration from simulation (circles and full curve), chain CM radius from simulation (box and full curve), model 1 fit (cross), and model 2 fit (plus).

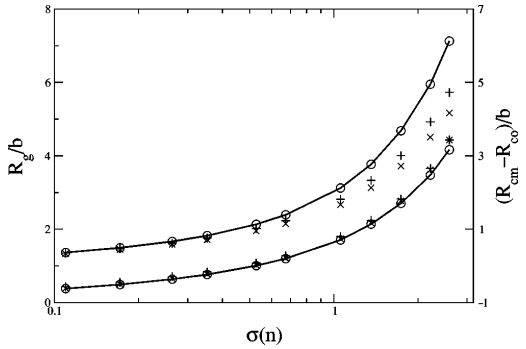

FIG. 9. Plot of the radius of gyration and chain CM radius for simulations when varying the chain length. Symbols as in Fig. 7.

those shown in Figs. 7 and 8. In Fig. 9 the chain length varies, which has a large impact on the radius of gyration, while varying the number of chains or the core radius only has an indirect effect on the radius of gyration, which expands slightly due to increased chain interactions.

A qualitative comparison of the estimate of the two models of R_g and the simulation result shows that model 1 provides a better estimate for the radius of gyration over a large range of surface densities, except for the simulations with long chains, where there is no discernible difference between the two models. We expect this to be caused by an overestimation of the radius of gyration, when the rod section is a significant percentage of the total chain length. Conversely, model 2 provides a better estimate of the chain CM radius, which is due to the fact that the rod section improves the representation of the radial density distribution caused by core expulsion. One exception is the simulations varying the number of chains, where both models consistently underestimate $R_{cm}-R_{co}$ (model 1 by 20%, model 2 by 12%), which is due to the bad phase match in Fig. 4. Model 2 consistently shows improved phase matching compared to model 1,

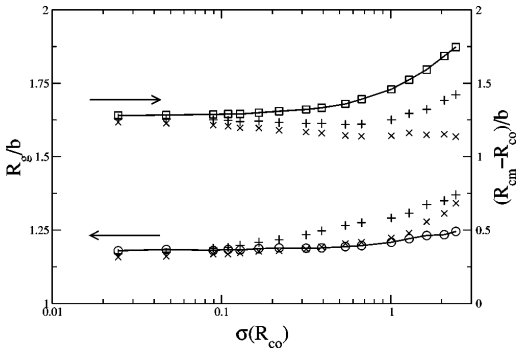

FIG. 8. Plot of radius of gyration and chain CM radius for simulations when varying the core radius. Symbols as in Fig. 7.

which explains why it provides a more accurate estimate of R_{cm}. For the high surface coverages, the fits only agree with the simulations results for low q values. However, they still provide estimates of the two fit parameters. This is because the location of the first inverted peak of the chain–core scattering provides an estimate of R_{cm}, while the low q behavior (of model 1), $S_{cs}(q)\approx 1-(3R_g^2+R_{cm}^2)q^2/6$, contains information on R_g and R_{cm}.

A quantitative comparison of the fit results shown in Figs. 7–9, show that for surface coverage $\sigma\sim 0.1$, the fits are very good, and the value of the fit parameters are very close to those obtained directly from the simulations. As the surface coverage is increased to $\sigma\sim 0.67$ (our reference micelle) clear deviations become apparent in the total chain scattering. The deviation between simulation and fits for R_g is 1% for model 1, and 7% for model 2, while the $R_{cm}-R_{co}$ deviation is 19%, and 12%, respectively. This translates into a deviation for R_{cm} of 5%, and 3%, respectively. For a surface coverage of $\sigma\sim 2.4$, the models only reproduce the simulation data in for low q values, but they still provide reasonable estimates for the radius of gyration and chain CM radius. For the simulation varying the number of chains $[\sigma(N)=2.44]$ the deviations for R_g is 5%, and 13% for model 1 and 2, respectively. The deviations for R_{cm} is 6% and 4%. The deviations for $R_{cm}-R_{co}$ is a about factor of 3 larger. For the simulation varying the core radius $[\sigma(R_{co})=2.43]$ the R_g deviations are less than 10%, however, the deviations for R_{cm} is 20%, and 11% for the two models, respectively. The deviations for $R_{cm}-R_{co}$ are a about factor of 2 larger. For the simulation varying the chain length $[\sigma(n)=2.59]$, both R_g deviations are 6%, while the deviations for R_{cm} are 21%, and 15%, respectively. The deviations for $R_{cm}-R_{co}$ are 1.5 times larger.

As already mentioned, we have also fitted the models to the simulations without excluded volume interactions, and both models produce good fits as expected. Model 2 yields a somewhat better fit to the simulations, and provides an improved estimate of the chains CM radius, when these are compared to the simulation results. Conversely, model 1 provides a slightly better estimate of the radius of gyration. This behavior is consistent with the results for simulations with

excluded volume interactions. These fits are not shown in the figures.

V. SUMMARY

We have performed Monte Carlo simulations of a model of spherical block-copolymer micelles, simulations have been performed with and without excluded volume interactions, in order to qualitatively probe the effects of excluded volume interactions on the micellar scattering function. We conclude, that the observed effects can be attributed to a correlation hole introduced by the excluded volume interactions, which strongly affects the inter-chain and chain–core contributions to the micellar scattering for micelles with high surface coverage.

Furthermore we have analyzed the simulation data in the context of the model of Pedersen and Gerstenberg and an improved model, where chains are connected to the micelle surface by a radially pointing rigid rod, which is a crude model for the chain stretching close to the core surface. Both models take explicit account of chain correlations due to single chain connectivity, but neglect excluded volume effects. Both models approximate the effects of core expulsion by lifting the polymer corona CM away from the core surface. We have fitted the models simultaneously to the two scattering contributions; the total chain scattering function and chain–core scattering contributions as obtained directly from the Monte Carlo simulations. The fits were performed with only two free parameters, i.e., the chain radius of gyration and the chain CM radius. Both models provide very good fits to simulations with core expulsion but without excluded volume interactions.

To avoid complications due to the semi-flexible chains we have simulated, the fit range was restricted to $qb<4.5$. This restriction could be removed by applying a more accurate model for the chain form factor and form factor amplitude (7 and 8) for instance a model derived from the Daniels distribution.[26] However, a chain form factor and form factor amplitude based on the Daniels approximation are not valid for our reference micelle, since it has only eight statistical independent segments. Another possibility is an empiric expression for semi-flexible chains.[21] The longest chains simulated shows the decay expected for excluded volume chains, and these require a chain form factor that can account for excluded volume effects.[14] We are currently working on deriving an empiric expression for the form factor and form factor amplitude of a semi-flexible excluded volume chain with a finite number of bonds, using Monte Carlo techniques.

For simulations with surface coverage less than unity, fits of model 1 and 2 to the simulation provide accurate estimates of the radius of gyration and the chain CM radius compared to those obtained directly from the simulation. The fitted parameters show systematic deviations due to excluded volume interactions for surface coverages above unity. However, the fits still provide reasonable estimates of the two parameters. Model 2, which attempts to include effects due to chain stretching close to the core, has improved the model estimate of the chain CM radius; however, it has had a detrimental effect on the radius of gyration estimate. We attribute this deviation to the fact that the addition of a rigid rod section overestimates the radius of gyration from the stretched chains, when the rod section is a relatively large percentage of the total chain length. However, the rod section modifies the model such that it provides a more realistic representation of the radial density distribution, and thus provides a more accurate chain CM radius estimate.

In the present paper we have used Monte Carlo simulations to analyze the effects of excluded volume interactions on spherical block copolymer micelles, and we have evaluated two models that describe these objects. Generally, models are necessary to extract data from scattering experiments, which do not allow for direct inversion of the experimental results in terms of physical structures and their associated parameters. Analysis and interpretation of experimental results require a large toolkit of different models. But the quality of the interpretation can only be as good as the quality of the model in representing a physically realistic structure. To evaluate the quality of a particular model, well-defined test cases need to be examined; for this Monte Carlo simulations are very well suited.

APPENDIX: CALCULATION OF PARTIAL SCATTERING FUNCTIONS

To resume: $\mathbf{r}_{ik}$ denotes the position of the kth vertex on the ith chain relative to the core center (ranges of indices as defined previously).

Let the phase sum of the ith chain be $z_i(\mathbf{q}) = \Sigma_k \exp(-i\mathbf{r}_{ik}\mathbf{q})$; then the phase sum of the entire polymer corona is given by $w(\mathbf{q}) = \Sigma_i z_i(\mathbf{q})$. The chain self-scattering function, chain–chain and chain–core interference contributions are then given by:

$$(n+1)^2 N\ F_c(q_n) = \left\langle \sum_i z_i^* z_i \right\rangle, \tag{A1}$$

$$(n+1)^2 N(N-1)\ S_{cc}(q_n) = \left\langle w^* w - \sum_i z_i^* z_i \right\rangle, \tag{A2}$$

$$(n+1) N\ S_{cs}(q_n) = \langle \mathrm{Re}(w) \rangle. \tag{A3}$$

Here w^* denotes complex conjugation of w. The averages are taken over the allowed chain conformations (an MC average) and micelle orientations. For each MC sample the scattering functions are sampled for a number of directions, M, of the $\mathbf{q}$ vector. The resulting partial scattering functions depend only on the magnitude of the scattering vector q_n. Let N_q be the number of q_n values sampled per MC sample.

Each time an MC sample is made, $MN_qN(n+1)$ complex exponentials (i.e., two trigonometric functions) have to be evaluated, which should be compared to the $N^2(n+1)^2$ evaluations that a direct space sampling method would require to calculate the pair-distance distribution. Reciprocal space sampling is clearly a vast improvement, since we are free to chose both M and N_q. However, this is still by far the most dominant contribution to the total execution time of a simulation, and a trick is clearly needed to calculate the complex exponentials in an efficient manner. An obvious choice would be a FFT technique;[27] however, FFT require that the q_n's are positioned on a lattice, and the number of points required to cover the range from $q_{\min}$ to $q_{\max}$ is N_q

$=q_{\max}/q_{\min}$, even though the cost of evaluating each of the exponentials is low, a huge number of points is required to cover 3–4 decades. We have chosen a hybrid approach to calculating the complex exponentials directly, using symmetry properties to derive them, while keeping the q_n's approximately equidistant on a logarithmic scale.

Let us abbreviate $\alpha q_n = \mathbf{r}_{ik} \cdot (q_n \hat{\mathbf{q}})$ where $\hat{\mathbf{q}}$ is a unit vector. In the following we will concentrate on calculating $\exp(-i\alpha q_n)$ in the case where $\exp(-i\alpha q_m)$ has already been calculated for all $m<n$. If q_m exists such that $q_n = 2q_m$, then $\exp(-i\alpha q_n) = \exp(-i\alpha q_m)^2$ (the double angle formulas), since we have previously evaluated $\exp(-i\alpha q_m)$, we only need to square that number. If q_m, q_p exists such that $q_n = q_m + q_p$ then $\exp(-i\alpha q_n) = \exp(-i\alpha q_m)\exp(-i\alpha q_p)$ (the addition formulas), since both exponentials have previously been evaluated, we only need to calculate the product of two numbers. Thus by an advantageous choice of the q_n distribution, we can use symmetry properties to convert many trigonometric evaluations into simple products of known complex numbers. The higher order symmetry properties require more algebraic operations, and do not provide a significant optimization.

Let the target distribution be given by

$$q_n^0 = 10^{(\log q_{\max} - \log q_{\min})\,(n/N_q) + \log q_{\min}}, \tag{A4}$$

which is an equidistant distribution, with N_q points covering the interval from $q_{\min}$ to $q_{\max}$ on a logarithmic scale.

The actual distribution of q_n's are chosen as to minimize

$$E[q_1, \ldots, q_{N_q}] = k\left(\frac{N_q}{\ln(10)(\log q_{\max} - \log q_{\min})}\right)^2 \times \sum_{i=1}^{N_q} \frac{(q_i - q_i^0)^2}{(q_i^0)^2} \tag{A5}$$

$$+ \beta N_{\text{calc}} + \gamma N_{\text{add}} + \delta N_{\text{double}}, \tag{A6}$$

where $N_{\text{calc}}, N_{\text{add}}$, and N_{double} is the number of exponentials that require direct evaluation, or can be deduced using the addition formulas, or formulas for the double angle, respectively. Thus $N_q \equiv N_{\text{calc}} + N_{\text{add}} + N_{\text{double}}$. The weights β, γ, and δ are chosen to represent the duration of the respective numerical operation; we have used $\beta = 1$ and $\gamma = \delta = 0.1$. The first term is a harmonic term that determines how large deviations from a perfect logarithmic distribution should be allowed, in order to speed up the evaluation; since the distribution is on a logarithmic scale, we have to divide by the local length scale, which is given by the parenthesis and the denominator. The constant k should be chosen so small that the ordering $q_m < q_n$ when $m<n$ is ensured, we have used $k = 0.01$. This penalty functional is easily minimized by a simulated annealing quench, with moves that shift q_n's, which require trigonometric evaluations into q_n's, which can be evaluated by simple algebraic operations on known numbers. If N_q is huge, care must be taken to avoid truncation errors in the evaluation. In our implementation only about 10% of the complex exponentials need to be evaluated directly.

[1] K. Mortensen and J. S. Pedersen, Macromolecules **26**, 805 (1993).
[2] G. A. McConnell, A. P. Gast, J. S. Huang, and S. D. Smith, Phys. Rev. Lett. **71**, 2102 (1993).
[3] W. M. Gelbart and A. Ben-Shaul, J. Phys. Chem. **100**, 13169 (1996).
[4] T. P. Lodge and M. Muthukumar, J. Phys. Chem. **100**, 13275 (1996).
[5] F. S. Bates, Science **251**, 898 (1991).
[6] S. T. Milner, Science **251**, 905 (1991).
[7] P. Lindner and T. Zemb, *Neutron, X-ray and Light Scattering: Introduction to an Investigative Tool for Colloidal and Polymeric Systems* (North Holland, Amsterdam, 1991).
[8] J. S. Pedersen, Adv. Colloid Interface Sci. **70**, 171 (1997).
[9] J. S. Pedersen and M. Gerstenberg, Macromolecules **29**, 1363 (1996).
[10] R. Toral and A. Chakrabarti, Phys. Rev. E **47**, 4240 (1993).
[11] A. P. Gast, Langmuir **12**, 4060 (1996).
[12] H. Li and T. A. Witten, Macromolecules **27**, 449 (1994).
[13] K. Procházka, J. Phys. Chem. **99**, 14108 (1995).
[14] S. Förster and C. Burger, Macromolecules **31**, 879 (1998).
[15] F. Schmid, J. Phys.: Condens. Matter **10**, 8105 (1998).
[16] Lord Rayleigh, Proc. R. Soc. London, Ser. A **84**, 24 (1884).
[17] P. Debye, J. Phys. Colloid Chem. **51**, 18 (1947).
[18] B. Hammouda, J. Polym. Sci., Part B: Polym. Phys. **30**, 1387 (1992).
[19] T. Neugebauer, Ann. Phys. (Leipzig) **42**, 509 (1943).
[20] H. J. Benoit, J. Polym. Sci. **11**, 507 (1953).
[21] J. S. Pedersen and P. Schurtenberger, Macromolecules **29**, 7602 (1996).
[22] S. D. Stellman and P. J. Gans, Macromolecules **5**, 516 (1972).
[23] S. D. Stellman, M. Froimowitz, and P. J. Gans, J. Comput. Phys. **7**, 178 (1971).
[24] P. Flory, *Statistical Mechanics of Chain Molecules* (Interscience, New York, 1969), p. 18.
[25] P. G. de Gennes, *Scaling Concepts in Polymer Physics* (Cornell University Press, Ithaca, NY, 1979).
[26] P. Sharp and V. A. Bloomfield, Biopolymers **6**, 1201 (1968).
[27] D. Frenkel, R. J. Vos, C. G. de Kruif, and A. J. Vrij, Chem. Phys. **84**, 4625 (1986).

Chapter 8

Article II

Block copolymer micelle coronas as quasi two-dimensional dilute/semi-dilute polymer solutions

Carsten Svaneborg and Jan Skov Pedersen*

Condensed Matter Physics and Chemistry Department, Risø national Laboratory, DK-4000 Roskilde, Denmark
*Present address: Department of Chemistry, University of Aarhus, Langelandsgade 140, DK-8000 Aarhus C, Denmark

Chain-chain interactions in a corona of polymers tethered to a spherical core under good solvent conditions are studied using Monte Carlo simulations. The total scattering function of the corona as well as different partial contributions are sampled. By combining the different contributions in a self-consistent approach it is demonstrated that the corona can be regarded as a quasi two-dimensional polymer solution, with a concentration dependence analogous to that of an ordinary polymer solution. Scattering due to the corona profile and density fluctuation correlations are separated in this approach. The osmotic compressibility is extracted from the latter, and it is shown to be a universal function of surface coverage, with some deviations at high coverage due to surface curvature effects.

This paper has been accepted by Physical Review E as an Rapid Communication.

Polymers can be tethered to a surface, thus forming a diffuse layer on the surface [1, 2]. The equilibrium properties of such a layer follow from the balance between entropic forces and excluded volume interactions. The latter favor a state with a minimum of monomer-monomer contacts, which can be achieved by increasing the available volume per chain by increasing the layer thickness. Entropic forces will tend to maximize the number of available chain configurations by opposing the chain stretching and by shifting the corona away from the surface to some extent. At low surface coverage the surface interaction will dominate, and the polymers will have a mushroom like shape. At very high surface coverage excluded volume interactions and chain-chain interactions dominate and chains will be strongly stretched forming a polymeric brush [3, 4]. Between the mushroom and brush regime there is a broad region of intermediate surface coverages [5], which is the typical regime accessible by experiments, see e.g. [6, 7].

In the present work we study the scattering from the polymeric layer of a spherical particle such as the polymer corona of a diblock copolymer micelle. We use Monte Carlo (MC) simulation-generated data to show that a model in which the the corona is regarded as a two-dimentional solution is applicable. The total corona scattering can be decomposed in two ways. In the analytical model of Pedersen and Gerstenberg [8], the intra-chain and inter-chain scattering contributions are combined to give the corona scattering, however, the same result can be obtained by combining the scattering contribution due to the *average* corona profile and density fluctuation correlations [9]. The latter decomposition can be interpreteted as being the scattering expected from a thin layer of dilute/semi-dilute solution confined to a thin layer around the core [10]. The approach presented in the present paper is based on self-consistent analysis of the MC results using the expressions provided by these two decompositions. The total corona scattering as well as the intra-chain, inter-chain, and corona profile scattering contributions were sampled during the simulations. The effects of excluded volume interactions, core expulsion, and chain semi-flexibility on the scattering was simulated and series of simulations varying the number of chains, chain length, and core radius were performed. In the analysis of the two expressions a Random Phase Approximation (RPA) was used for the fluctuation scattering contribution, and excellent agreement was obtained when inserting the partial scattering contributions as obtained from MC simulations. The excellent agreement of the two expressions enables us to extract the scattering contribution due to density fluctuation correlations within the corona. These carry thermodynamic information about the apparent second virial coefficient and the osmotic compressibility of the polymer layer. These quantities show a surface coverage dependence analogous to that expected from an ordinary polymer solution.

Numerous approaches such as self-consistent field theory [27, 28], variational techniques [29], and numerical simulations [13, 14] have all been applied for investigating the profiles of brushes on curved interfaces. Polymer layers at low and medium surface coverages are not amenable to analytically treatment, due to the presence of large density fluctuations. However, the small-angle scattering from a polymeric interface depends not only on the profile but also on the

correlations of density fluctuations [9]. The scattering from a dilute or semi-dilute solution of star polymers were treated by Marques et al. using an empirical 'blob' approach [16]. Our approach offers a clear quantitative picture of the interaction effects in micellar coronas, which are based firmly on Monte Carlo simulation results.

We describe the density of chains in a polymer corona on the surface of a spherical particle using a reduced surface coverage. Due to the chain entropy, the center of mass of a chain will be located at approximately a distance R_g from the core surface, where R_g is the unperturbed chain radius of gyration. The effective core surface area is thus $4\pi(R_{co} + R_g)^2$, where R_{co} is the core radius, whereas the cross-sectional area of N chains is $\pi R_g^2 N$. The reduced surface coverage is given by the ratio of cross-sectional chain area to available surface area as $\sigma = N\pi R_g^2/[4\pi(R_{co} + R_g)^2]$. The reduced surface coverage is a two-dimensional analogy of the c/c^* concentration [20, 25] for ordinary polymer solutions. A surface coverage of unity corresponds to critical overlap, where the area occupied by an unperturbed chain equals the available surface area per chain. For $\sigma < 1$ chains are few and far apart and weakly perturbed by the presence of other chains, and the scattering is well described by the model of Pedersen and Gerstenberg [8]. However, in the brush regime ($\sigma \gg 1$) the surface will induce chain ordering perpendicular to the surface as chains are stretched. The scattering in this regime is expected to be described by a core-shell model [19]. Experimentally $\sigma < 5$ is found for copolymer micelles [20, 16, 17].

The normalized corona scattering [$F_{cor}(q = 0) = 1$] consists of two weighted contributions: an intra-chain contribution F_c and an inter-chain contribution S_{cc} as

$$F_{cor}(q) = \frac{1}{N} F_c(q) + \left(1 - \frac{1}{N}\right) S_{cc}(q). \tag{8.1}$$

Here q is the magnitude of the scattering vector, and F_c is the Fourier transform of the pair-distance distribution between sites on the same chain. The intra-chain scattering is mainly due to chain connectivity and self-avoidance, and single-chain properties such as the radius of gyration, the contour length L, and the Kuhn length b can be determined from it. For a long semi-flexible chain the Kuhn length is the step length of an equivalent random walk. The inter-chain scattering S_{cc} is the Fourier transform of the pair-distance distribution between sites on different chains. The inter-chain scattering contains information about the corona profile, and the radius of the core. However, it also includes correlations due to chain-chain interactions such as the 'correlation hole', which is known to be present in ordinary polymer solutions [20, 25].

Core-shell models [19] describe the corona scattering in terms of the configurationally averaged profile, and as a result all density fluctuation correlations due to chain connectivity, self-avoidance, and chain-chain interactions are neglected. The core-shell approximation is $F_{cor} = A_{cor}^2$, where the profile scattering is given by $A_{cor}(q) = \int_0^\infty f(r)\sin(qr)/(qr)4\pi r^2 \mathrm{d}r$, and where $f(r)$ is the corona profile. If chain-chain interactions are negligible, different chains will be uncorrelated, and the inter-chain scattering will be given by $S_{cc} = A_{cor}^2$. Chain-chain interactions will yield an additional contribution to the inter-chain scattering

due to short-ranged density fluctuation correlations, which will dominate the inter-chain scattering at high q values. These fluctuations are caused by the repulsive excluded volume interactions between different chains. Based on this we define an fluctuation scattering contribution F_{fluc}, leaving only correlations due to the average profile (given by A^2_{cor}). Thus the corona scattering is rewritten as

$$F_{sol}(q) = \frac{1}{N} F_{fluc}(q) + \left(1 - \frac{F_{fluc}(q=0)}{N}\right) A^2_{cor}(q). \tag{8.2}$$

The weighting ensures that F_{sol} is normalized for $q = 0$ since F_{fluc} is not normalized. Rewriting (1) as (2) has the effect of shifting the influence of the correlation hole from S_{cc} into F_{fluc}. Therefore, inter-chain correlations has to be included in an expression for the $F_{fluc}(q)$ term. We apply an expression based on the PRISM theory for polymer solutions and melts, see e.g. [23]:

$$F_{fluc}(q) = \frac{F_c(q)}{1 - \rho c(q) F_c(q)}. \tag{8.3}$$

Here $c(q)$ is the Fourier transform of the direct correlation function between sites on different chains in an equivalent site approximation, which depends on the site-site interaction potential, and ρ is the density of scattering sites. The F_{sol} expression has the interpretation as being the scattering of a dilute or semi-dilute solution with a profile $f(r)$, and will be called solution scattering.

We use Monte Carlo (MC) simulation results for comparing F_{cor} and F_{sol}. The micelle was modelled as a number of semi-flexible chains tethered to a spherical core. Interactions were included by placing six hard spheres of radius $0.1b$ per Kuhn length b of the chains as this reproduces the excluded volume effects found experimentally for polystyrene in a good solvent [24]. Chains were excluded from the core region. The MC moves consisted of pivoting the chain tails [25], and two moves, that moved and reorientated chains on the core surface. We note that chains are not free to move about on the surface of a micelle with a glassy or crystalline core. However, the observed scattering is an ensemble average of all allowed corona configurations, and this includes an average over the location of the chain tethering points, which requires a surface move. The configurational ensemble averages of the F_c, S_{cc}, and A_{cor} scattering contributions were simultaneously sampled during the MC simulations [26]. The unperturbed chain radius of gyration was obtained from a separate set of simulations of a single chain. We chose a reference micelle defined as having $N = 44$ chains, chain length $L = 8.33b$, and core radius $R_{co} = 3.33b$, this choice mimics a Pluronic P85 micelle [8]. We performed three series of simulations, where one of the three parameters was varied in turn, while keeping the remaining two fixed at their reference values. The range of variation was chosen to correspond to a variation of surface coverage σ in the range from 0.01 to about five, thus covering the experimental regime ranging from isolated chains to a reasonable chain overlap. It should be noted that the equilibrium corona configuration does not only depend on the reduced surface coverage but also on the surface curvature R_g/R_{co} and number of chains N.

Comparing (8.1), (8.2), and (8.3) for the sampled scattering contributions allows us to obtain the $-\rho c(q)$ term from the simulation results. We found that it has a weak dependence on q, and as a result we approximate it with an effective excluded volume parameter $\nu(\sigma) \equiv -\rho c(q)$. This converts the PRISM expression (8.3) into the form of a Random Phase Approximation. The excluded volume parameter is related to a virial expansion of the reduced osmotic compressibility as $\nu(\sigma) = 2A_2\sigma + 3A_3\sigma^2 + \ldots = 2A_2(\sigma)\sigma$ where $A_2(\sigma)$ is the reduced apparent second virial coefficient [28]. A_{cor} oscillates around zero, and we have determined $\nu(\sigma)$ from the first zero point of A_{cor}.

The sampled corona scattering from simulations varying the number of chains is shown in fig. 1 normalized such that they coincide for large q values. The huge increase in oscillations as the number of chains increases is caused by the change in weighting between the highly oscillatory inter-chain contribution, and the non-oscillatory intra-chain contribution. Also shown in fig. **??** is the solution scattering. The two sets of curves show an excellent match, which demonstrates the self-consistency of our model of the corona scattering. Similar excellent agreement is obtained for simulations varying length of chains and core radius (not shown). Finally, the fluctuation scattering contribution F_{fluc} is shown. This contribution is seen to decrease with increasing surface coverage, analogous to the concentration dependence of the scattering from a polymer solution, see e.g. [28]. The corona scattering is dominated by profile scattering at low q values, whereas the fluctuation scattering dominates at large q values.

A fluctuation-dissipation theorem relates the Fourier transform of the density fluctuation correlation function to the osmotic compressibility [20]. The reduced osmotic compressibility is given by $\kappa \equiv \frac{\partial \Pi^*}{\partial \sigma} = F_{fluc}(q = 0)^{-1} = 1 + 2A_2(\sigma)\sigma$ where the reduced osmotic pressure is $\Pi^* = \pi R_g^2 \Pi/(k_b T)$. In this expression Π,k_b, and T are the osmotic compressibility, Boltzmann constant, and temperature, respectively. Fig. 2 shows the reduced osmotic compressibility obtained from simulations varying number of chains, chain length, and core radius, and the points fall on an universal curve as function of surface coverage. Similar behaviour have been predicted for polymers at flat interfaces by Carignano and Szleifer for Π^* [5] for $\sigma < 6$. The osmotic compressibility shows a weak dependence of surface coverage for $\sigma < 1$, as one would expect from the dilute polymer solution analogy, see e.g. [25]. The insert of fig. 2 shows the apparent second virial coefficient. The values from the three series of simulations approximately collapse onto a common power law relation: $A_2(\sigma)\sigma = \alpha\sigma^\beta$ with $\alpha = 0.68 \pm 0.01$ and $\beta = 0.95 \pm 0.02$. PRISM theory in the thread limit [23] predicts that $A_2(c/c^*)$ is a constant for low concentrations. We observe a weak dependence on surface coverage in the range of surface coverages we have simulated. At high surface coverages the deviations from power law behaviour observed in the insert of fig. 2 is reflected in the compressibility. We attribute these deviations to effects of chain stretching, which shows some dependence on the surface curvature.

In this paper we have demonstrated that the scattering from a corona of chains tethered to a spherical core for experimentally relevant surface coverages can be self-consistently re-expressed as the scattering one would expect from a quasi two-dimensional dilute/semi-dilute polymer solution confined to a thin

layer on the core surface. We note that the radius of gyration as well as the correlation length are comparable to the corona thickness, which is why the polymer layer can be regarded as being quasi two-dimensional. In the brush limit the chains will be aligned perpendicular to the surface. This is clearly far from the case of a semi-dilute solution, and we expect the RPA expression to break down in this limit. It should be noted that we do not observe any deviations between the corona scattering and the solution scattering even for the largest surface coverages simulated. The expression we have proposed for the solution scattering bridges the gap between the model of Pedersen and Gerstenberg, valid at low surface coverage, and the core-shell models expected to be valid at very high surface coverage, while retaining formal similarities with both models.

We have also demonstrated that the scattering contributions due to the corona profile and fluctuations decouple, allowing us to deduce the osmotic compressibility of the corona from the density fluctuation correlation function. The compressibility shows a universal dependence on surface coverage analogous to that observed for ordinary polymer solutions as function of concentration. We furthermore expect similar expressions to be valid for the scattering from micelles with elliptical and cylindrical cores, however, with some deviations due to the variation of the local surface curvature for such geometrical shapes. The model, we have presented, can be used for separating corona profile and chain-chain correlation information in real experiments, and thus allows more detailed information to be gained by analysis of experimental data.

Bibliography

[1] A. Halperin, M. Tirell, and T. P. Lodge, Adv. Pol. Sci. **100**, 31 (1991).

[2] I. Szleifer and M. A. Carignano, Adv. Chem. Phys **94**, 165 (1996).

[3] P-G. de Gennes, J. Phys. (Paris) **37**, 1443 (1976).

[4] S. Alexander, J, Phys. (Paris) **38**, 983 (1977).

[5] I. Szleifer and M.A. Carignano, Adv. Chem. Phys. **94**, 165 (1996).

[6] M. S. Kent *et al.*, J. Phys. Chem. **103**, 2320 (1995).

[7] M. S. Kent *et al.*, J. Phys. Chem. **108**, 5635 (1998).

[8] J. S. Pedersen and M. C. Gerstenberg, Macromolecules **29**, 1363 (1996).

[9] L. Auvray and P.-G. de Gennes, Europhys. Lett. **2**, 647 (1986).

[10] An empirical model based on the same assumption has been used for describing the dynamics of brushes: P.-G. de Gennes, C. R. Acad. Paris Ser. II **302**, 765 (1986), and B. Farago *et al.*, Phys. Rev. Lett **71**, 1015 (1993).

[11] N. Dan and M. Tirrell, Macromolecules **25**, 2980, (1992).

[12] C. M. Wijmans E. B. Zhulina, Macromolecules **26**, 7214, (1993).

[13] H. Li and T. A. Witten, Macromolecules **27**, 449, (1994).

[14] R. Toral and A. Chakrabarti, Phys. Rev. E. **47**, 4240 (1993).

[15] M. Murat and G. S. Grest, Macromolecules **24**, 704 (1991).

[16] C. M. Marques *et al.*, Eur. Phys. J. B **3**, 353 (1998).

[17] M. Daoud et al., Macromolecules **8**, 804 (1975).

[18] P-G. de Gennes, *Scaling Concepts in Polymer Physics* (Cornell University Press, London, 1979).

[19] S. Förster and C. Burger, Macromolecules **31**, 879 (1998).

[20] G. A. McConnel *et al.*, Faraday Discuss **98**, 121 (1994).

[21] L. Derici *et al.*, Phys. Chem. Chem. Phys. **1**, 2773, (1999).

[22] J. S. Pedersen *et al.*, Macromolecules **33**, 542 (2000).

[23] M. Fuchs and M. Müller, Phys. Rev. E. **60**, 1921 (1999).

[24] J. S. Pedersen, M. Laso and P. Schurtenberger, Phys. Rev. E **54**, 5917 (1996).

[25] M. Lal, Molecular Physics **17**,57 (1969).

[26] C. Svaneborg and J. S. Pedersen, J. Chem. Phys. **112**, 9661 (2000).

[27] H. Benoit and M. Benmouna, Polymer **25**, 1059 (1984).

[28] J. S. Pedersen and P. Schurtenberger, Europhys. Lett. **45**, 666 (1999).

Figures

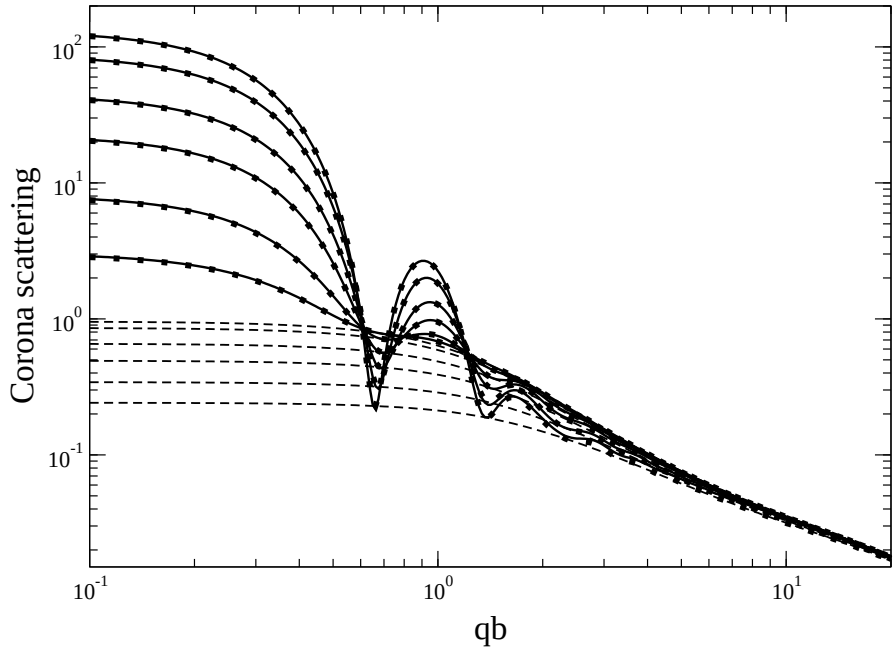

Figure 1: Comparison between corona scattering F_{cor} and solution profile scattering $F_{sol.prof}$ for micelles with number of chains: $N = 3, 8, 22, 44, 87, 131$ (bottom to top). F_{cor} (thick line), $F_{sol.prof}$ (full boxes), and the fluctuation scattering F_{fluc} (thin dashed line). These are normalised such that the single chain scattering coincides in the large q limit.

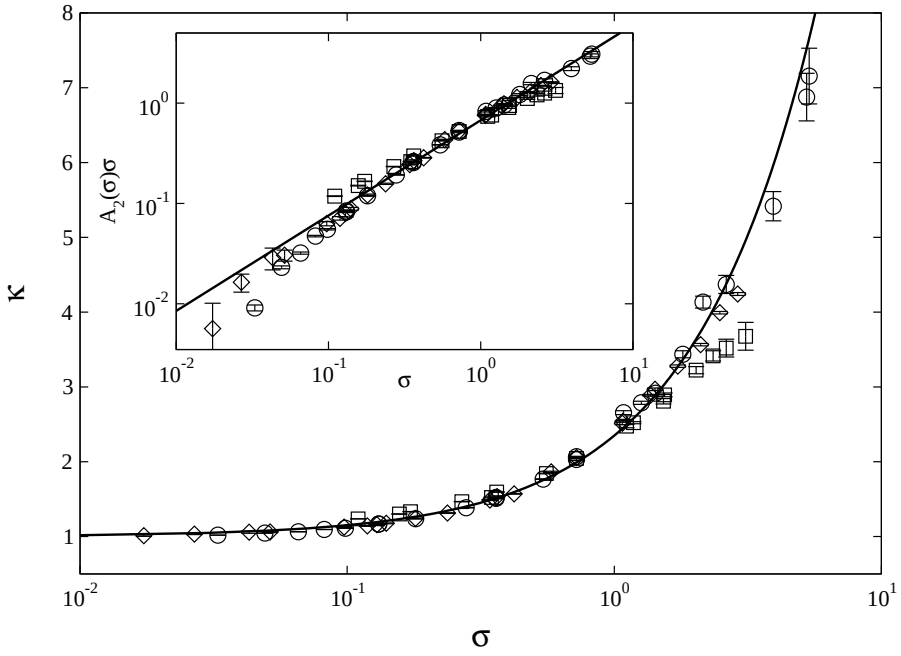

Figure 2: The reduced osmotic compressibility κ plotted against surface coverage for simulations varying number of chains (circle), varying chain length (box), and varying core radius (diamond). The insert shows the $A_2(\sigma)\sigma$ plotted against surface coverage. The line in the insert is the power law $A_2(\sigma)\sigma = 0.675\sigma^{0.95}$ and the corresponding osmotic compressibility is shown as a line in the figure.

Chapter 9

Article III

Form factors of block copolymer micelles with excluded volume interactions of the corona chains determined by Monte Carlo simulations

Carsten Svaneborg and Jan Skov Pedersen*

Condensed Matter Physics and Chemistry Department, Risø national Laboratory, DK-4000 Roskilde, Denmark
*Present address: Department of Chemistry, University of Aarhus, Langelandsgade 140, DK-8000 Aarhus C, Denmark

The scattering of a diblock-copolymer micelle has been simulated using Monte Carlo techniques. The scattering is analysed using a novel model, where the corona is represented as a dilute/semi-dilute polymer solution with a radial profile. This approach decouples the scattering due to interaction and connectivity induced density fluctuations and the average radial profile of the corona. Three different profiles have been used to fit the simulated corona scattering: a box with a Gaussian tail, and two maximum entropy (ME) profiles; chain penetration into the core region is not allowed for any of the profiles. Excellent fits are obtained, especially for a ME profile with three parameters. An excluded volume parameter and the corona compressibility are obtained, and show a strong dependence on surface coverage. The derived expressions for the form factor provides a new approach for analyzing experimental data obtained by neutron or x-ray small-angle scattering for block copolymer micelles with significant intra and inter-chain excluded volume interactions interactions.

This paper has been submitted to Macromolecules.

9.1 Introduction

When a diblock copolymer is dissolved in a solvent which is good of one block and bad for the other block, micelles are spontaneously formed. These micelles have a relatively dense core of the insoluble blocks surrounded by a diffuse corona consisting of the solvated blocks. The core can have various geometric shapes such as spherical, elliptical, or cylindrical, depending on solvent and the length of the polymer blocks [1]. Such micelles provide a model system for studying the interactions between polymer chains tethered to a curved surface [2][3].

Much work have been invested in understanding properties of such systems, as tethering polymers to a surface provide a way of modifying the physical, chemical, and biological properties of surfaces [4][5]. There are numerous studies in the literature of polymers tethered to a flat interface forming a polymer layer, see e.g. [6][7][8][9]. For chains tethered to a convex surfaces such as a sphere the available volume per chain segment will grow rapidly along the chain as segments moves away from the surface, and this has a strong effect on the properties of the polymer layer. The profiles of brushes on convex surface have been examined using variational minimisation of mean field theory [10], self-consistent field theory [11][12][2][3], and simulation techniques such as Monte Carlo and Molecular Dynamics simulations [13][14].

Under good solvent conditions a reduced surface coverage of a flat polymer layer can be defined as $\sigma = \pi R_{go}^2/A'$, where R_{go} is the radius of gyration of an unperturbed polymer chain, and A' is the surface area available per chain (the inverse grafting density). For $\sigma \ll 1$ (the mushroom regime) all chains are essentially isolated. The polymer layer will be laterally inhomogeneous, and the conformation of a single polymer chain depends only on self-interactions and the presence of the surface. The profile of a polymer layer has recently been investigated by renormalization group calculation [15] in the low coverage limit. For $\sigma \gg 1$ (the brush regime) each chain will interact with many neighbouring chains, and chains will stretch away from the surface in an attempt to reduce the excluded volume energy contribution by a reduction of the monomer density, which is achieved by increasing the height of the polymer layer. However, chain stretching will be accompanied by a decrease in the configurational entropy caused by the reduction of the number of possible chain configurations. The height of the polymer layer is determined by the balance of these two effects. In the brush regime the layer will be laterally homogeneous, and the chain stretching will be uniform except at the outer edge of the layer, where there will be some fluctuations due to the increased degrees of freedom of the chain ends [10].

For a spherical micellar core we define specifically the reduced surface coverage as

$$\sigma = \frac{N\pi R_{go}^2}{4\pi(R_{co} + R_{go})^2}. \tag{9.1}$$

Here R_{go} is the unperturbed radius of gyration of the chains, while R_{co} is the core radius, and N is the number of chains. The reduced surface coverage is the packing fraction of chains on the surface, assuming that chains are spherical

objects on the surface of the core. Due to the non-penetration of the chains into the core region the center-of-mass of a chain is displaced a distance about R_{go} from the core surface yielding an effective surface area per chain of $4\pi(R_{co} + R_{go})^2/N$, while the cross-sectional area of a chains is πR_{go}^2.

The topic of the present article is to present results from computer simulations for the scattering from micelles as well as an analysis of the results by a novel semi-empirical model. The model is a generalization of core-shell models that takes the scattering due to density fluctuation correlations into account. The model allows the radial profile, chain radius of gyration, and the corona osmotic compressibility to be obtained from micellar scattering data.

We have performed simulations of the scattering for surface coverages $\sigma < 5$, which correspond to the region of surface coverages experimentally available for copolymer micelles, see e.g. [2][16][17]. The computer simulations have been performed using semi-flexible chains with excluded volume interactions, where chains are excluded from the spherical core region. Monte Carlo simulation techniques (MC) allow us to sample the scattering contributions from the micelle just as in a real experiment using contrast variation techniques, but using a well-defined model for the scattering object, here a micelle. This allows us to test models for the scattering from complex objects using simulation results, and it allows us to correlate the observed scattering to properties of the simulated model system, which will improve the interpretation of experimental scattering data. The simulation results are analysed using a semi-empirical model, which combines expressions for the scattering from a core-shell model with that of a dilute/semi-dilute polymer solution; a similar model have been used by de Gennes for describing the dynamics of brushes at flat interfaces [18][19]. We have used three radial profiles for describing the average radial profile, a box with a Gaussian tail, and two Maximum Entropy profiles [20][21][22], where knowledge of the two or three first momenta of the profile is assumed.

The paper is organised as follows: In section 2 we present a derivation of the model, section 3 presents the Monte Carlo simulations, and the quantities that are sampled during the MC simulations. In section 4 our MC results are presented and discussed, while section 5 contains our analysis and modelling of the data, and our conclusions are summarised in section 6.

9.2 Analytical Models

In a dilute polymer solution polymers are well separated, and as a result the conformation and position of different polymer chains are uncorrelated. The scattering from the solution is given by the single chain form factor, which for an ideal flexible chain is given by $F_{Debye}(x) = 2[x - 1 + \exp(-x)]/x^2$ with $x = (qR_g)^2$, where R_g is the radius of gyration, and q the magnitude of the scattering vector [23]. For $qR_g \gg 1$ the form factor follows a $(qR_g)^{-2}$ power law; this is a reflection of the $< R_{ij}^2 > \propto |i-j|$ scaling relation between the root-mean-square (RMS) distance between two sites on the chain and the contour length of the chain segments connecting the two sites. Topologically the ideal chain is a connected string-like object with a fractal dimension of two, while

actual polymer chains are multi-fractals due to their finite size and the semi-flexibility of the polymer backbone.

The reduced density for a polymer solution is defined as $\Sigma = 4\pi R_{go}^3\rho/3$ (identical to the reduced overlap concentration c/c^*, where c^* is the overlap concentration of a polymer solution), and ρ is the number density of chains. If the reduced density is well below unity, the solution is dilute, and polymers are well separated. If the reduced density is well above unity, the solution is in the semi-dilute regime, where polymers are entangled, forming a transient network of intermeshed chains [24][25]. Using a discrete model with n sites per chain, the scattering from a semi-dilute solution follows the predictions from PRISM theory [26][27], which states that it depends on the single chain scattering and a direct inter-chain correlation function $c(q)$ as

$$F_{PRISM}(q) = \frac{F_{Debye}(q)}{1 - n\rho c(q) F_{Debye}(q)}. \tag{9.2}$$

Here we have neglected the effects of self-avoidance and we do therefore not consider the screening at higher concentrations. Let us assume that the di rect correlation function can be approximated by its low q limit, then $-noc(q)$ can be approximated by an effective concentration dependent excluded volume interaction parameter $\nu(\Sigma)$[27]. This turns the PRISM expression into the form of a Random Phase Approximation (RPA) [28]. Defining the reduced surface compressibility as $\kappa \equiv \partial\Pi^*/\partial\Sigma$, where the reduced osmotic pressure is $\Pi^* = 4\pi R_g^3\Pi/(3k_bT)$ ($\Pi^* = \pi R_g^2\Pi/(k_bT)$ in the case of a two-dimensional system of tethered chains to a surface). Here Π, k_b, and T are the osmotic pressure, Boltzmann constant, and absolute temperature, respectively. The RPA excluded volume interaction parameter can be related to a virial expansion of the reduced osmotic compressibility as $\kappa = 1 + 2A_2\Sigma + 3A_3\Sigma^2 + \ldots = 1 + 2A_2(\Sigma)\Sigma = 1 + \nu$, where the $A_2(\Sigma) = A_2 + 3A_3\Sigma/2 + \ldots$ function defines the apparent second virial coefficient [28]. In the dilute limit the RPA expression reduces to the form factor of an ideal chain, while in the $q \to 0$ limit the inverse forward scattering is $F_{RPA}^{-1}(q = 0) = 1 + \nu = \kappa$ which is expected from a fluctuation dissipation theorem.

A block copolymer micelle consists of a diffuse corona of the dissolved block and a dense core of the insoluable block. The normalised form factor [$F_{micelle}(q = 0) = 1$] of a block copolymer micelle with a homogeneous spherical core can be written in terms of partial scattering contributions as

$$F_{micelle}(q) = \frac{1}{(\beta_{cor} + \beta_s)^2}\left[\beta_s^2\Phi^2(q) + \beta_{cor}^2 F_{cor}(q) + 2\beta_s\beta_{cor}A_{cor}(q)\Phi(q)\right], \tag{9.3}$$

where the three contributions correspond to scattering from the core, the corona, and an interference term between the core and the corona, respectively. The corona and core excess scattering lengths are denoted β_c and β_s, respectively, and they are defined as $\beta_{cor} = NV_{cor}\Delta\rho_{chain}$ and $\beta_s = NV_s\Delta\rho_{core}$, where V_{cor}, V_s, $\Delta\rho_{chain}$, and $\Delta\rho_{core}$ are the volume of a corona and core block, the excess scattering length densities of a corona block, and core block, respectively. A

diblock copolymer micelle has implicitly been assumed, such that N denotes the aggregation number. In this paper the corona, core and corona-core interference contributions to the micelle scattering are normalised to unity in the $q \to 0$ limit. The normalised form factor amplitude of a sphere is given by Rayleigh as $\Phi(qR_{co}) = 3[\sin(qR_{co}) - qR_{co}\cos(qR_{co})]/(qR_{co})^3$, where R_{co} is the radius of the micelle core [29].

Because the core is assumed to be spherical and homogeneous, A_{cor} only depends on the radial distribution of segments $\varphi(r)$, i.e. the corona profile, and A_{cor} will in the rest of the paper be denoted profile scattering. It is given by

$$A_{cor}(q) = \int_0^\infty \mathrm{d}r 4\pi r^2 \frac{\sin(qr)}{qr}\varphi(r). \tag{9.4}$$

If the single chain scattering contribution is neglected as well as correlations due to density fluctuations caused by chain-chain interactions, the corona scattering is given by $F_{cor} = A_{cor}^2$. This is the approximation that yields a core-shell model of the micellar scattering[30], which is the scattering from a configurationally averaged micelle, rather than the configurationally averaged scattering from a micelle, which is the scattering observed experimentally. As single chain scattering is neglected, a core-shell model is unable to reproduce the characteristic single chain power law decay at large q values, which is a signature of the chain connectivity, nor is a core-shell model able to represent the finite scattering observed in the minima where $A_{cor}(q) = 0$. Only in the limit $\sigma \gg 1$ where the density of chains is very high, e.g. when the corona is in the brush regime, do we expect these fluctuations to be sufficiently suppressed for core-shell models to give a reasonable description.

For a micelle the corona scattering is the sum of two contributions: a contribution from the intra-chain scattering $F(q)$ (proportional to the number of chains N), and inter-chain scattering $H(q)$ (proportional to the number of different pairs of chains $N(N-1)$). The normalised $[F_{cor}(q=0) = 1]$ corona scattering is thus given by

$$F_{cor}(q) = \frac{F(q)}{N} + \frac{N-1}{N}H(q). \tag{9.5}$$

The separation of the corona scattering into inter-chain and intra-chain scattering contributions is somewhat arbitrary. Another way of separating the corona scattering is in terms of the scattering from the configurationally averaged radial profile, and from the correlations of the density fluctuations [31][32] about this average profile. The scattering due to the radial profile is given by A_{cor}^2 as in a core-shell model. The density fluctuation correlation function depends on chain interactions and chain connectivity, and we model this by the scattering from a two dimensional dilute/semi-dilute solution using the RPA approximation:

$$F_{sol.prof}(q) = \frac{F_{RPA}(q)}{N} + \frac{N - F_{RPA}(q=0)}{N}A_{cor}^2(q). \tag{9.6}$$

Here the weighting of the two terms has been adjusted to account for the fact that scattering have been shifted from the profile scattering contribution into the

fluctuation scattering contribution, and the fluctuation scattering contribution is not normalized. This expression for the corona scattering has separated the total scattering into a term that only depend on the scattering from a single chain and an excluded volume parameter, and a term that only depends on the radial profile of the corona, and can be interpreted as being the scattering one would observed from a polymer solution with a particular radial profile being confined to the micellar surface. The first term is denoted the fluctuation scattering in the rest of this paper, while the second term is denoted profile scattering.

9.3 Monte Carlo Simulation

We have performed Monte Carlo (MC) simulations on block copolymer micelles [33]. Micelles was modeled as a spherical core with a number N of semi-flexible chains tethered to it, where each chain consists of n bonds of length l_0. The valence angle between segments was fixed at 135.585 degrees, which yielded a Kuhn length $b = 6l_0$ such that the semi-flexible chain reproduces the radius of gyration of a flexible chain in the long chain limit. The excluded volume interaction was simulated by placing six hard spheres along each Kuhn length of the chain. The radius of the hard spheres was fixed at $0.1b$, which is known to reproduce the binary cluster integral of polystyrene in a good solvent [35]. The MC moves consisted of pivoting the individual chains [36], and two surface MC moves, that moved and reorientated chains on the micelle surface. These were performed by pivoting the entire chain about the core center or the tether vertex, respectively. Configurations where a chain was found to overlap with other chains or the core region were rejected. We used the "zippering" algorithm [37] when checking for chain overlap, taking into account the semi-flexibility of the chains, and taking care to avoid introducing local stiffness by allowing neighbouring vertices along the chain to overlap. The initial micelle configuration was constructed using slightly stretched chains, which were grown while avoiding overlaps. This initially biased configuration was equilibrated by performing MC moves until the number of accepted moves was in excess of one hundred times the number of degrees of freedom in the model. The three parameters controlling the step size of the MC moves were adjusted during the equilibration stage to yield approximately 50% acceptance probability for each of the three moves.

The chain was periodically reconstructed after every 50000 pivot moves using the tabulated dihedral angles to avoid the build up of numerical errors due to the many repeated rotations needed to sample the micellar configurations space. This was made possible because each chain carries a virtual zeroth segment around with it, and the zeroth segment and the first segment, define a coordinate system in which it is easy to add another segment with a specific dihedral angle, valence angle, and segment length. This procedure, when iterated, uniquely reconstructs the chain based on a table of dihedral angles, a table which was created during chain formation, and which was updated each time a pivot move was accepted. This is a cheap and effective operation compared to solving 3 linear equations for each segment as in the chain correction algorithm of Stell-

man and Gans [36], and also provides an easy way of creating the initial chain configuration. The deviation between the actual and expected dihedral angle was constantly below 3×10^{-12} during the simulation of the longest chain (229 segments), with deviations in segment length and valance angle below about a third of that. During a MC simulation the configuration was sampled for every 1000 attempted MC steps, and a simulation consisted of 100 blocks, each block being the average of 100 samples. Error bars was derived by analysing the fluctuations of the block averages.

During MC simulations the radial density profiles $\varphi(R_j)$ were sampled in a number of bins at radii R_j as the number of vertices lying in a spherical shell centered on the core with outer radius $(R_j + R_{j+1})/2$ and inner radius $(R_{j-1} + R_j)/2$. Each bin was normalised by the volume of that spherical shell. We sampled the radius of gyration of the individual chains defined as

$$R_g^2 = \left\langle \frac{1}{(n+1)N} \sum_i^N \sum_k^{n+1} (\mathbf{R}_{cm,i} - \mathbf{r}_{ik})^2 \right\rangle \quad \text{with} \quad \mathbf{R}_{cm,i} = \frac{1}{n+1} \sum_k^{n+1} \mathbf{r}_{ik}, \tag{9.7}$$

where $\mathbf{r}_{ik}$ is the position of the k'th vertex on the i'th chain. N is the number of chains and $n+1$ is the number of vertices/scattering sites. The scattering from the micelle corona is given by the scattering from the set of vertices and core as

$$F_{micelle}(q) \propto \left\langle \left| \beta_{cor} \sum_i^N A_i + \beta_s \Phi \right|^2 \right\rangle, \tag{9.8}$$

where the form factor amplitude of the i'th chain is

$$A_i(\mathbf{q}) = \frac{1}{N(n+1)} \sum_k^{n+1} e^{i\mathbf{q}\cdot\mathbf{r}_{ik}}. \tag{9.9}$$

Since the micelle core is assumed to be spherical and homogeneous, the core form factor amplitude Φ is real and can be moved outside the configurational and orientational average. The remaining configurational averages can be compared to the corresponding terms in (9.3). The normalised corona scattering and the profile scattering can be identified as

$$F_{cor}(q) = \frac{1}{N^2} \left\langle \left| \sum_i^N A_i \right|^2 \right\rangle, \tag{9.10}$$

and

$$A_{cor}(q) = \frac{1}{N} \left\langle \mathrm{Re} \sum_i^N A_i \right\rangle. \tag{9.11}$$

In this notation the single chain scattering and inter-chain scattering can be written as the sum of diagonal and off-diagonal members of (9.10) as:

$$F(q) = \frac{1}{N} \left\langle \sum_i^N |A_i|^2 \right\rangle \quad \text{and} \quad H(q) = \frac{1}{N(N-1)} \left\langle \sum_{i \neq j}^N A_i A_j^* \right\rangle. \tag{9.12}$$

Comparing these equations to (9.10) demonstrates the weighting used in the expression for corona scattering (9.5). The averages consist of a configurational as well as a orientational average. These were performed using MC sampling, and by evaluation of the scattering for 13 directions for each q value, and choosing a new set of random directions each time a block of 100 samples was completed. The set of q values were chosen as approximately logarithmic distributed, but slightly tweaked such that many q values are the sum of two smaller q values, or twice another q value. This converted many of the complex exponentials needed to evaluate (9.9) into simple products and squares of previously calculated complex numbers. This method of sampling yields a significant optimisation of the sampling of micellar scattering [33].

9.4 Results and Discussion

We have chosen a reference micelle defines as having $N = 44$ chains, chain length $L = 8.33b$, and core radius $R_{co} = 3.33b$, as this mimics the configuration of the Pluroic P85 micelles [106]. We use the Kuhn length b as a length scale. We have performed three series of simulations where one of the parameters N, L, and R_{co} was varied while keeping the remaining two fixed at their reference values. The range of variation was chosen to correspond to a variation of surface coverage in the range from 0.01 to five, covering the experimentally accessible regime for copolymer micelles [2][16][17].

Figure 1 shows the corona scattering for simulations where the number of chains is varied. A qualitative examination shows a huge decrease of scattering at high q values relative to the scattering at low q values as the number of chains is increased, while the amplitude of the first subsidiary oscillation increases and higher-order oscillations progressively become more pronounced. This is caused by the weighting between the highly oscillatory inter-chain scattering $H(q)$, and the non-oscillatory intra-chain scattering $F(q)$. The scattering is dominated by single chain scattering and its $1/N$ dependence at high q values, while the rapidly decaying profile scattering contribution dominates at low q values. The minima of the corona scattering correspond to q values where $A_{cor}(q) = 0$, and in those minima the scattering intensity is given solely by the chain scattering F.

Figure 2 shows the corona scattering corresponding to simulations where the core radius is decreased for fixed number of chains and core radius. Decreasing the core radius, causes the oscillations due to the radial profile to shift towards larger q values. Simultaneously the oscillations are reduced as the inter-chain scattering becomes progressively less dominant compared to the chain scattering $F(q)$, which is essentially unchanged by a decrease in core radius.

The logarithm of the absolute value of the profile scattering is shown in figures 3 and 4. Each sign change gives rise to an inverted peak due to the logarithm. A qualitative examination shows that increasing the number of chains has only a slight effect on the profile scattering i.e. the corona profile, as the first inverted peaks are shifted slightly towards smaller q values indicating a slight increase of the corona width. As the core radius is decreased a huge shift is seen in the shift of the oscillations towards larger q values shown in figure

4, which indicates that varying core radius has a large impact on the corona profile. Simulations where the chain length is increased will display similar effects as those where the core radius is decreased, as this provides two opposite mechanisms of controlling the surface curvature, which can be quantified by the dimensionless ratio of the radius of gyration to core radius. A broadening of the first subsidiary and second subsidiary oscillation is observed in figure 3 and 4, and this is attributed to effects of surface coverage and surface curvature, respectively, on the shape of the corona profile.

Figure 5 shows the reduced density profiles sampled during the simulations, where the number of chains, or core radius was varied. Simulations varying the chain length yields the same reduced density profile as simulations varying the core radius, as these simultaneously varies the surface coverage and curvature in a similar manner. The reduced density profiles are defined as $\varphi'(r') = \varphi(r')/C$ where $C = \int \varphi(r')dr'$ is an area normalisation constant, and the reduced radius is defined as $r' = (r - R_{co})/(\langle r \rangle - R_{co})$, where $\langle r \rangle = \int r\varphi(r)\, 4\pi r^2 \mathrm{d}r$ is the first moment of the simulated profile. This representation shows the change of the profile shape rather than the change of the profile itself.

At low surface coverage all profiles indicate a depletion zone close to the core, however, no depletion zone is present when the surface coverage is increased above unity. At sufficiently large surface curvatures the $\varphi(r) \propto r^{-4/3}$ scaling behaviour predicted by Halperin [24] is clearly observed in the vicinity of the core surface, however, further away from the core the radial profiles decay faster than predicted by Halperin, which is due to the finite length of the simulated chains. Upon variation of the number of chains, the profile only shows a dependence on the number of chains for surface coverages above unity, indicating that chain interactions are negligible for surface coverages below unity. The profile for simulations where the chain length is varied shows a large change of shape. This is due to the fact that the effective surface curvature R_g/R_{co} is simultaneously increased.

9.5 Analysis and modelling of the results

For a quantitative analysis of the simulated chain scattering, two parameters are required for the chain scattering, namely the radius of gyration R_g , and the excluded volume parameter in the RPA expression, which is assumed to be a function of the surface coverage $\nu(\sigma)$. We have assumed that the excluded volume coefficient only depends on the reduced surface coverage, in analogy with an ordinary polymer solution where it is a function of the reduced density Σ as shown in the theory section. We have simulated semi-flexible chains, as this provides a relatively realistic model for real polymer chains. The simple RPA expression is modified using a Daniels form factor in the denominator [55], which takes the semi-flexibility of the chains into account in an approximate manner, while we retain the Debye form factor in the numerator of the RPA expression. Simulations have shown, that this provides a quite accurate expression for the scattering from semi-dilute solutions of semi-flexible polymers [40]. The full

expression for the fluctuation scattering contribution is

$$F_{RPA}(qR_g) = \frac{F_{Daniels}\left(\frac{q^2R_g^2}{e(L/b)}\right)}{1+\nu(\sigma)F_{Debye}(q^2R_g^2)}, \tag{9.13}$$

$$F_{Daniels}(x) = F_{Debye}(x) + \frac{b}{15L}\left(4+7x^{-1}-(11+7x^{-1})e^{-x}\right),$$

$$F_{Debye}(x) = \frac{2[x-1+\exp(-x)]}{x^2},$$

and

$$e(n) = 1 - \frac{3}{2n} + \frac{3}{2n^2} - \frac{3}{4n^3}\left(1-e^{-2n}\right).$$

Here $e(n)$ is a correction to the radius of gyration of the Daniels expression due to the finite number of statistically independent segments in our simulations [41]. The profile scattering A_{cor} is the Fourier transform of the radial profile, and requires an expression for the radial monomer profile $\varphi(r)$. To our knowledge, no theoretical expressions exist for the radial density profiles of spherical micelles in the low to medium coverage limit, which we explore in the present paper. As a result we use three empirical profiles, all of which are generalisations of a Gaussian distribution.

The first profile we use is a box with a Gaussian tail, abbreviated BoxGauss profile, which is defined as follows

$$\varphi(r) = \begin{cases} 0 & r < R_{co} \\ B & R_{co} \le r < R_{ch} \\ B\exp\left[-(r-R_{ch})^2/(2s^2)\right] & R_{ch} \le r \end{cases}.$$

Here $B^{-1} = \int \varphi(r) 4\pi r^2 \mathrm{d}r$ is a normalisation constant, R_{ch} is the outer edge of the box, and s defines the length scale on which the Gaussian tail decays. The normalised scattering from this profile is given by:

$$A_{cor}(q,s,R_{ch}) = \frac{S_g(q,s,R_{ch}) + V(R_{ch})\Phi(qR_{ch}) - V(R_{co})\Phi(qR_{co})}{V_o + V(R_{ch}) - V(R_{co})}. \tag{9.14}$$

Here $\Phi(qR)$ is the normalised form factor amplitude for a homogeneous sphere with a volume $V(R) = 4\pi R^3/3$. And the normalised scattering contribution of the half-Gaussian is

$$S_g(q,s,r) = \left\{qr\left(4rs + \sqrt{2\pi}(r^2+s^2)\right)\right\}^{-1} \times$$

$$\left\{2rs\sin(qr) + \sqrt{2\pi}\exp(-\frac{(qs)^2}{2})\left(qrs^2\cos(qr) + r^2\sin(qr)\right)\right.$$

$$+2\sqrt{2}D[\frac{qs}{\sqrt{2}}]\left(r^2\cos(qr)-qrs^2\sin(qr)\right)\Big\},$$

while the corresponding volume of the Gaussian profile is

$$V_g(s,r)=2\pi s\left(4rs+\sqrt{2\pi}(r^2+s^2)\right)$$

The Dawson integral is given by $D[y]=\exp(-y^2)\int_0^y\exp(t^2)\mathrm{d}t$ and a numerical expression for this integral is given in Numerical Recipes [46]. An expression for the scattering from a Gaussian-shaped profile has previously been reported by H. Bagger-Jörgensen et al. [42], however, the published expression contains errors.

We also use two maximum entropy (ME) [20][21][22] profiles for analysing the data. These profiles are based on the assumptions that no chains enter the micellar core, such that $\varphi(r)=0$ for $r<R_{co}$. We furthermore assume knowledge of the first two or three momenta of the profile. In general assuming knowledge of the first m momenta of profile leads to an entropy functional

$$S[\varphi]=\int_{R_{co}}^{\infty}\mathrm{d}r4\pi r^2\varphi(r)\left(-K\ln\varphi(r)+\sum_{n=0}^{m}\lambda_n r^n\right),$$

where a uniform prior is assumed. Here λ_n is a set of Lagrange multipliers to ensure the $m+1$ constraints of the momenta of the distribution $\varphi(r)$. The zeroth constraint ensures normalisation. Upon variation of the entropy functional it is seen that the maximum entropy profile can be written as

$$\varphi^m(r;a_1,\ldots,a_m)=\begin{cases}0 & r<R_{co}\\ B\exp\left[-\sum_{n=1}^{m}a_n(r-R_{co})^n\right] & r\geq R_{co}\end{cases},$$

where B is a normalisation constant, and the set of a_n's are related to the Lagrange multipliers. We take these as fit parameters when fitting the scattering. For $m=2$ the normalised profile scattering produced by this profile, hence denoted the ME2 profile, can be worked out for $a_2>0$. This yields

$$A_{cor}(q,a_1,a_2)=$$

$$\frac{4a_2^{3/2}\sin(qR_{co})+2a_2\sqrt{\pi}Re\left\{\mathrm{Erfc}(x+iy)\exp(x^2-y^2)(q+ib)e^{ic}\right\}}{\sqrt{\pi}(2a_2+b^2)q\mathrm{Erfc}(x)\exp(x^2)-2\sqrt{a_2}\,(a_1-4a_2R_{co})\,q},\qquad(9.15)$$

where $b=2a_2R_{co}-a_1$, $c=2xy-qR_{co}$, $x=a_1/(2\sqrt{a_2})$, and $y=q/(2\sqrt{a_2})$. $\mathrm{Re}\{z\}$ is the real part of the complex number z, and $\mathrm{Erfc}(z)$ is the complementary error function of complex argument; an expression for $\mathrm{Erfc}(x+iy)\exp(x^2-y^2)$ is also given in the appendix. In the limit of $R_{ch}\to R_{co}$ and $a_1\to 0$ both profiles converges towards a simple Gaussian profile, and the two scattering expressions (9.14) and (9.15) are identical.

We have also used a ME profile with $m = 3$ denoted the ME3 profile. The profile scattering was obtained by numerical Fourier transformation of the profile. The profile was represented by 500 piecewise linear segments in the range from R_{co} to $R_{co} + 6R_g$, and an analytical expression for the Fourier transform was used for the scattering from each segment.

The corona and profile scattering obtained from the MC simulations using (9.10) and (9.11) were fitted simultaneously by the corresponding theoretical expressions (9.6) and (9.4), where we model the fluctuation scattering by (9.13), and we model the profile by one of the three profiles: box with a Gaussian tail (abbreviated BoxGauss), and a maximum entropy profile assuming knowledge of the first two or three momenta (abbreviated ME2 and ME3). The fit parameters for the fluctuation scattering are the radius of gyration R_g and the excluded volume coefficient ν. The fit parameters for the radial profiles are R_{co} and s for the BoxGauss profile, while the first two or three a_n parameters are fitted for the two ME profiles. The fit range for the profile scattering was $qb < 10$ and $qb < 4$ for the corona scattering. The latter range is dictated by the fact that the Daniels expression is not valid for larger values of qb, as it fails to reproduce the rigid rod scattering behaviour observed at large q values.

The results of fitting the model using the three profiles to the simulation results for the corona scattering and profile scattering are shown in figures 1-4. For $\sigma < 1$ all the fits have reduced chi-square value [43] $\chi^2_{red} < 5$, except for the simulations with the shortest chains $L = 2b$ and $L = 4b$ which have a $\chi^2_{red} < 30$. These large values are due to the fact that the Daniels distribution is not valid for chains with so few statistical segments. In the $\sigma < 1$ range the ME2 and ME3 profiles are identical since the a_3 parameter is estimated to zero within the statistical errors for the ME3 profile. For simulations with very large core radii both ME fits consistently have somewhat smaller χ^2_{red} values compared to the BoxGauss profile fits, however, for simulations with a low aggregation number, all three profiles provide fits of similar quality. The agreement between model and simulation data is excellent for surface coverage $\sigma < 1$ for all three profiles. However, for $\sigma > 1$ the fits provided by the ME2 profile are comparable to those using the BoxGauss profile, while the ME3 profile consistently provides significantly better fits, where χ^2_{red} is reduced by at least an order of magnitude. This vast improvement can be understood by observing the deviations shown in the high q part of corona scattering shown in figure 1 and 2 for the largest surface coverage. These deviations are caused by the inability of the profile in representing the actual profile scattering, as shown in figure 3 and 4, where the ME3 profile can be seen to give a much better fit to the profile scattering compared to the BoxGauss and ME2 profiles.

Profiles obtained by fitting the scattering and profiles sampled during the simulation are shown in figure 5 and 6. They have been plotted using the scaling transformation of the corresponding simulation profile to avoid introducing artifacts when comparing the two scaled profiles. For low surface coverages the fitted profiles are very similar, and show a good agreement with the simulated profiles. For high surface coverages the ME3 profile give significantly better estimates than the two other profiles. These deviations at high surface coverages are reflected in the deviations in the profile scattering shown in figures 3-4. The

deviations in the vicinity of the core do not appear to have any effect on the profile scattering.

For $\sigma < 1$ fitting the three profiles yields identical estimates of the radius of gyration and the excluded volume parameter, while for $\sigma > 1$ significant deviations are observed between the estimates provided by fitting the three model expressions. These are caused by the inability of the BoxGauss and ME2 profiles in fitting the sampled profile scattering and corona scattering at high q values. Both the radius of gyration and the excluded volume parameter are estimated from the corona scattering at high q values, and as a result of this we only report the results obtained from the fits using the ME3 profile.

The radius of gyration obtained from the simulations is shown in figure 7. For the simulations where the surface coverage is increased by increasing the number of chains or decreasing the core radius show a radius of gyration with a similar dependence on surface coverage. Radius of gyration estimated by the fits is also shown, and they are in good agreement with the simulations results with less than 2% deviation for simulations with a low number of chains or large core radius. Larger deviations (12% for the highest surface coverage) are apparent for simulations with long chains.

The insert in Figure 8 shows the $\nu(\sigma)$ parameters obtained from fits using the ME3 profile. While this parameter also depends on the surface coverage and the number of chains, the points from simulations varying number of chains, core radius, and chain length collapse on the same curve, which shows a power law dependence on surface coverage. The power law is $\nu(\sigma) = \alpha\sigma^{\beta}$ with $\alpha = 1.42 \pm 0.03$ and $\beta = 1.04 \pm 0.02$. The simulations with the shortest chains can be observed to deviate from this behaviour, which we attribute to the Daniels form factor not being valid for such short chains. Previously we have analysed the scattering data using a self-consistent approach [44], where the single chain scattering, sampled using (9.12) during MC simulations, was used in numerator and denominator in the RPA expression (9.13). $\nu(\sigma)$ was derived by equating (9.5) and (9.6) in the first minima of the profile scattering where $S_{ch}(q) = 0$, and a power law behaviour with $\alpha = 1.35 \pm 0.02$ and $\beta = 0.95 \pm 0.02$ was found. This indicates that while $\nu(\sigma)$ shows a simple power law relation on σ, the corresponding constant and exponent shows a weak dependence on the particular expressions used for the chain and profile scattering.

The forward scattering due to density fluctuations is related to the osmotic compressibility κ through a fluctuation dissipation theorem, which states that the osmotic compressibility is inversely proportional to the $q \to 0$ limit of the Fourier transform of the density fluctuation correlation function. For a polymer solution the observed scattering is due to density fluctuations, and as a result it is easy to obtain the osmotic compressibility by extrapolating the observed scattering to the $q \to 0$ limit. For a micellar corona the scattering at low q values is dominated by profile scattering due to the average radial profile. Thus the profile scattering dominates the scattering due to the density fluctuations, making a simple extrapolation impossible, however, by modelling the profile and fluctuation scattering separately as we have done in this paper is is trivial to obtain the $q \to 0$ limit of the fluctuation scattering contribution as $\kappa(\sigma) = F_{RPA}^{-1}(q = 0) = 1 + \nu(\sigma)$ just as for a polymer solution [24]. The osmotic

compressibility is shown in figure 8, the osmotic compressibility can be seen to follow a universal dependence on the surface coverage except for high surface coverages where deviations due to a dependence on the number of chains and surface curvature can be seen.

9.6 Conclusions

We have presented Monte Carlo simulation results performed on the scattering from a micelle as function of number of chains, chain length, and core radius. We have, furthermore, presented a novel empirical model expressions for the scattering from block copolymer micelle with a spherical core and that includes the effects of excluded volume interactions. The corona scattering is represented as a sum of scattering contributions due to the average radial density profile and the density fluctuations correlations about this profile. We model the fluctuation contribution to the scattering as that of a dilute/semi-dilute polymer solution. The proposed model depends on the radius of gyration, an excluded volume parameter, which is proportional to the apparent second virial coefficient, and an expression for the radial profile of the micellar corona. To our knowledge, there is no theoretical expression available for the radial profile except in the high curvature limit. We used three empirical expressions for the corona profile, one with a box with a Gaussian tail and two maximum entropy estimates where knowledge of the two or three first momenta was assumed. The model expressions for the corona scattering and profile scattering were simultaneously fitted to the scattering obtained directly from the MC simulations. These fits show an excellent agreement for low surface coverages $\sigma < 1$ for all three profiles, while the ME3 profile shows an excellent agreement also for $\sigma > 1$, where the BoxGauss and the ME2 profile show significant deviations at high q values for the corona scattering. These deviations are caused by the fact that the BoxGauss and ME2 profiles provide a poor represention of the actual corona profile. This is reflected in the estimates of radius of gyration and the excluded volume parameter by these two models, as these are estimated from the high q behaviour of the corona scattering where the fluctuation scattering dominates. For $\sigma < 1$ all profiles provides identical estimates for the radius of gyration and excluded volume parameter. Besides providing estimates for the radius of gyration and the excluded volume parameter, the fits also provide estimates for the radial profile, which can be compared to the actual radial profiles obtained from the MC simulation.

Profiles obtained by fitting the simulated scattering are in good agreement with the profiles obtained directly from simulations, except for small deviations close to the core. For $\sigma < 1$ the three profiles obtained from the fits of the simulated scattering are very similar, however, at high surface coverages, the ME3 profile yields a significantly better estimate for the radial profile.

The fits yields estimates of the radius of gyration which are in good agreement with the radius of gyration obtained directly from simulations. Plotting the excluded volume parameter against reduced surface coverage for simulations varying chain length, number of chains and core radius shows that the results

approximately fall on a common curve corresponding to a power law behaviour. However, the coefficients and exponents are slightly different from those we have previously obtained through a self-consistent analysis, where simulation results for the single chain scattering were used in the RPA expression for the corona scattering, thus forming a complete self-consistent expression for the corona scattering. This suggests that the power law behaviour is sensitive to the model expressions used for fitting the scattering.

We have shown that the effects from chain connectivity and excluded volume interactions between tethered chains on the scattering of a micelle with a spherical core can be described by a relatively simple model, where the corona is modelled as a dilute/semi-dilute solution with a particular radial profile. We note that this method of including connectivity and excluded volume interactions effects in the scattering from colloidal aggregates can be generalised to geometries such as micelles with elliptical and cylindrical cores. The models of the scattering from colloidal aggregates presented in the present paper allows more accurate and detailed information to be obtained from the analysis of experimental results. We are currently applying the expressions in the analysis of small-angle neutron contrast variation data and small-angle x-ray scattering data for micelles of polystyrene-polyisoprene in decane. The results will be presented in a future article.

9.7 Appendix

The real and imaginary parts of $G(x,y) = \exp(x^2 - y^2)\mathrm{Erfc}(x + iy)$ can be separated into real and imaginary parts using an infinite series approximation [45]

$$\begin{aligned} G(x,y) = \quad & e^{x^2-y^2}\mathrm{Erfc}(x) - \tfrac{e^{-y^2}}{2\pi x}\cos(2xy) - \tfrac{2}{\pi}\textstyle\sum_{n=1}^{\infty} \tfrac{e^{-\frac{n^2}{4}-y^2}}{n^2+4x^2} f_n(x,y) \\ & + i\left\{ -\tfrac{e^{-y^2}\sin(2xy)}{2\pi x} - \tfrac{2}{\pi}\textstyle\sum_{n=1}^{\infty} \tfrac{e^{-\frac{n^2}{4}-y^2}}{n^2+4x^2} g_n(x,y) \right\}, \end{aligned}$$

where

$$\begin{aligned} f_n(x,y) &= 2x - 2x\cosh(ny)\cos(2xy) + n\sinh(ny)\sin(2xy) \\ g_n(x,y) &= 2x\cosh(ny)\sin(2xy) + n\sinh(ny)\cos(2xy) \end{aligned} .$$

Here $\mathrm{Erfc}(x)$ is the real complimentary error function. An expression for it is given in Numerical Recipes [46]. Evaluation of the two auxiliary functions f_n and g_n can be optimised using the addition formulae in which case only $\cosh(y)$ and $\sinh(y)$ need to be evaluated, and subsequent evaluations of $\cosh(ny)$ and $\sinh(ny)$ require only a few simple arithmetic operations of precalculated constants.

Bibliography

[1] Mortensen K.; Pedersen, J.S. *Macromolecules* **1993**, 26, 805.

[2] McConnel, G.A.; Lin, E.K.; Gast, A.P.; Huang, J.S., Lin, M.Y., Smith, S.D.; *Faraday Discuss.* **1994**, 98, 121.

[3] Gast, A.P. *Langmuir* **1996**, 12, 4060.

[4] Szleifer, I.; Carignano, M.A. *Adv. Chem. Phys.* **1996**, 94, 165.

[5] Halperin, A.; Tirrell, M.; Lodge, T.P., *Adv. Polym. Sci.* 1992, 100, 31.

[6] Carignano, M.A.; Szleifer, I. *J. Chem. Phys.* **1993**, 98, 5006.

[7] Carignano, M.A.; Szleifer, I. *Macromolecules* **1995**, 28, 3197.

[8] Carignano, M.A.; Szleifer, I. *J. Chem. Phys.* **1994**, 100, 3210.

[9] Netz, R.R.; Schick, M. *Macromolecules* **1998**, 31, 5105.

[10] Li, H.; Witten, T.A. *Macromolecules* **1994**, 27, 449.

[11] Dan, N.; Tirrell, M. *Macromolecules* **1992**, 25, 2890.

[12] Wijmans, C.M.; Zhulina, E.B. *Macromolecules* **1993**, 26, 7214.

[13] Toral, R.; Chakrabarti, A. *Phys. Rev. E* **1993**, 47, 4240.

[14] Murat, M.; Grest, G.S. *Macromolecules* **1991**, 24, 704.

[15] Adamuti-Trache, M.; McMullen, W.E.; Douglas, J.F. *J. Chem. Phys.* **1996**, 105, 4798.

[16] Derici, L.; Ledger, S.; Mai, S-M.; Booth, C. Hamley, I.W.; Pedersen, J.S. *Phys. Chem. Chem. Phys.* **1999**, 1, 2773.

[17] Pedersen, J.S.; Hamley, I.W.; Ryu. C.Y.; Lodge. T.P. *Macromolecules* **2000**, 33, 542.

[18] de Gennes P-G., *C. R. Acad. Paris Ser.* II, **302** (1986) 765.

[19] Farago, B.; Monkenbusch, M.; Richter, D.; Huang, J.S.; Fetters L.J.; Gast, A.P. *Phys. Rev. Lett.* **1993**, 71, 1015.

[20] Gilmore, C.J. *Acta Cryst.* **1996**, A52, 561.

[21] Bricogne, G. *Acta Cryst.* **1984,** A40, 410.

[22] Jaynes, E.T. *Phys. Rev.* **1957**, 106, 620.

[23] Debye, P. *J. Phys. Colloid. Chem.* **1947**, 51, 18.

[24] Daoud, M.; Cotton, J.P.; Farnoux, B.; Jannink, G.; Sarma, G.; Benoit, H.; Duplessix, R.; Picot, C.; de Gennes, P.G. *Macromolecules* **1975**, 8, 804.

[25] de Gennes, P.G. *Scaling Concepts in Polymer Physics;* Cornell University Press: Ithaca, New York, 1979.

[26] Schweizer K.S.; Curro J.G., *Adv. Polym. Sci.* **1994**, 116, 319.

[27] Fuchs, M.; Müller, M. *Phys. Rev. E* **1999**, 60, 1921.

[28] Benoit, H.; Benmouna, M.; *Polymer* **1984**, 25, 1059.

[29] Lord Rayleigh *Proc. Roy. Soc. London* **1911**, A84, 25.

[30] Förster, S.; Burger, C. *Macromolecules* **1998**, 31, 879.

[31] Auvray, L.; de Gennes, P.G.; *Europhys. Lett.* **1986**, 2, 647.

[32] Cosgrove, T.; Heath, T.G.; Ryan, K.; Crowley, T.L. *Macromolecules* **1987**, 20, 2879.

[33] Svaneborg, C.; Pedersen, J.S. *J. Chem. Phys.* **2000**, 112, 9661.

[34] Pedersen, J.S.; Gerstenberg, M.C. *Macromolecules* **1996**, 29, 1363.

[35] Pedersen, J.S.; Schurtenberger, P. *Macromolecules* **1996**, 29, 7602.

[36] Stellman, S.D.; Gans, P.J. *Macromolecules* **1972**, 5, 516.

[37] Stellman, S.D.; Froimowitz, M.; Gans, P.J. *J. Comput. Phys.* **1971**, 7, 178.

[38] Halperin, A. Macromolecules **1987**, 20, 2943.

[39] Burchard, W.; Kajiwara, K. *Proc. Roy. Soc. London* **1970**, A316, 185.

[40] Pedersen, J.S.; Schurtenberger, P. *Europhys. Lett.* **1999**, 45, 666.

[41] Benoit, H.; Doty, P. *J. Phys. Chem.* **1953**, 57, 958.

[42] Bagger-Jörgensen, H.; Olsson, U.; Mortensen, K. *Langmuir* **1997**, 13, 1413.

[43] Pedersen, J.S. Adv. Colloid Interface Sci. **1997**, 70, 171.

[44] Svaneborg, C.; Pedersen, J.S. submitted *to Phys. Rev. E.*

[45] Abramowich, M.; Stegun, I.A *Handbook of mathematical functions; Dover, 1965.* eq. 7.1.29.

[46] Press, W.H.; Teukolsky, S.A.; Vetterling, W.T.; Flannery B.P. *Numerical Recipes*; University press, Cambridge 1992.

Figures

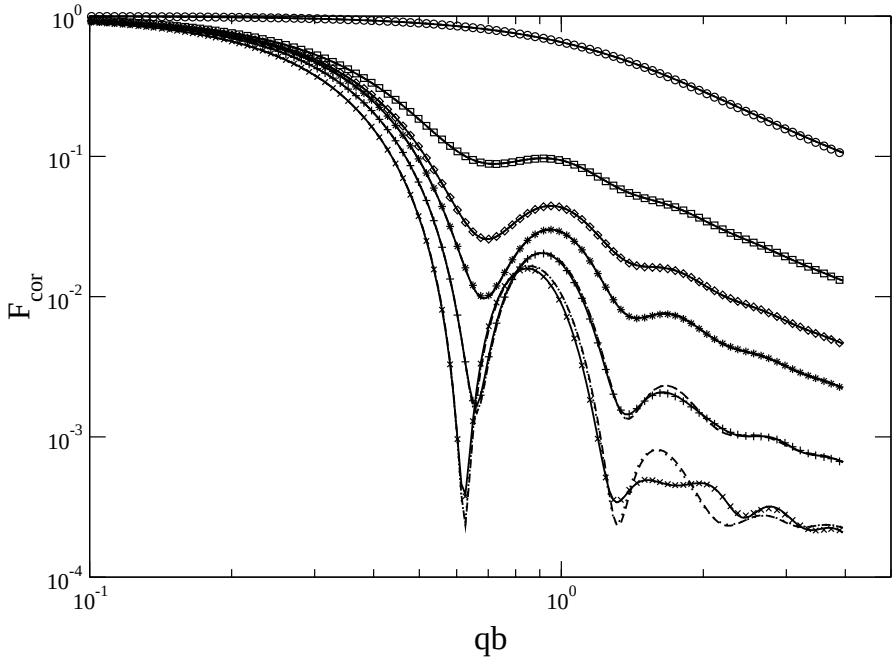

Figure 9.1: Corona scattering for simulations varying the number of chains corresponding to surface coverages $\sigma = 0.016, 0.13, 0.36, 0.72, 2.15$,and 5.37 (top to bottom using symbols). Lines are model fits. Dotted line: BoxGauss, dashed line: ME2, and solid line: ME3 profile.

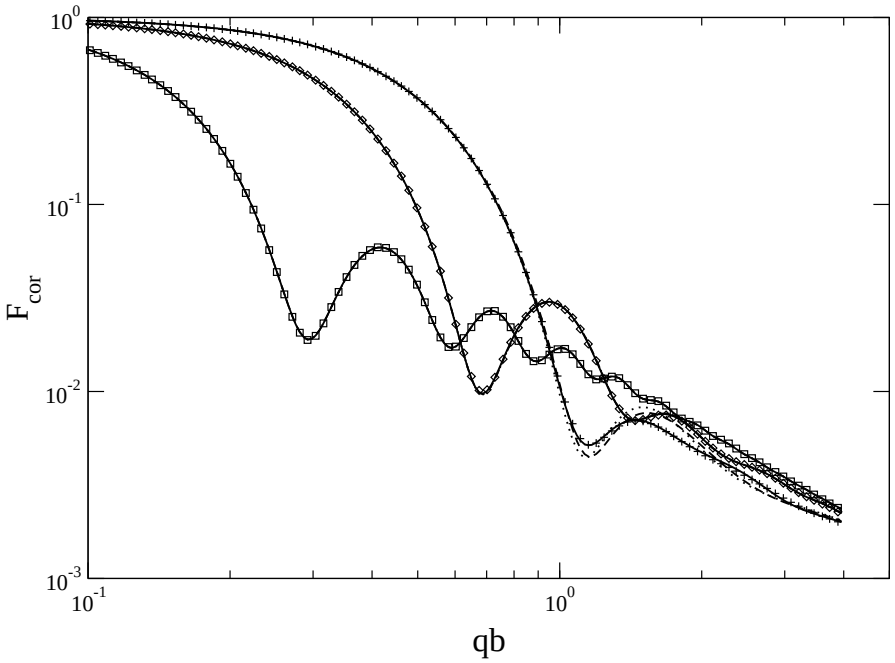

Figure 9.2: Corona scattering for simulations varying the core radius corresponding to surface coverages $\sigma = 0.13, 0.72$, and 2.10, respectively (using box, diamond, and plus symbols respectively). Lines are model fits. Dotted line: Box-Gauss, dashed line: ME2, and solid line: ME3 profile.

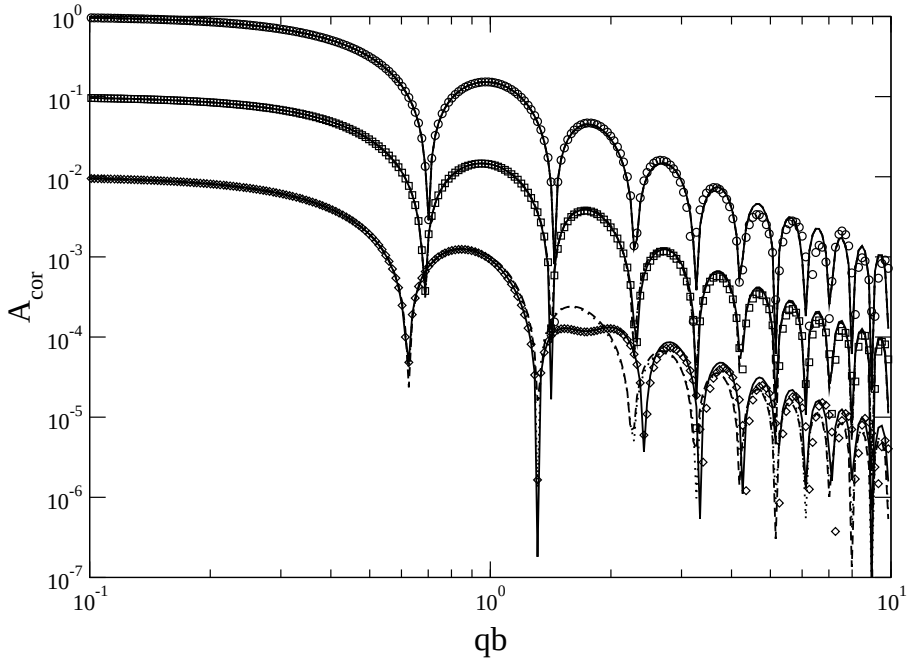

Figure 9.3: Profile scattering for simulations varying the number of chains corresponding to surface coverages $\sigma = 0.016$, $\sigma = 0.72$ (shifted down one decade), and $\sigma = 5.37$ (shifted down two decades). Lines are model fits using BoxGauss profile (dotted), ME2 profile (dashed line), and ME3 profile (solid line).

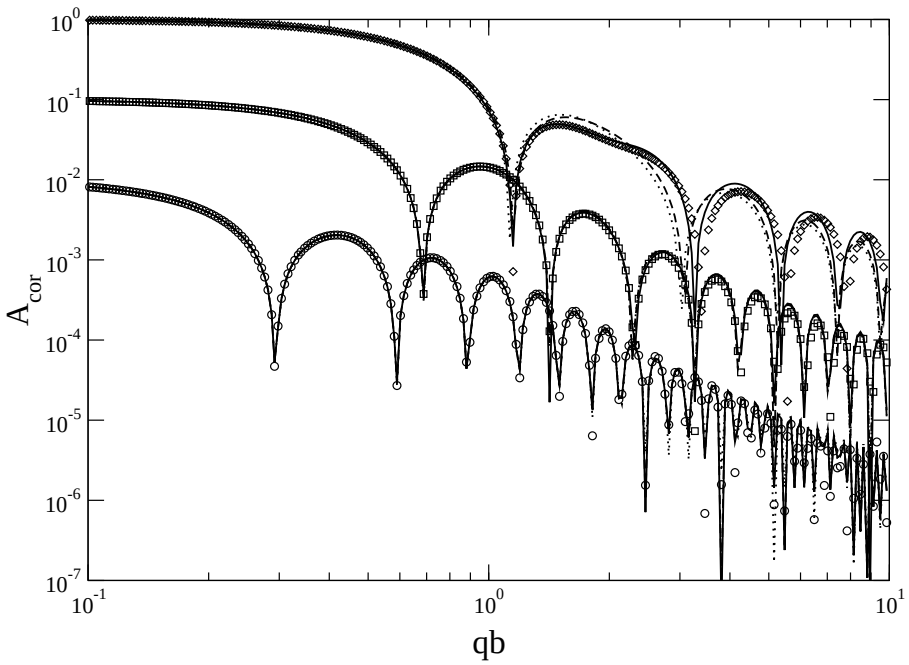

Figure 9.4: Profile scattering for simulations varying the core radius corresponding to surface coverages $\sigma = 0.13$ (shifted down two decades), $\sigma = 0.72$ (shifted down one decade), and $\sigma = 2.10$. Lines are model fits using BoxGauss profile (dotted), ME2 profile (dashed line), and ME3 profile (solid line).

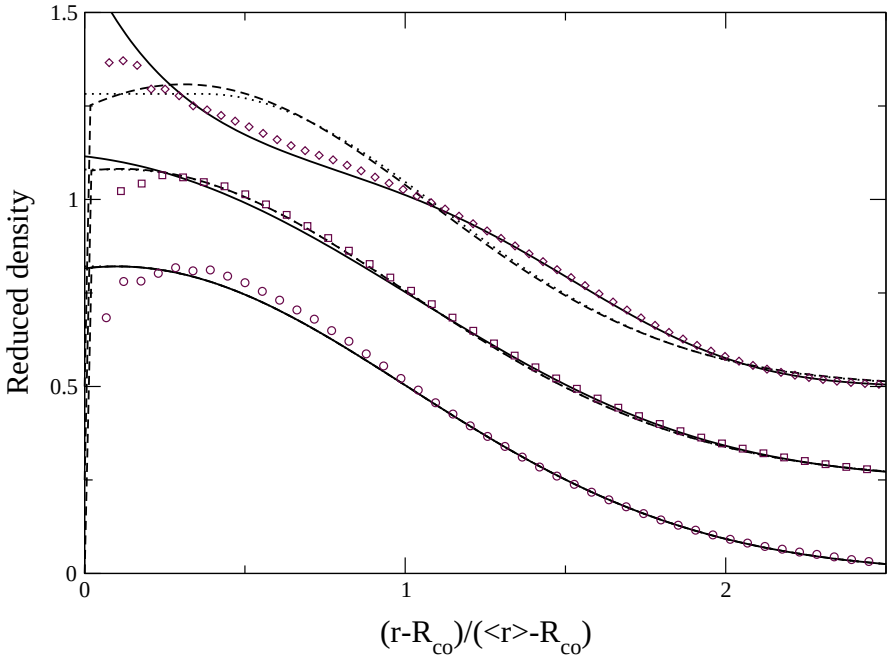

Figure 9.5: Reduced radial density profiles obtained from simulations varying number of chains (symbols) and profiles obtained by fitting the scattering using the BoxGauss (dotted lines), ME2 (dashed lines), and ME3 profile (solid line). The fitted profiles have been transformed using the parameters as for the simulation profile. Simulation profiles are shown for a number of chains corresponding to surface coverages $\sigma = 0.05$ (circle), $\sigma = 0.72$ (box shifted up 0.25), and $\sigma = 5.37$ (diamond, shifted up 0.5).

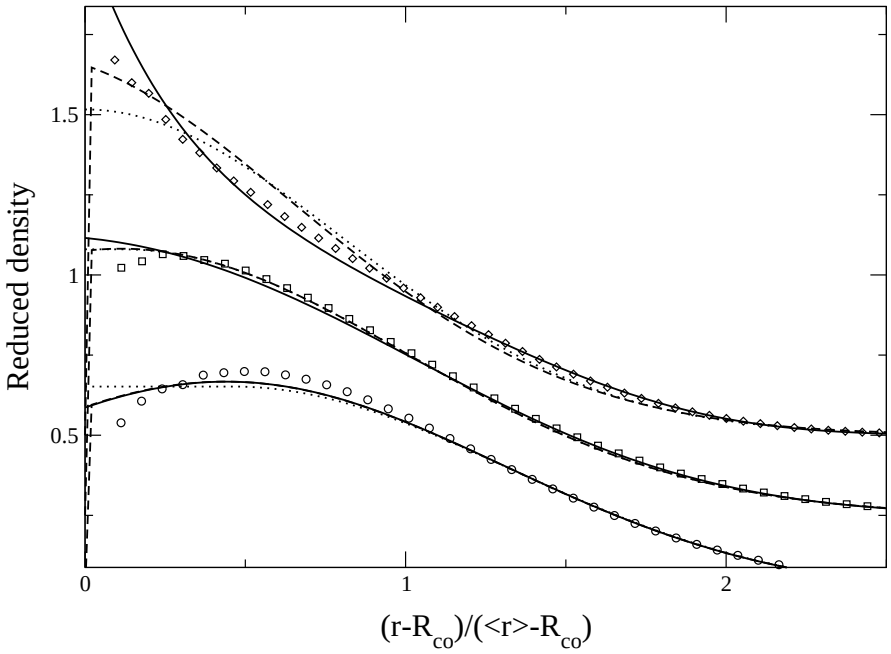

Figure 9.6: Reduced radial density profiles obtained from simulations varying the core radius (symbols) and profiles obtained by fitting the scattering using the BoxGauss (dotted lines), ME2 (dashed lines), and ME3 profile (solid line). The fitted profiles have been transformed using the parameters for the simulation profile. Simulation profiles are shown for a core radius corresponding to surface coverages $\sigma = 0.13$ (circle), $\sigma = 0.72$ (box, shifted up 0.25), and $\sigma = 2.10$ (diamond, shifted up 0.5).

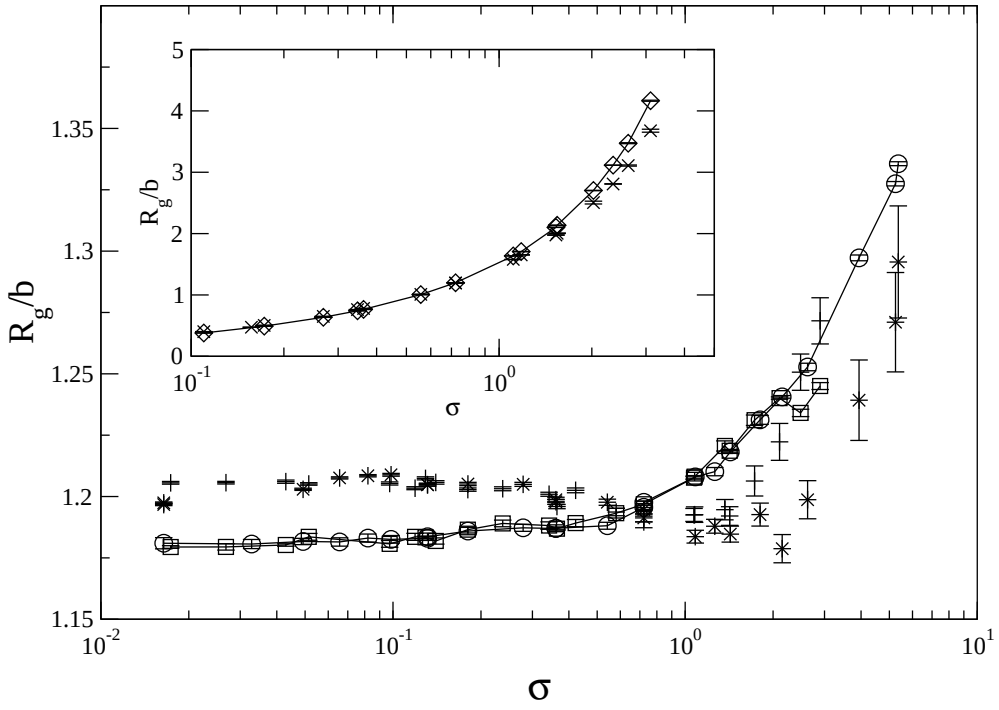

Figure 9.7: Radius of gyration obtained from simulation (lines and symbols) and from fits (symbols) varying number of chains (circle and line) and core radius (box and line). The inset shows the radius of gyration for simulations varying chain length (diamond and line). Radius of gyration estimated by fitting the scattering using the ME3 profile for simulations varying the number of chains (star), core radius (plus) and chain length (cross).

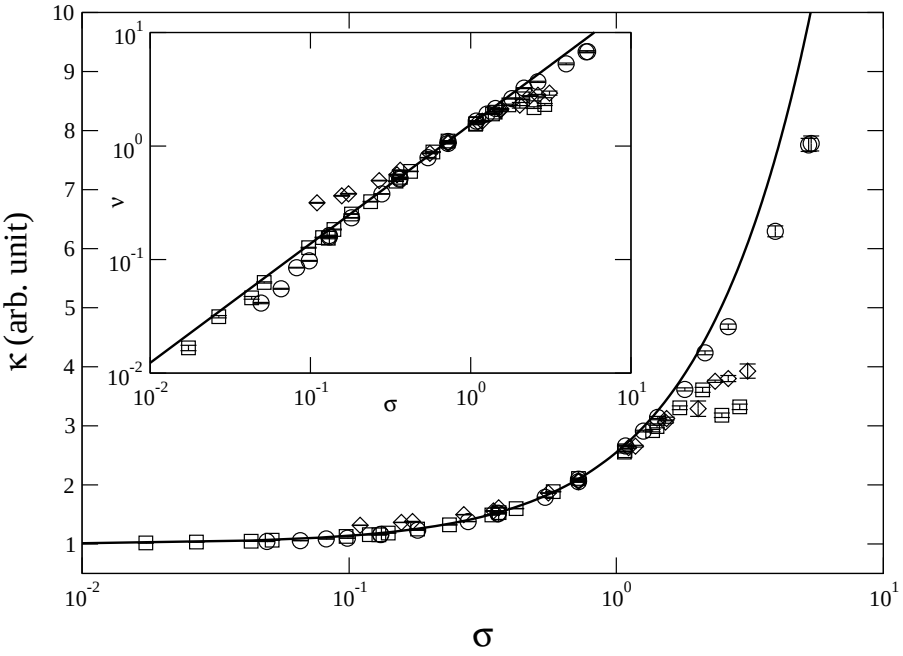

Figure 9.8: Compressibility κ vs. surface coverage σ obtained from fitting the ME3 profile to the simulation data. Inset shows excluded volume coefficient $\nu(\sigma)$ plotted against surface coverage for fits using the ME3 profile. Simulations varying number of chains (circle), core radius (diamond) and chain length (box). The solid line in the inset is the power law relation $\nu(\sigma) = 1.42\sigma^{1.04}$ and the solid line is the corresponding compressibility.

Chapter 10

Article IV

Analytical calculations of scattering form factors of stars, branched polymers and block copolymer micelles for chains with excluded volume interactions

Carsten Svaneborg and Jan Skov Pedersen*

Condensed Matter Physics and Chemistry Department, Risø National Laboratory, DK-4000 Roskilde, Denmark
*Present address: Department of Chemistry, University of Aarhus, Langelandsgade 140, DK-8000 Aarhus C, Denmark

A general formalism is presented for scattering of acyclic polymer structures, and expressions for the form factor of arbitrary branched polymers are derived. In addition expressions are give for the form and intermolecular structure factor for micelles with an arbitrary core geometry, and star polymers with arms consisting of arbitrary block copolymers. Excluded volume interactions are included on the level of a linear chain through the applied scattering expressions. The results for copolymer stars are used for fitting scattering data obtained by Monte Carlo simulations for triblock copolymer stars with $f = 2, 3$, and 6 with and without interactions.

This is an incomplete draft of an article, however, the theory section is complete and forms the majority of the article. The draft article will probably converted into two or three articles, and generalised to structures that include loops. Citations in this article refer to the thesis reference list.

10.1 Introduction

Scattering techniques, such as light scattering, small-angle neutron or x-ray scattering (LS, SANS and SAXS, respectively) are ideally suited for probing the structure of colloidal suspensions [18]. However, a prerequisite for the useful application of scattering methods is the availability of expressions for the form and structure factor, corresponding, respectively to various geometrical models for colloidal aggregates and to their interactions, as this is a requirement for an accurate interpretation and modelling of experimental scattering data, from which parameters related to the structure and interaction of colloidal aggregates can be extracted in an reliable manner.

10.2 Theory

The scattering from a solution of identical composite particles such as micellar aggregates or structures such as branched polymers consists of two terms

$$I(q) = F(q) + H(q).$$

Here the first term is the form factor, i.e. the Fourier transform of the pair-distance distribution function between scatterers within the composite particle, and the second term is the Fourier transform of the pair-distance distribution function between scatterers belonging to different composite particles. This is the intermolecular structure factor. By defining an apparent structure factor as

$$S_{app}(q) = 1 + \frac{H(q)}{F(q)},$$

the total scattering can be recast in the simple form associated with the scattering from dispersions of mono-disperse spheres.

$$I(q) = F(q)S_{app}(q).$$

The normalised ($F(q=0) = 1$) form factor of a composite particle is defined as

$$F(q) = \left(\sum_k b_k\right)^{-2} \left\langle \left| \sum_k \Delta b_k e^{i\mathbf{q}\cdot\mathbf{r}_k} \right|^2 \right\rangle .$$

Here $\mathbf{r}_k$ is a vector describing the location of the k'th scatterer in the composite particle, which has an excess scattering length Δb_k. The average is over all the possible conformations and orientations of the composite particle or structure. The composite particle is assumed to consist of a number of subunits which could be subchains in branched polymer structures, blocks in block copolymers, or corona and core in the case of micelles. In this case

$$F(q) = \left(\sum_k \beta_k\right)^{-2} \left\langle \sum_{j,k} \beta_j \beta_k A_{jk}(\mathbf{q}) \right\rangle ,$$

where the interference from pairs of sites in the j'th and k'th subunits is

$$A_{jk}(\mathbf{q}) = (\beta_j \beta_k)^{-1} \left(\sum_l \sum_i \Delta b_{j_l} \Delta b_{k_i} e^{i\mathbf{q}\cdot(\mathbf{r}_{j_l} - \mathbf{r}_{k_i})} \right),$$

where j_l and k_i denote the subset of all the scatterers contained in the l'th and i'th subunit, respectively. The total excess scattering of the i'th subunit is $\beta_i = \sum_i \Delta b_{k_i}$. Assuming that each subunit has a reference point $\mathbf{R}_i$, such as the center-of-mass of a solid particle, the end of a polymer chain, or the boundary between two adjacent blocks in a copolymer, we can define the form factor amplitude of a subunit i as

$$A_i(\mathbf{q}) = \left(\sum_i \Delta b_{k_i} \right)^{-1} \sum_i \Delta b_{k_i} e^{i\mathbf{q}\cdot(\mathbf{r}_{k_i} - \mathbf{R}_i)}.$$

Using this definition the form factor amplitude is normalised to unity in the limit of small q values, and the scattering from pairs of sites can be expressed as

$$A_{jk}(\mathbf{q}) = A_j^*(\mathbf{q}) A_k(\mathbf{q}) e^{i\mathbf{q}\cdot(\mathbf{R}_j - \mathbf{R}_k)},$$

where A_j^* denotes complex conjugation of A_j. The form factor can be expressed in terms of subunit form factor amplitudes as

$$F(q) \propto \left\langle \sum_j \beta_j^2 A_j^* A_j + \sum_{j \neq k} \beta_j \beta_k A_j^* A_k e^{i\mathbf{q}\cdot(\mathbf{R}_j - \mathbf{R}_k)} \right\rangle.$$

If, for instance, subunits j and k are two distant blocks on a N-block copolymer, then a unique path consisting of steps from one block boundary to the next can be constructed connecting the two reference points of the distant subparticles. The vector connecting the two reference points is nothing more than the sum of all the vectors representing the individual steps. Thus assuming in general that for any pair of subunits j and k a path of $n_{jk} \geq 0$ steps exists, denote by $\mathbf{R}_{jk}^i$ the i'th step in that path, and define $\mathbf{R}_{jk}^0 = \mathbf{R}_k$ and $\mathbf{R}_{jk}^{n_{jk}} = \mathbf{R}_j$, the vector connecting the two reference points can be written in terms of individual steps as

$$\mathbf{R}_j - \mathbf{R}_k = \sum_{i=1}^{n_{jk}} \left(\mathbf{R}_{jk}^i - \mathbf{R}_{jk}^{i-1} \right).$$

In this case the form factor of the composite particle is

$$F(q) \propto \left\langle \sum_j \beta_j^2 A_j A_j^* + \sum_{j \neq k} \beta_j \beta_k A_j^* A_k \prod_{i=1}^{n_{jk}} e^{i\mathbf{q}\cdot\left(\mathbf{R}_{jk}^i - R_{jk}^{i-1}\right)} \right\rangle.$$

At this stage no approximations have been made. However, if we assume that we can carry out the configurational and orientational average of the subunits

independently of each other, which corresponds to an assumption that the pair-distance distribution between scattering sites on different subunits can be factorised into products of site-to-reference, reference-to-reference, and reference-to-site probabilities, we can identity the form factor of the j'th subunit by $F_j(q) = \left\langle A_j A_j^* \right\rangle$, which is a real function, that only depends on the magnitude of the q vector due to the orientational average. If we furthermore assume that the configurational and orientational average of the individual steps can be carried out separately, we can define the phase factor of the i'th step between subunits j and k as

$$\Psi_{jk}^i(q) = \left\langle e^{i\mathbf{q}\cdot\left(\mathbf{R}_{jk}^i - \mathbf{R}_{jk}^{i-1}\right)} \right\rangle,$$

which is the Fourier transform of the distance distribution of each step. For example in the case of a polymer connecting two subunits, the phase factor is the Fourier transform of the end-to-end distance distribution of the connecting block. Subject to these assumptions the normalised form factor $[F(q=0)=1]$ of the composite particle is

$$F(q) = \left(\sum_i \beta_i\right)^{-2} \left\{ \sum_i \beta_i^2 F_i + 2 \sum_{j<k} \beta_j \beta_k A_j \left(\prod_{i=1}^{n_{jk}} \Psi_{jk}^i \right) A_k \right\}.$$

The expression for the form factor of a single composite particle resembles the scattering expression for a solution of different particles, where the product of phase factors plays the role of a partial structure factor between subunits of the composite particle. This is due to the somewhat arbitrary distinction between composite particle and subunit.

The Fourier transform of the pair-distance distribution between sites on different composite particles can be derived through an analogous argument, assuming that the configuration, orientation and location of different particles are uncorrelated [110]. Assuming one of the reference points coincide with the center of mass of the composite particle, then there exists a unique path of $n_{ck} \geq 0$ steps ($n_{cc} = 0$) connecting the center (reference point denoted by index "c") to the k'th reference point, where the i'th step is denoted Ψ_{ck}^i. In this case the inter-particle structure factor is

$$H(q) = \left(\sum_i \beta_i\right)^{-2} \left\{ \sum_k \beta_k A_k \left(\prod_{i=1}^{n_{ck}} \Psi_{ck}^i \right) \right\}^2 \left(S_{cc}(q) - 1\right),$$

where $S_{cc}(q)$ denotes the center-to-center structure factor of the composite particles, which has to be supplied by some other means, such as PRISM theory using an effective interaction potential between the composite particles. The term in the curly parenthesis plays the role of the form factor amplitude of the entire composite particle as it can be identified as the Fourier transform of the radial scattering length distribution [110].

The expressions for the form factor and structure factor were derived assuming that different composite particles, as well as different sub-particles within

the composite particle, are uncorrelated. These approximations are valid at low concentrations of particles, and in cases where the sub-particles are not strongly interacting, such as micellar aggregates with a low surface coverage. It was furthermore assumed that subsequent steps between reference points were not orientationally correlated, and that individual steps only depend on the radial distance. These assumptions are valid for sub-particles connected by flexible and long semi-flexible chain molecules.

The expressions for the form and structure factor are geometrical statements containing only information about the relative positions of sub-particles. Information about the pair distance distribution within a sub-particle is described through the form factor of that sub-particle, while the form factor amplitude contains information about the distance distribution relative to the reference point, and the phase factor contains information about the distance distribution between two reference points, such as the end-to-end distance distribution of the polymer chain connecting two sub-particles. Interactions between scatterers within each sub-particle is included in this description through the particular equations used to describe these three contributions to the scattering functions.

10.3 Subunits consisting of chain molecules

For a chain molecule we chose as reference point one of the ends. The three scattering function contributions: the phase factor, form factor amplitude, and form factor, respectively, are the Fourier transforms of the end-to-end P_{ee}, end-to-site P_{es}, and site-to-site P_{ss} pair-distance probability distributions, respectively. These probability distributions are typically given by the same function, that describes the probability that two sites on the chain, that are separated by a contour length l along the chain, are located at a direct distance r from each other. The scattering functions are defined as

$$\Psi(q,L) = \int \mathrm{d}r 4\pi r^2 \frac{\sin(qr)}{qr} P_{ee}(r,L), \tag{10.1}$$

$$A(q,L) = \int_0^L \mathrm{d}l \frac{1}{L} \int \mathrm{d}r 4\pi r^2 \frac{\sin(qr)}{qr} P_{es}(r,l), \tag{10.2}$$

and

$$F(q,L) = \int_0^L \mathrm{d}l \frac{2(L-l)}{L^2} \int \mathrm{d}r 4\pi r^2 \frac{\sin(qr)}{qr} P_{ss}(r,l), \tag{10.3}$$

where L is the total contour length of the chain. These integral expressions can be recast into sums over the number of segments using the substitutions $L = bN$ and $l = bn$, where b is the Kuhn length, and N the total number of segments. The Kuhn length of a semi-flexible chain is the segment length of the corresponding flexible chain, and thus it is a measure for the length scale below which the chain effectively becomes a rigid rod. The Kuhn length of a flexible chain is identical to the step length of the chain as the direction of subsequent steps are uncorrelated.

The most basic example is a randomly orientated infinitely thin rigid rod with length L. In this case the end-to-end probability distribution is $P_{ee}(r, L) = \delta(L - r)/(4\pi r^2)$. The rigid rod is special as the contour length l and direct distance r are degenerate parameters, and only the contour length integral has to be performed. The end-to-internal point and internal-to-internal point distributions are both given by $P_{es}(r, l) = P_{ss}(r, l) = \Theta(L - r)\delta(r - l)/(4\pi r^2)$, where $\delta(r - l)$ takes care of the degeneracy. Here $\delta(x)$ denotes the delta function, while $\Theta(x)$ denotes the step function. Using these distributions it is straight forward to perform the integrations (10.1)-(10.3) and one obtains

$$\Psi_{rod}(q, L) = \frac{\sin(qL)}{qL}, \quad A_{rod}(q, L) = \frac{\mathrm{Si}(qL)}{qL},$$

and

$$F_{rod}(q, L) = \frac{2\mathrm{Si}(qL)}{qL} - \frac{4}{(qL)^2}\sin^2\left(\frac{qL}{2}\right),$$

where $\mathrm{Si}(x) = \int_0^x \mathrm{d}y \sin(y)/y$ is the Sin integral. The expression for the rod form factor was previous derived by Neugebauer [111]. For a flexible chain without excluded volume interactions, all the pair distance distributions are given by a Gaussian distribution

$$P(r, l) = \left(\frac{3}{2\pi bl}\right)^{\frac{3}{2}} \exp\left(-\frac{3}{2}\frac{r^2}{bl}\right)$$

Based on the Gaussian distribution the integrals (10.1)-(10.3) can be carried out. The result for the form factor amplitude and form factor has previously been given by Hammouda [108] and Debye [71]. Using the abbreviation $x = (qR_g)^2$ where $R_g^2 = bl/6$, the results can be stated as

$$\Psi_o(x) = \exp(-x) \quad A_H(x) = \frac{1 - \exp(-x)}{x} \quad \text{and} \quad F_D(x) = \frac{2[\exp(-x) - 1 + x]}{x^2}.$$

Semi-flexible chains without excluded volume interactions are reasonably described by the second Daniels approximation [55, 58], which is given by

$$P(r, l) = \left(\frac{3}{2\pi bl}\right)^{3/2}\left(1 - \frac{5b}{8l} + \frac{2r^2}{l^2} - \frac{33}{40}\frac{r^4}{bl^3}\right)\exp\left(-\frac{3r^2}{2bl}\right)$$

The three scattering functions can immediately be obtained by integrating this distribution, and they can be written as a perturbation to the expressions for flexible chains as follows

$$\Psi_{Daniels}(x, N_{seg}) = \Psi_o(x) + \frac{x}{2N}\left(1 - \frac{11}{15}x\right)e^{-x},$$

$$A_{Daniels}(x, N_{seg}) = A_H(x) + \frac{1}{30N}\left(4 - 4e^{-x} + 11xe^{-x}\right),$$

and

$$F_{Daniels}(x, N_{seg}) = F_D(x) + \frac{1}{15N}\left\{4 + \frac{7}{x} - \left(11 + \frac{7}{x}\right)e^{-x}\right\}.$$

Here N is the number of statistically independent segments i.e. $N = L/b$. These expressions are valid when $qb < 3.1$ and $l > 10b$ [52]. The expression for the form factor and phase factor was previously given in [58].

For flexible chains with excluded volume interactions the end-to-end, end-to-internal site, and internal-to-internal site distributions are commonly regarded as being best described by the des Cloizeaux distribution [70], which has the form

$$P(r; r_o) = Br_o^{-d}\left(\frac{r}{r_o}\right)^{2+\theta}\exp\left(-D\left(\frac{r}{r_o}\right)^{\delta}\right),$$

where $r_o = \sqrt{\left\langle R_{xy}^2/d\right\rangle}$ is the averaged site-to-site distance, for instance the end-to-end R_{ee}, end-to-site R_{es}, or site-to-site R_{ss} average distance, and d is the space dimensionality. For a flexible chain with excluded volume interactions the site-to-site distance is related to the number of segments as $\left\langle R_{xy}^2\right\rangle = b^2n^{2\nu} = 2(1+\nu)(1+2\nu)R_g^2$, where n is the number of segments connecting the two sites, ν the excluded volume length exponent, and R_g the radius of gyration of the chain. The two exponents δ and θ are given by $\delta = 1/(1-\nu)$ and $\theta = (\gamma-1)/\nu$, where γ is the entropic exponent of an excluded volume chain. In the limit of long flexible chains renormalization group theory estimates the exponents as $\nu = 0.588$ and $\gamma = 1.1619$ for $d = 3$ [68]. The γ exponent vary slightly depending on whether one considers the end-to-end, end-to-internal site, or internal-to-internal pair distance distribution. This is due to the increased degrees of freedom associated with the end points compared to an internal point [60, 64]. B and D are normalisation constants, and they are fixed by requiring that $\int_0^\infty \mathrm{d}^d r P(r, r_0) = 1$ and $\int_0^\infty \mathrm{d}^d r P(r, r_o) r^2 = \langle r_{xy}^2\rangle$, where $\mathrm{d}^d r = 2\pi^{d/2} r^{d-1}/(\Gamma[d/2])\mathrm{d}r$ is the volume of an infinitesimal spherical shell in d-dimensions.

Based on this distribution the phase factor, form factor amplitude, and form factor can be calculated and expressed in terms of a series and an asymptotic expansion valid at low and high q values, respectively. Details are given in the appendix. The results are summarised below using the following abbreviations

$$X = \frac{(1+2\nu)(1+\nu)}{2}\frac{\Gamma(a)}{\Gamma(a+b)}(qR_g)^2, \quad C = \frac{\Gamma[d/2]}{\Gamma[a]},$$

$$a = \frac{2+d+\theta}{\delta}, \quad \text{and} \quad b = \frac{2}{\delta},$$

where $\Gamma[x]$ is the Gamma function. Using these abbreviations the phase factor has an series expansion

$$\Psi(q, R_g) = C\sum_{n=0}^{\infty}\frac{\Gamma[a+bn](-X)^n}{\Gamma[\frac{d}{2}+n]n!},$$

and an asymptotic expansion

$$\Psi(q, R_g) = \frac{C\delta}{2} \sum_{n=0}^{\infty} \frac{(-1)^n \Gamma[\frac{a+n}{b}]}{\Gamma[\frac{d}{2} - \frac{a+n}{b}] n!} X^{-\frac{a+n}{b}}.$$

The form factor amplitude has a series expansion

$$A(q) = C \sum_{n=0}^{\infty} \frac{\Gamma[a+bn]}{\Gamma[\frac{d}{2}+n](2\nu n+1)} \frac{(-X)^n}{n!},$$

and an asymptotic expansion

$$A(q) = \frac{C\Gamma[\frac{1}{2\nu}]\Gamma[a - \frac{b}{2\nu}]}{2\nu\Gamma\left[\frac{d}{2} - \frac{1}{2\nu}\right]} X^{-\frac{1}{2\nu}}$$

$$+C \sum_{n=0}^{\infty} \frac{(-1)^n \Gamma\left[\frac{a+n}{b}\right]}{[b - 2\nu(a+n)]\Gamma\left[\frac{d}{2} - \frac{a+n}{b}\right] n!} X^{-\frac{a+n}{b}}.$$

The form factors based on the des Cloizeaux distribution was derived by Utiyama et al. [70, 112], and is stated here for the sake of completeness; the series expression is

$$F(q) = C \sum_{n=0}^{\infty} \frac{\Gamma\left[a+bn\right](-X)^n}{(1+\nu n)(1+2\nu n)\Gamma\left[\frac{d}{2}+n\right] n!}, \tag{10.4}$$

while the asymptotic expansion is

$$F(q) = \frac{C\Gamma\left[a - \frac{b}{2\nu}\right]\Gamma\left[\frac{1}{2\nu}\right]}{\nu\Gamma\left[\frac{d}{2} - \frac{1}{2\nu}\right]} X^{-\frac{1}{2\nu}} - \frac{C\Gamma\left[a - \frac{b}{\nu}\right]\Gamma\left[\frac{1}{\nu}\right]}{\nu\Gamma\left[\frac{\delta}{2} - \frac{1}{\nu}\right]} X^{-\frac{1}{\nu}}$$

$$+Cb \sum_{n=0}^{\infty} \frac{(-1)^n \Gamma\left[\frac{a+n}{b}\right]}{[b - 2\nu(a+n)][b - \nu(a+n)]\Gamma\left[\frac{d}{2} - \frac{a+n}{b}\right] n!} X^{-\frac{a+n}{b}}.$$

The limit where chains are flexible and non-interacting is given by $d = 3$, $\nu = 0.5$, and $\gamma = 0$. In this case the des Cloizeaux distribution reduce to a Gaussian distribution, and the des Cloizeaux scattering expressions reduce to the previously stated Gaussian expressions.

All these sums can be written in the form

$$S(qR_g) = \sum_{n=0}^{\infty} s_n a_n (qR_g)^{\beta_n} = \sum_{n=0}^{\infty} s_n e^{b_n + \beta_n x} \quad \text{where} \quad x = \ln(qR_g),$$

and $s_n = \text{sign}(a_n)$ in which case the a_n constants can be defined to be positive, e.g. if $a_n = 0$ then the choice $s_n = 0$ and $a_n = 1$ produce the same term. A sufficient number of constants $b_n = \ln(a_n)$ can be calculated in advance, allowing the sums to be estimated with the required precision, without a need for the repeated evaluation of Gamma functions.

10.4 Excluded volume interactions

When writing the Fourier transform of the pair-distance distribution as a product of form factor amplitudes and phase factors, it was implicitly assumed that the pair-distance distribution could be factorised into a convolution of independent site-to-reference, reference-to-reference, and reference-to-site probabilities. This is only true if the correlations caused by interactions between subunits can be neglected. In the case where the same probability distribution describes an entire linear chain consisting of several blocks, the interference term can be calculated exactly. When assuming that the same pair-distribution describes the entire chain, the interference between two distant different blocks j and k on a linear chain, separated by a contour length of L_{ik}, is given by the interference is given by

$$A_{jk}(q; L_j, L_{jk}, L_k) = \int_0^{L_j} \frac{\mathrm{d}l_j}{L_j} \int_0^{L_k} \frac{\mathrm{d}l_k}{L_k} \int_0^{\infty} \mathrm{d}r 4\pi r^2 \frac{\sin(qr)}{qr} P_{ss}(r, l_j + L_{jk} + l_k), \tag{10.5}$$

where P_{ss} is the site-to-site probability distribution. For a Gaussian distribution $A_{jk}(q; L_j, L_{jk}, L_k) = A_H(q, L_j)\Psi_o(q, L_{jk})A_H(q, L_k)$ where the form factor amplitudes and phase factor was presented in the previous section. For a excluded volume chain the des Cloizeaux distribution is used, and a series expansion of the phase factor and performing the contour length integrations, the interference term can be expressed, using the radius of gyration of the two blocks $R_{g,j}$ and $R_{g,k}$ and of the inter-connecting chain segment $R_{g,jk}$, as

$$A_{jk}(q; R_{g,j}, R_{g,jk}, R_{g,k}) = \frac{C}{2} \left(f[R_{g,2}] + f[R_{g,123}] - f[R_{g,12}] - f[R_{g,23}] \right),$$

with the radius of gyration abbreviations

$$R_{g,12} = \left(R_{g,j}^{\frac{1}{\nu}} + R_{g,jk}^{\frac{1}{\nu}} \right)^{\nu}, \quad R_{g,23} = \left(R_{g,jk}^{\frac{1}{\nu}} + R_{g,k}^{\frac{1}{\nu}} \right)^{\nu},$$

and

$$R_{g,123} = \left(R_{g,j}^{\frac{1}{\nu}} + R_{g,jk}^{\frac{1}{\nu}} + R_{g,k}^{\frac{1}{\nu}} \right)^{\nu},$$

and the function f is given by

$$f(R) = \left(\frac{R^2}{R_{g,i} R_{g,k}} \right)^{\frac{1}{v}} g\left(\frac{\Gamma[a](1+\nu)(1+2\nu)}{2\Gamma[a+b]} q^2 R^2 \right),$$

where g has a series expansion

$$g(y) = \sum_{n=0}^{\infty} \frac{\Gamma[a+bn](-y)^n}{(1+\nu n)(1+2\nu n)\Gamma[\frac{d}{2}+n]n!}$$

and an asymptotic expansion

$$g(y) = \frac{\Gamma[a - \frac{b}{2\nu}]\Gamma[\frac{1}{2\nu}] y^{-\frac{1}{2\nu}}}{\nu\Gamma[\frac{d}{2} - \frac{1}{2\nu}]} - \frac{\Gamma[a - \frac{b}{\nu}]\Gamma[\frac{1}{\nu}] y^{-\frac{1}{\nu}}}{\nu\Gamma[\frac{d}{2} - \frac{1}{\nu}]}$$

$$+\sum_{n=0}^{\infty}\frac{b(-1)^n\Gamma[\frac{a+n}{b}]y^{-\frac{a+n}{b}}}{[b-2(a+n)\nu][b-(a+n)\nu]\Gamma[\frac{d}{2}-\frac{a+n}{b}]n!}.$$

In practice the crossover between the series and asymptotic expansion should be located around $y = 15$.

10.5 Arbitrary linear block copolymer

The scattering from a linear copolymer consisting of an arbitrary number of blocks, interacting with excluded volume interactions is given by

$$F_{lin}(q) = \sum_i \beta_i^2 F_i(q, L_i) + 2\sum_{j<k}\beta_j\beta_k A_{jk}(q, L_{jk}),$$

here L_i is the contour length of the i'th block, while $L_{jk} = \sum_{i=j+1}^{k-1} L_i$ is the contour length of all the blocks between the i'th and j'th block. Note that it has been assumed that the pair-distance distribution between blocks is still given by the same des Cloizeaux distribution.

10.6 Arbitrary branched polymer

For an arbitrary branched polymer there are two contributions to the total scattering: One from the form factor of individual sub-chains yielding an F_i for each subchain, and another from interference terms between all pairs of different sub-chains. It is assumed that a unique path consisting of steps from one branch to the next branch exists, which connect any two sub-chains in an arbitrary branched polymer. We then denote the i'th step from branch to branch point between the j'th and k'th polymer segment out of $n_{jk} \geq 0$ steps by $\Psi(q, L^i_{jk})$, where L^i_{jk} is the contour length of the step along the chain. Here it has been assumed that all sub-chains have the same Kuhn length, such that the phase factor is only a function of the contour length of a sub-chain. It is a trivial extension to include different Kuhn lengths of the various segments. In this case the pair distance distribution between any two sites on two different sub-chains consists of a step from the site on the j'th subchain to the reference point (yielding a factor A_j), each of the n_{jk} steps the path connecting the two sites yields a factor, which for the i'th step is $\Psi(q, L^i_{jk})$, and a step from the reference point to a site on the k'th chain (yielding a factor A_k). The form factor of the branched polymer is the sum of the form factors of the individual sub-chains, and the sum of all such possible paths between sites on chains weighted by the respective scattering lengths.

$$F_{branch}(q) = \left(\sum_i \beta_i\right)^{-2}\left(\sum_i \beta_i^2 F_i(q) + 2\sum_{j<k}\beta_j\beta_k A_j(q)A_k(q)\prod_{i=1}^{n_{jk}}\Psi(q, L^i_{jk})\right)$$

This expression have previously been given in the limit of Gaussian chains [19].

10.7 Micelles with an arbitrary core

The form factor of a micelle with an arbitrary core geometry consists of contributions from scattering between the following sub-units: core-core, core-chain, chain-chain on the same chain, and chain-chain between two different chains. The reference point of the core is the center of mass, while reference point for the tethered chains is the tethering point, i.e. the reference point of the chains is the entire core surface. Index "ch" denotes chains, "co" core and "s" denotes the surface.

The pair distance between a scatterer in the core and a chain is given by the step from the core scatterer to the core reference point (A_{co}), a step from the core reference point to any tethering point on the surface (Ψ_s), and from a tethering point to any site on a chain (A_{ch}). However, as the core and core surface are fixed relative to each other the orientational average has to be performed on the product of the respective steps yielding a term proportional to $\langle A_{co}\Psi_s\rangle A_{ch}$ for the core-chain contribution to the total scattering. The pair distance distribution between two sites on two different chains can be regarded as a step from a site on one chain to the tethering point of that chain (A_{ch}), the step from one tethering point on the surface to another tethering point (F_s), and a step from that tethering point to a site on the other chain (A_{ch}), which yields a term $A_{ch}F_sA_{ch}$ for the chain-chain scattering between different chains. The scattering contribution from a pair of scatterers within the same chain is proportional to the chain form factor F_{ch}. β_{ch} is the total scattering length of the corona and contains all sites within the corona, however, intra-chain scattering contributes β_{ch}^2/N while the inter-chain scattering contributes $\beta_{ch}^2(N-1)/N$ to the total corona scattering length. Taking care to introduce all the numerical prefactors the form factor of a micelle becomes

$$F_{micelle}(q) = \frac{1}{(\beta_{co}+\beta_{ch})^2}\left(\beta_{co}^2F_{co} + 2\beta_{co}\beta_{ch}\langle A_{co}\Psi_s\rangle A_{ch}\right.$$

$$\left. + \frac{1}{N}\beta_{ch}^2F_{ch} + \frac{N-1}{N}\beta_{ch}^2A_{ch}^2F_s\right).$$

Assuming that the center of mass of the core coincides with the center of mass of the micelle, we can also give the intermolecular structure factor of the micelles. This consists of the pair distance distribution from a scatterer in the core to the center of the core, yielding a term A_{co}, and a core-chain contribution from the core center to any site on any chain. This consists of a step from the center of the core to the surface (Ψ_s), and a step from the tethering point to any site on a chain (A_{ch}), yielding a term Ψ_sA_{ch}. The result when the excess scattering lengths are included becomes [110]

$$H_{micelle}(q) = \frac{1}{(\beta_{co}+\beta_{ch})^2}\left(\beta_{co}A_{co} + \beta_{ch}A_{ch}\Psi_s\right)^2\left[S_{cc}(q)-1\right].$$

In the special case where the core is spherical the phase and form factor of surface, and the form factor amplitude and form factor of the core, respectively, are given by

$$\Psi_s(qR_{co}) = \frac{\sin(qR_{co})}{qR_{co}} \quad F_s(qR_{co}) = \Psi_s^2,$$

and

$$A_{co} = \frac{3[\sin(qR_{co}) - qR_{co}\cos(qR_{co})]}{(qR_{co})^3} \quad F_{co} = A_{co,}^2$$

where R_{co} denotes the radius of the core. Inserting these expression in the micellar form factor will reproduce the model of Pedersen and Gerstenberg [106, 107]. As correlations between chains and the core have been neglected chains are able to enter the core region, however, core repulsion can be mimicked by increasing the radius in the surface expressions relative to the radius used in the core expressions.

10.8 Stars of arbitrary block copolymers

The form factor of a star polymer made of block copolymers contains three contributions: The form factor of each block, the interference between two blocks on the same chain, and the interference between two blocks on two different chains. We denote the form factor amplitude of the j'th block on the i'th chain as $A_j^{(i)}$, and the corresponding phase factor as Ψ_{ij}. The interference term describing the pair distance between two sites on block j and l, respectively, on the i'th chain consists of a jump from the site to the block boundary closest to the other site (providing a $A_j^{(i)}$ factor), then a number of steps from block boundary to boundary along the chain, each step providing a phase factor until the reference point l is reached yielding $\prod_{\alpha=j+1}^{l-1}\Psi_\alpha^{(i)}$. A step from the reference point to the site on the block provides a form factor amplitude $A_l^{(i)}$.

Similarly the interference term between two sites j and l on two different chains i and k consists of a jump from the site to the block boundary closest to the star center (providing a factor $A_j^{(i)}$), then $j-1$ steps between block boundaries towards the center providing a factor $\prod_{\alpha=1}^{j-l}\Psi_\alpha^{(i)}$, and a number of steps from the center to the l'th block boundary on the k'th chain providing $\prod_{\beta=1}^{l-1}\Psi_\beta^{(k)}$, and a single step from the block boundary to the site providing the form factor amplitude $A_l^{(k)}$.

Let f be the number of arms, and n_i the number of segments on chain i. Then, neglecting the correlations introduced by steric interactions between the different arms and different blocks, the normalised $[F_{star}(q=0)=1]$ form factor of the star consists of the sum of all such paths connecting any two sites:

$$F_{star}(q) = \left(\sum_{i=1}^{f}\sum_{j=1}^{n_i}\beta_j^{(i)}\right)^{-2}\left(\sum_{i=1}^{f}\sum_{j=1}^{n_i}\left(\beta_j^{(i)}\right)F_j^{(i)} + 2\sum_{i=1}^{f}\sum_{\substack{j,l=1\\ j<l}}^{n_i}\beta_j^{(i)}\beta_l^{(i)}A_j^{(i)}A_l^{(i)}\prod_{\alpha=j+1}^{l-1}\Psi_\alpha^{(i)}\right.$$

$$+2 \sum_{\substack{i,k=1 \\ i<k}}^{f} \sum_{j=1}^{n_i} \sum_{l=1}^{n_k} \beta_j^{(i)} \beta_l^{(k)} A_j^{(i)} A_l^{(k)} \prod_{\alpha=1}^{j-1} \Psi_\alpha^{(i)} \prod_{\beta=1}^{l-1} \Psi_\beta^{(k)} \Bigg) . \qquad (10.6)$$

Here $F_j^{(i)}$ is the form factor, $A_j^{(i)}$ is the chain form factor amplitude, $\Psi_j^{(i)}$ is the phase factor, and $\beta_j^{(i)}$ is the excess segmental scattering length of the j'th block on the i'th chain. $R_{g,ij}$ denotes the radius of gyration of block j on the i'th chain. We use a notation where $\prod_{\alpha=j}^{l} \Psi_{i\alpha} = 1$ if $l < j$. The corresponding normalised structure factor is given by the sum of all paths connecting any site on any chain to the center and it is

$$H_{star}(q) = \left(\sum_{i=1}^{f} \sum_{j=1}^{n_i} \beta_{ij} \right)^{-2} \left(\sum_{i=1}^{f} \sum_{j=1}^{n_i} \beta_{ij} A_{ij} \prod_{\alpha=1}^{j-1} \Psi_{i\alpha} \right)^2 (S_{cc}(q) - 1) .$$

10.9 Monte Carlo simulations

Monte Carlo simulations of the scattering from stars of semi-flexible triblock copolymers with and without excluded volume interactions have been performed. The chains on the stars were modelled by a discrete Kratky-Porod model with $L/b = 100$ or 400 segments per arm. Excluded volume interactions were included by placing six hard-spheres with radius $\epsilon = 0.1b$ per Kuhn length of the chain. This is a choice which is known to reproduce the binary cluster intergral of polystyrene in a good solvent [93]. The scattering at homogeneous contrast ($\beta_1 = \beta_2 = \beta_3 = 1$), as well as the scattering from the inner ($\beta_1 = 1$, $\beta_2 = \beta_3 = 0$), middle ($\beta_2 = 1$, $\beta_1 = \beta_3 = 0$), and outer ($\beta_3 = 1$, $\beta_1 = \beta_2 = 0$) scattering have been obtained.

10.10 Results and Discussion

In the special case of a triblock copolymer star with f arms eq. (10.6) reduce to

$$\begin{aligned} F_{star}(q) = f^{-1} (\beta_1 + \beta_2 + \beta_3)^{-2} \{ & \beta_1^2 F_1 + \beta_2^2 F_2 + \beta_3^2 F_3 \\ & +2 (\beta_1 \beta_2 A_1 A_2 + \beta_2 \beta_3 A_2 A_3 + \beta_1 \beta_3 A_1 A_3 \Psi_2) \\ & +(f-1) (\beta_1^2 A_1^2 + \beta_2^2 A_2^2 \Psi_1^2 + \beta_3^2 A_3^2 \Psi_1^2 \Psi_2^2 \\ & +2 (\beta_1 \beta_2 A_1 A_2 \Psi_1 + \beta_2 \beta_3 A_2 A_3 \Psi_1^2 \Psi_2 + \beta_1 \beta_3 A_1 A_3 \Psi_1 \Psi_2)) \} , \end{aligned}$$

This expression was fitted simultaneously to the simulation data using the four scattering contrasts calculated with the Daniels expressions for the form factors, form factor amplitudes, and phase factors and fitting the radius of gyration of each block, as well as the number statistical independent segments in the range of qb from 0.1 to 10. The fits shown in figures 10.1 - 10.3 are in excellent agreement with the simulation results, and the reduced $\chi^2_{red} < 1.2$ for all fits.

The form factor of triblock copolymer stars including excluded volume effects on the linear level is given by

$$F_{star}^{exvol}(q) = f^{-1}\left(\beta_1+\beta_2+\beta_3\right)^{-2}\left\{\beta_1^2F_1+\beta_2^2F_2+\beta_3^2F_3\right.$$
$$+2\left[\beta_1\beta_2A(L_1,0,L_2)+\beta_2\beta_3A(L_2,0,L_3)+\beta_1\beta_3A(L_1,L_2,L_3)\right]$$
$$+(f-1)\left[\beta_1^2A(L_1,0,L_1)+\beta_2^2A(L_2,2L_1,L_2)+\beta_3^2A(L_3,2L_1+2L_2,L_3)\right.$$
$$\left.\left.+2\left(\beta_1\beta_2A(L_1,L_1,L_2)+\beta_2\beta_3A(L_2,2L_1+L_2,L_3)+\beta_1\beta_3A(L_1,L_1+L_2,L_3)\right)\right]\right\}. \tag{10.7}$$

Here the form factor F and form factor amplitude A is given by eq. (10.4) and (10.5), respectively. Excluded volume interactions within each arm are accounted for in this expression, while the excluded volume interactions between arms ignore the presence of the $f-2$ arms. Hence for $f=2$ eq. (10.7) includes the full excluded volume effects. Note the middle block has twice the length of the other blocks. The form factor has been fitted to simulation results for the scattering from a two-arm star with excluded volume interactions and semi-flexibility. Fit parameters were the radius of gyration of the three blocks, and the critical exponents ν and γ as well as four flat backgrounds that is added to the scattering, thus effective exponents averaged over the entire star is obtained. These backgrounds has the effect of mimicking the effects of semi-flexibility on the scattering. The fit has $\chi^2_{red}=2.7$ and is shown on figure 10.4.

The fit yields the exponents $\nu=0.583$ and $\gamma=0.449$. Renormalization group theory [68] yields $\nu=0.588$ and $\gamma=1.1619$ in the long flexible chain limit.

10.11 Appendix

The des Cloizeaux distribution [64, 60] is

$$P(r, r_0) = \frac{B}{r_o}\left(\frac{r}{r_o}\right)^{2+\theta} \exp\left(-D\left(\frac{r}{r_o}\right)^{\delta}\right)$$

with

$$r_o = \sqrt{\frac{\langle R_{ss}^2\rangle}{d}} = \sqrt{\frac{b^2 n^{2\nu}}{d}} = R_g\sqrt{\frac{2(1+2\nu)(1+\nu)}{d}},$$

where b is the Kuhn length of the chain and n the number of segments, while R_g is the radius of gyration. ν, γ are the critical length and entropy exponent, respectively, which for $d = 3$ is estimated to be $\nu = 0.588$ and $\gamma = 1.1619$ from RGT theory [68] for infinite long flexible chains. The Gaussian limit is $d = 3$, $\nu = 0.5$, and $\gamma = 0$ in this limit $r_o^2/2 = b^2 n/6 = R_g^2$

B and D are normalisation constants, derived from the zeroth and second momenta of the des Cloizeaux distribution:

$$B = \frac{\delta\Gamma\left(\frac{d}{2}\right)D^a}{2\pi^{d/2}\Gamma(a)} \qquad D = \left[\frac{1}{d}\frac{\Gamma\left(a+b\right)}{\Gamma\left(a\right)}\right]^{1/b},$$

where the following abbreviations are used: $\delta = 1/(1-\nu)$ and $\theta = (\gamma-1)/\nu$. We use the method and notation used by Förster and Burger[70]. Scattering from a distribution is in arbitrary dimension given by

$$\Psi(q, r_o) = \int_0^\infty P(r, r_o)\,{}_0F_1(\frac{d}{2}; -\frac{(qr)^2}{4})\frac{2\pi^{\frac{d}{2}}r^{d-1}}{\Gamma[d/2]}\mathrm{d}r.$$

For $d = 3$, this reduces to

$$\Psi(q, r_o) = \int_0^\infty P(r)\frac{\sin qr}{qr}4\pi r^2\mathrm{d}r.$$

The definition of the ${}_oF_1$ hyper geometric function is

$${}_0F_1(b; z) = \sum_{n=0}^{\infty}\frac{\Gamma[b]}{\Gamma[b+n]}\frac{z^n}{n!}.$$

Inserting the expression into the integral and integrating produces the series expansion of the phase factor:

$$\Psi(q, R_g) = \frac{2\pi^{d/2}B}{\delta D^a}\sum_{n=0}^{\infty}\frac{\Gamma[a+bn]}{\Gamma[\frac{d}{2}+n]n!}\left(-\frac{(1+2\nu)(1+\nu)}{2dD^{2/\delta}}(qR_g)^2\right)^n$$

We can obtain the asymptotic expansion by rewriting the sum as

$$\Psi(q, X) = C\sum_{n=0}^{\infty}\frac{\Gamma[a+bn]}{\Gamma[d/2+n]}\frac{(-x)^n}{n!} \tag{10.8}$$

where the following abbreviations were used

$$a = \frac{2+d+\theta}{\delta} \quad b = \frac{2}{\delta} \quad x = \frac{(1+2\nu)(1+\nu)}{2dD^b}(qR_g)^2 \quad C = \frac{\Gamma[d/2]}{\Gamma\left[a\right]}.$$

Note that a series can be expressed as a complex integral as

$$\sum_{n=0}^{\infty} \frac{a(n)(-x)^n}{n!} = -\int_{c-i\infty}^{c+i\infty} \frac{dz}{2\pi i} a(z)\Gamma[-z]x^z,$$

where the integration path is chosen to include all poles of the Gamma function, which are located at zero and all positive (real) integers. The asymptotic series expansion is obtained by summing the residues of all poles for $\mathrm{Re}(z) < 0$, i.e. the poles of the prefactor

$$a(z) = \frac{\Gamma[a+bz]}{\Gamma[d/2+z]},$$

which are located at $a + bz = -m$, where m is zero or a positive integer. The residue of the integrand in the m'th pole is

$$\mathrm{Res}[a(s)\Gamma[-s]x^s, s = -(a+m)/b] = \frac{\Gamma[\frac{m+a}{b}]x^{-\frac{m+a}{b}}}{b\Gamma[-\frac{m+a}{b}+\frac{d}{2}]},$$

which yields the asymptotic series as

$$\Psi(q,X) = \frac{C}{b}\sum_{m=0}^{\infty} \frac{(-1)^m\Gamma[\frac{m+a}{b}]x^{-\frac{m+a}{b}}}{\Gamma[\frac{d}{2}-\frac{m+a}{b}]m!}.$$

The form factor is obtained by integrating the phase factor as

$$A(q) = \int_0^N \frac{\mathrm{d}n}{N}\Psi(q, r_o(n))$$

Inserting the sum, using $r_o^2(n) = b^2n^{2\nu}/d$, and interchanging the order of the sum and the integration, the integration can be carried out term by term yielding the series expansion of the form factor amplitude as

$$A(q) = C\sum_{n=0}^{\infty} \frac{\Gamma[\frac{2+d+\theta+2n}{\delta}]}{\Gamma[\frac{d}{2}+n](2\nu n+1)n!}\left(-\frac{(1+2\nu)(1+\nu)}{2dD^{2/\delta}}q^2R_g^2\right)^n.$$

The asymptotic expansion is derived analogous to that of the phase factor. Simple poles are located at $z = -(a+m)/b$ and $z = -1/(2\nu)$ and summation of the corresponding residues yields the asymptotic expansion

$$A(q,N) = C\left(\frac{\Gamma[\frac{1}{2\nu}]\Gamma[a-\frac{b}{2\nu}]x^{-\frac{1}{2\nu}}}{2\nu\Gamma\left[\frac{d}{2}-\frac{1}{2\nu}\right]} + \sum_{m=0}^{\infty}\frac{(-1)^m\Gamma\left[\frac{a+m}{b}\right]x^{-\frac{a+m}{b}}}{m!(b-2(a+m)\nu)\Gamma\left[\frac{d}{2}-\frac{m+a}{b}\right]}\right)$$

Figures

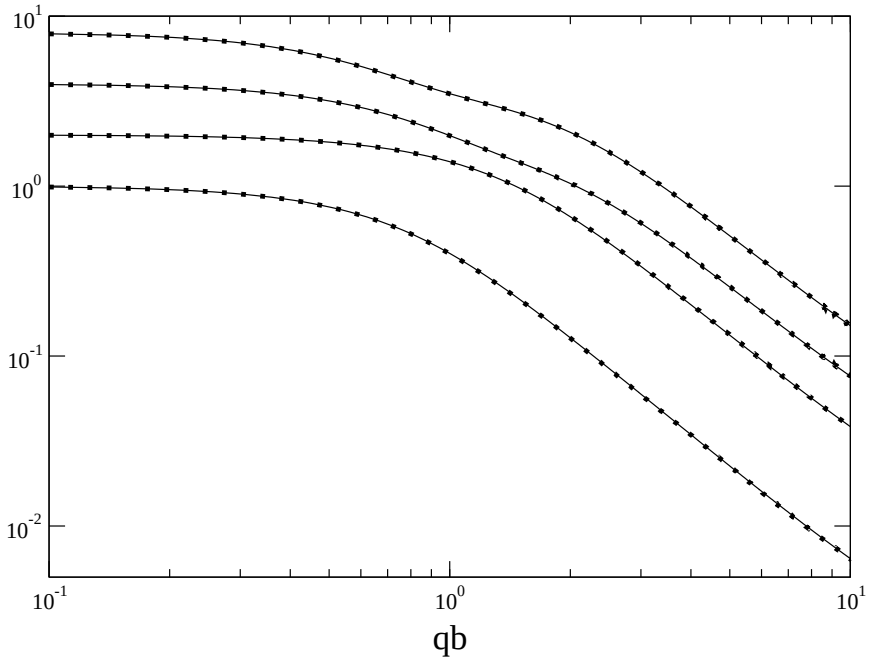

Figure 10.1: Triblock copolymer star (two arms) scattering for semi-flexible chains without excluded volume interactions ($L/b = 100$). Scattering for bulk contrast, inner block, middle block, and outer block (from bottom to top using boxes), fit (line).

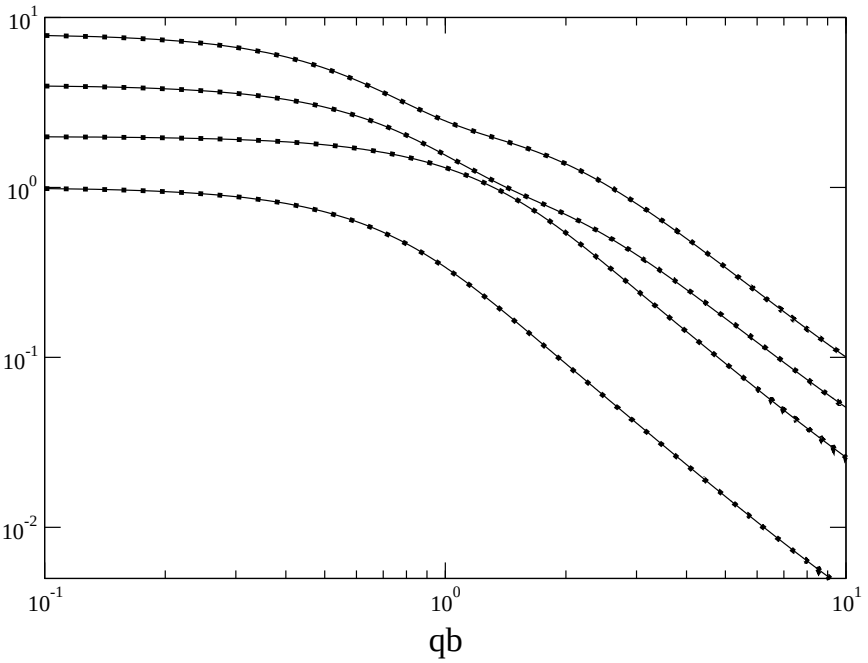

Figure 10.2: Triblock copolymer star (3 arms) scattering for semi-flexible chains without excluded volume interactions ($L/b = 100$). Scattering for bulk contrast, inner block, middle block, and outer block (from bottom to top using boxes), fit (line).

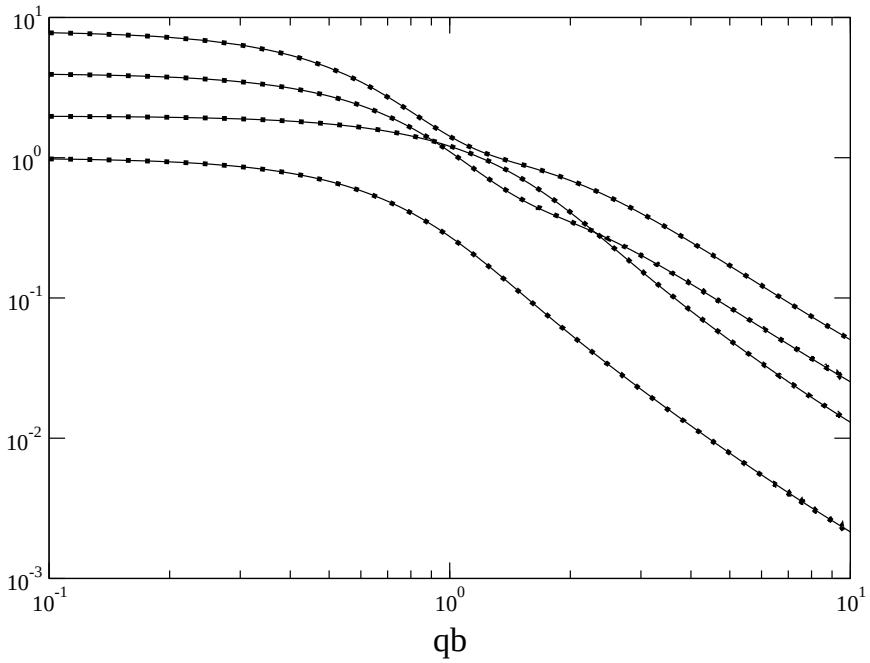

Figure 10.3: Triblock copolymer star (6 arms) scattering for semi-flexible chains without excluded volume interactions ($L/b = 100$). Scattering for bulk contrast, inner block, middle block, and outer block (from bottom to top using boxes), fit (line).

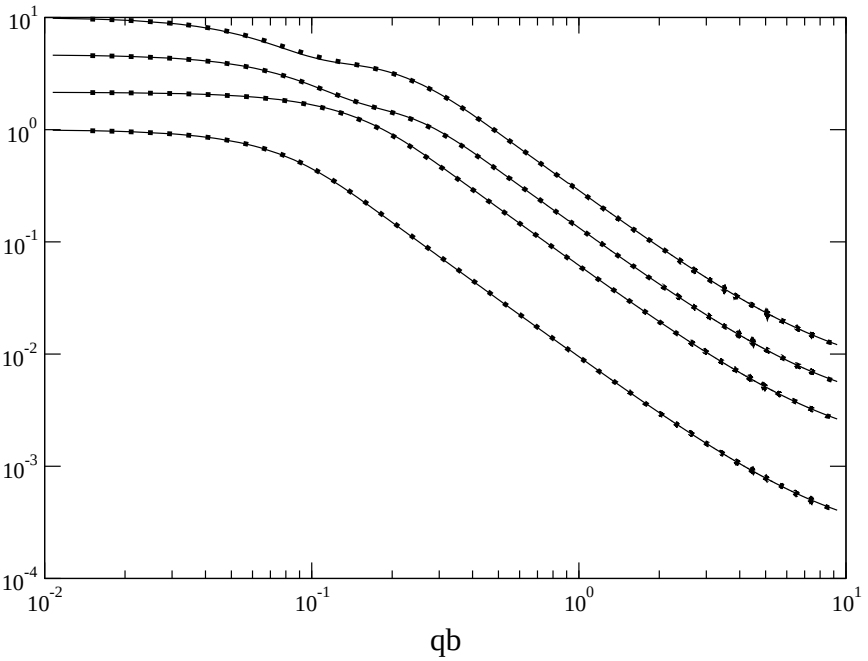

Figure 10.4: Triblock copolymer star (2 arms) scattering for semi-flexible chains with excluded volume interactions ($L/b = 400$). Scattering for bulk contrast, inner block, middle block, and outer block (from bottom to top using boxes), fit (line).

Chapter 11

Conclusion

The aim of the work presented in this thesis was to investigate the scattering from diblock copolymer micelles with a spherical core using Monte Carlo (MC) simulations. The purpose of the simulations was to formulate an expression for the micellar form factor, that can be used when analysing experimental scattering data. Using the solution profile scattering to represent the corona form factor such an expression was formulated, and the expression was validated using self-consistent analysis based on Monte Carlo simulation data in article II. These MC simulations were performed varying the number of chains, chain length and core radius within the experimentally available range of surface coverages for diblock copolymer micelles. The corona form factor was obtained directly from simulation results for the intra-chain and inter-chain scattering, while the solution profile scattering was derived based on the simulation scattering results for the intra-chain and corona form factor amplitude. Comparing the two results for the corona form factor shows an excellent agreement for all simulation data, even at the highest surface coverages. This demonstrates that the scattering from the micellar corona can be regarded as being that of a quasi two dimensional dilute/semi-dilute polymer solution, a solution that is confined to the micellar corona region given by a radial profile with a width comparable to the chain radius of gyration. The comparison shows that the polymer solution scattering can be accurately approximated by an RPA approximation.

Article I investigated the validity of the model due to Pedersen and Gerstenberg. This model includes effects due to single chain scattering and approximates the effects of core expulsion, but it neglects excluded volume interactions within the corona. The conclusion was that this model provides reasonable accurate estimates of the radius of gyration and the corona center of mass distance from the core center for surface coverages less than unity, while deviations increased for increasing surface coverages above unity. The solution profile expression for the corona form factor includes excluded volume interactions as well as core expulsion, and the expression provides excellent fits to the observed scattering which was shown in article III. The estimated parameters have been compared to the same parameters obtained directly from the MC simulation, and it was shown that very accurate estimates for the radius of gyration and the shape of the radial profile are obtained for all simulations. This has validated the pro-

posed solution profile expression for the corona scattering, not just as being a good description of the corona form factor, but also as an excellent tool for estimating physical parameters from the experimental scattering data.

The solution profile concept also allows scattering due to the average radial profile and scattering due to density fluctuations within the profile to be separated, even though the scattering due to the radial profile is the dominant contribution to the corona form factor for low q values. This enables the scattering due to density fluctuations in the forward direction to be obtained using both an model fitting approach and a self-consistent approach. This has enabled the extraction of the corona compressibility and apparent second virial coefficient due to the chain interactions within the micellar corona from the simulated scattering.

The osmotic compressibility has a universal dependence on surface coverage, with small deviations at very high surface coverages, which we attribute to a weak dependence on surface curvature and number of chains. The apparent second virial coefficient for all simulations approximately collapses onto a common power law relation, and the power laws obtained from the self-consistent analysis and model fitting approaches are in reasonable agreement. The osmotic compressibility and apparent second virial coefficient have an dependence on reduced surface coverage analogous that of an ordinary polymer solution on the reduced concentration c/c^*, hence validating the claim that the micellar corona can be regarded as a quasi-two dimensional polymer solution.

Article IV provides a way of calculating the form factor and structure factor of polymer structures such as star copolymers, branched polymers, copolymer micelles, and other structures that can be regarded as consisting of a number of connected subunits. General expressions are presented for the form and structure factor for the polymer structures at level of approximation of the model of Pedersen and Gerstenberg, i.e. interactions between subunits are neglected, however, it is shown how to include excluded volume interactions between subunits on a linear chain, such as the effects of excluded volume interactions between blocks in a copolymer. The formalism requires the knowledge of phase factors, form factor amplitudes, and form factors for all the subunits, for a polymer. These are the Fourier transforms of the end-to-end, end-to-internal site, and internal-to-internal site distance distributions. In the article, results are presented or reviewed for subunits consisting of flexible and semi-flexible chains, as well as chains with excluded volume interactions.

Expressions without excluded volume interactions have been fitted simultaneously to four contrasts of a triblock copolymer star with two, three and six arms, respectively, and the fits are in excellent agreement with the simulation results. An expression with excluded volume interactions has, furthermore, been fitted to a triblock copolymer star with two arms, e.g. a linear pentablock copolymer, and this fit also shows excellent agreement

The articles and the present thesis describe some new simulation techniques. The chain creation technique using a virtual zeroth bond have lead to a considerable simplification of creating a chain with a particular configuration, and has significantly simplified the computational task of correcting vertex positions for numerical errors introduced by the repeated pivot moves compared to the

technique due to Stellman and Gans [102]. A hybrid Fast-Fourier-Transform algorithm for sampling the scattering on a logarithmically distributed q scale has been presented, which greatly reduces the time required for sampling the partial scattering contributions.

A prerequisite for an accurate analysis and interpretation of experimental data is the existence of advanced models. This thesis and the articles included have shown that a relatively simple expression exists for the scattering from diblock copolymer micelles. And a general formalism for calculating form factors of polymer micelles and branched polymer structures has been presented. It is the author's hope that the results presented in the report will be applied for interpreting experimental scattering results, and provide not only information but also knowledge about the structure of complex fluids.

11.1 Suggestions for future work

The chapter summary of articles ended by proposing a generalisation of the scattering from a micelle with an arbitrary core geometry by recasting the corona scattering expression using a solution profile scattering term. However, this expression has yet to be checked using simulation results. Simulations of the scattering from micelles with end-capped cylindrical cores have already been performed, but has yet to be analysed. It would also be interesting to perform simulations with surface coverages in the brush regime, to compare Monte Carlo results with the many theories that exists in this limit, and, for instance, to investigate the compressibility dependence on surface curvature and number of chains.

All the simulations in this thesis have been performed for an athermal solvent. This is sufficient to provide accurate expressions for the scattering from polymers in a good solvent, however, it would be interesting to include an chain-chain interaction potential such that, for instance, the effects of the screened electrostatic interactions polyelectrolyte corona could be investigated.

The RPA approximation in the solution profile scattering contribution works very well within the range of surface coverages simulated, but a full PRISM treatment of the micellar corona should be possible, and this would yield the direct correlation function $c(q)$ as function of number of chains, chain length, and core radius. This would provide an expression for the solution profile scattering which does not rely on the RPA approximation.

The effects due to the structure factor has yet to be explored. In the chapter with the summary of articles an equation for the structure factor using the solution profile expression was proposed for a micellar solution, however, the center-to-center structure factor $S_{cc}(q)$ is assumed to be given in this expression. However, this center-to-center structure factor should also be amenable to a PRISM treatment for instance by defining an effective micelle-micelle potential based on the degree of overlap of the two micellar coronas, which in a mean field approach is simply provided by the overlap of the radial monomer distributions for two micelles.

In article three maximum entropy (ME) estimate for the radial profile was

proposed based on knowledge of the first two/three moments of the profile. These parameters were subsequently obtained by fitting the corona form factor amplitude based on the ME profile to the simulated scattering. It should be possible to formulate a direct maximum entropy expression that provides the corona profile by maximising the entropy subject to the constraints posed by the known scattering data without the assumption that the profile can be represented by a particular functional expression.

The formalism for calculating form and structure factors, which generally neglects excluded volume interactions, has been extended to include excluded volume interactions on the level of linear molecules. An interesting problem would be how to introduce correlations due to interactions for instance between the arms of star polymers. Renormalization group theory calculations for the scattering from star polymers with excluded volume interactions exist, and similar techniques would probably be required for the general problem of introducing interactions. An alternative approach would be to add some general expansion that approximate the effects due to excluded volume interactions, where the expansion parameters could be obtained by fitting numerical simulations. This would provide a general method for parameterising Monte Carlo scattering results from polymer structures.

Chapter 12

Acknowledgements

The first half of this Ph.D. project was spend on fitting models that did not fit, running simulations that crashed due to dark pointer magic, chain correction algorithms that instead made chains explode, fit programs that spontaneously code decayed into gibberish, and doing long calculations that amounted to nothing but a waste basket full of paper. However, when everything finally works and the fits stops throwing fits science is fun, and this makes up for all the time spend on all the now forgotten difficulties. Advice and guidance from my supervisor Jan Skov Pedersen is gratefully acknowledged, as well as for making this Ph.D. project a fun experience.

The pleasant company of my two office mates Asger and Martin as well as fellow students and colleagues wandering by the office in the search for coffee and staying for a chat is acknowledged, even if a chat involved a dosis of whatever theory I found interesting that week.

I would also like to express an appreciation of the support provided by my parents, and acknowledge the family dog Malu (a german shepard) for consistently reminding me of the fact that no matter how important physics is, it is also important to sleep, to eat and drink, and to play with the dog.

The department secretaries are acknowledged for effective assistance with practical problems, and while the Risø Library is very good, the ready assistance from the Risø librarians when I needed some paper or book is gratefully acknowledged, as well as the Danish Polymer Center for giving me a temporary position to finish the papers and prepare the defence of this thesis.

I would also like to acknowledge the time spend by people around the world on making freely available software in their spare time, software such as the Linux operating system, the Latex typesetter, the Lyx editor, the Gnu compiler, and the Xmgrace plot program, programs that have greatly facilitated making the results the project is based on, and writing this thesis.

Bibliography

[1] W.M. Gelbart and A. Ben-Shaul. The new science of complex fluids. *J. Phys. Chem.*, 100:13169–13189, 1996.

[2] P.-G. de Gennes. Soft matter. *Reviews of Modern Physics*, 64(3):645–648, 1992.

[3] T.A. Witten. Structured fluids. *Physics Today*, July:21–28, 1990.

[4] T. Lodge and M. Muthukumar. Physical chemistry of polymers: Entropy, interactions, and dynamics. *J. Phys. Chem.*, 100:13275–13292, 1996.

[5] F.S. Bates and G.H. Fredrickson. Block copolymer-designer soft materials. *Physics Today*, Feb.:32–38, 1999.

[6] A.P. Gast. Polymeric micelles. *Curr. Opin. Colloidal Interface Sci.*, 2:258–263, 1997.

[7] G.A. McConnell, E.K. Lin, A.P. Gast, J.S. Huang, M.Y. Lin, and S.D. Smith. Structure and interactions in tethered-chain systems. *Faraday Discuss.*, 98:121–138, 1994.

[8] K. Mortensen and J.S. Pedersen. Structural study on the micelle formation of poly(ethylene oxide) -poly(propylene oxide)-poly(ethylene oxide) triblock copolymer in aqueous solution. *Macromolecules*, 26:805–812, 1993.

[9] A. Halperin, M. Tirrell, and T.P. Lodge. Tethered chains in polymer microstructures. *Adv. Polym. Sci.*, 100:31–71, 1992.

[10] I. Szleifer and M.A. Carignano. Tethered polymer layers: phase transitions and reduction of protein adsorption. *Macromol. Rapid. Commun.*, 21(8):423–448, 2000.

[11] S.T. Milner. Polymer brushes. *Science*, 251:905–914, 1991.

[12] R. Zana. Micellization of amphiphiles: selected aspects. *Colloids and Surfaces A*, 123-124:27–35, 1997.

[13] T.A. Witten and P.A. Pincus. Colloid stabilization by long grafted polymers. *Faraday Discuss.*, 19:2509–2513, 1986.

[14] J.F. Joanny. Lubrification by molten polymer brushes. *Langmuir*, 8:989–995, 1992.

[15] H. Ji and P.-G. de Gennes. Adhesion via connector molecules: The many-stitch problem. *Macromolecules*, 26:520–525, 1993.

[16] R.S. Ward. Surface modifying additives for biomedical polymers. *IEEE Eng. Med. Biol.*, June:22–25, 1989.

[17] R.L. Lee and P.S. Low. Delivery of liposomes into cultured KB cells via folate receptor-mediated endocytosis. *J. Biol. Chem.*, 269(5):3198–3204, 1994.

[18] P. Lindner and Th. Zemb, editors. *Neutron, X-ray and light scattering: Introduction to an investigative tool for colloidal and polymeric systems.* North-Holland, 1991.

[19] J.S. Pedersen. Analysis of small-angle scattering data from micelles and microemulsions: free-form and model fitting. *Curr. Opin. Colloidal Interface Sci.*, 4:190–196, 1999.

[20] M. Daoud, J.P. Cotton, B. Farnoux, G. Jannink, G. Sarma, H. Benoit, R. Duplessix, C. Picot, and P.G. de Gennes. Solutions of flexible polymers. Neutron experiments and interpretation. *Macromolecules*, 8(6):804–818, 1975.

[21] P.-G. de Gennes. *Scaling concepts in polymer physics.* Cornell University Press, New York, 1979.

[22] P.J. Flory. The configuration of real polymer chains. *J. Chem. Phys.*, 17(3):303–310, 1949.

[23] M. Daoud and J.P. Cotton. Star shaped polymers: A model for the conformation and its concentration dependence. *J. Physique*, 43:531–538, 1982.

[24] A. Halperin. Polymer micelles: A star model. *Macromolecules*, 20:2943–2946, 1987.

[25] S.T. Milner and T.A. Witten. Theory of the grafted polymer brush. *Macromolecules*, 21:2610–2619, 1988.

[26] R.C. Ball, J.F. Marko, S.T. Milner, and T.A. Witten. Polymers grafted to a convex surface. *Macromolecules*, 24:693–703, 1991.

[27] N. Dan and M. Tirrell. Polymers tethered to curved interfaces. A self-consistent-field analysis. *Macromolecules*, 25:2890–2895, 1992.

[28] C.M. Wijmans and E.B. Zhulina. Polymers brushes curved surfaces. *Macromolecules*, 26:7214–7224, 1993.

[29] H. Li and T.A. Witten. Polymers grafted to convex surfaces: A variational approach. *Macromolecules*, 27:449–457, 1994.

[30] K.F. Freed. Functional integrals and polymer statistics. *Adv. Chem. Phys.*, 22:1–128, 1972.

[31] R.R. Netz and M. Schick. Polymer brushes: From self-consistent field theory to classical theory. *Macromolecules*, 31:5105–5122, 1998.

[32] M.A. Carignano and I. Szleifer. Statistical thermodynamic theory of grafted polymeric layers. *J. Chem. Phys.*, 98(6):5006–5018, 1993.

[33] M.A. Carignano and I. Szleifer. Pressure isotherms, phase transitions, instability, and structure of tethered polymers in good, Θ, and poor solvents. *J. Chem. Phys.*, 100(4):3210–3223, 1994.

[34] M.P. Pépin and M.D. Whitmore. Monte Carlo and numerical self-consisent field study of end-tethered polymers in good solvent. *J. Chem. Phys.*, 111(22):10381–10388, 1999.

[35] R. Toral and A. Chakrabarti. Monte Carlo study of polymer chains end-grafted onto a spherical interface. *Phys. Rev. E.*, 47:4240–4246, 1993.

[36] M. Murat and G.S. Grest. Polymers end-grafted onto a cylindrical surface. *Macromolecules*, 24:704–708, 1991.

[37] G.L. Squires. *Introduction to the theory of thermal neutron scattering.* Dover, 1978.

[38] P. M. Chaikin and T. C. Lubensky. *Principles of condensed matter physics.* Cambridge University Press, 1995.

[39] J. P. Hansen and I. R. McDonald. *Theory of simple liquids.* Academic Press, 1986.

[40] E. Merzbacher. *Quantum mechanics.* John Wiley & Sons, New York, 1970.

[41] J.S. Pedersen, I.W. Hamley, C.Y. Ryu, and T.P. Lodge. Contrast variation small-angle neutron scattering study of the structure of block copolymer micelles in a slightly selective solvent at semidilute concentrations. *Macromolecules*, 33:542–550, 2000.

[42] S. Cusack and A. Miller. An investigation of the structure of Alfalfa Mosaic Virus by small-angle neutron scattering. *J. Mol. Biol.*, 145:525–543, 1981.

[43] H.B. Stuhrmann. Contrast variation. In O. Kratky O. Glatter, editor, *Small angle x-ray scattering*, pages 197–213. Academic Press, 1982.

[44] B. Jacrot. The study of biological structures by neutron scattering from solution. *Rep. Prog. Phys.*, 39:911–953, 1976.

[45] T. Ohta and Y. Oono. Conformation space renormalization theory of semidilute polymer solutions. *Physics Lett.*, 89A(9):460–464, 1982.

[46] Y. Oono. Statistical physics of polymer solutions: Conformation-space renormalization-group approach. *Adv. Chem. Phys.*, 61:301–437, 1985.

[47] F. Schmid. Self-consistent-field theories for complex fluids. *J. Phys. Condens. Mater*, 10:8105–8138, 1998.

[48] K.F. Freed. Excluded volume effects in polymers attached to surfaces: Chain conformational renormalization group. *J. Chem. Phys.*, 79(6):3121–3132, 1983.

[49] H. Sagan. *Introduction to the calculus of variations.* Dover, 1992.

[50] M. Plischke and B. Bergersen. *Equilibrium statistical physics.* Prentice-Hall, 1989.

[51] B. Zimm. The scattering of light and the radial distribution function of high polymer solutions. *J. Chem. Phys.*, 16(9):1093–1099, 1982.

[52] R.G. Kirste and R.C. Oberthür. Synthetic polymers in solution. In O. Kratky O. Glatter, editor, *Small angle x-ray scattering*, pages 387–431. Academic Press, 1982.

[53] E. Ott. *Chaos in dynamical systems.* Cambridge University Press, 1993.

[54] P.J. Flory. *Statistical mechanics of chain molecules.* Interscience, 1969.

[55] H.E. Daniels. The statististical theory of stiff chains. *Proc. Roy. Soc. Edinb.*, 63:290–311, 1952.

[56] J.J Hermans and R. Ullman. The statistis of stiff Chains, with applications to light scattering. *Physica*, 18(11):951–971, 1952.

[57] H. Benoit and P. Doty. Light scattering from non-gaussian chains. *J. Chem. Phys.*, 57:958, 1953.

[58] W. Burchard and K. Kajiwara. The statistics of stiff chain molecules I. The particle scattering factor. *Proc. Roy. Soc. Lond. A.*, 316:185–199, 1970.

[59] J. Mazur. On the limiting shape of the distribution function of lengths of a single polymer molecule with excluded-volume effects. *J. Phys. Chem.*, 43(12):4354–4356, 1965.

[60] W. Wittkop, S. Kreitmeier, and D. Göritz. The distribution function of internal distances of a single polymer chain with excluded volume in two and three dimensions: A Monte Carlo study. *J. Phys. Chem.*, 104(1):351–358, 1996.

[61] B. Li, N. Madras, and A.D. Sokal. Critical exponents, hyperscaling and universal amplitude ratios for two- and three-dimensional self-avoiding walks. *J. Stat. Phys.*, 80(3–4):661–754, 1995.

[62] P. Grassberger and R. Hegger. Simulations of three-dimensional Θ polymers. *J. Chem. Phys.*, 102(17):6881–6899, 1995.

[63] A.L. Kholodenko and K.F. Freed. Renormalization group treatment of polymer excluded volume by t'Hooft–Veltman–type dimensional regularization. *J. Chem. Phys.*, 78(12):7390–7411, 1983.

[64] J. des Cloizeaux. Short range correlation between elements of a long polymer in a good solvent. *J. Physique*, 41:233–238, 1980.

[65] A. Jaeckel and J. Dayantis. Statistics of confined self-avoiding walks. Part I: Chain dimensions and concentration profiles. *J. Phys. A. Math. Gen.*, 27:2653–2667, 1994.

[66] S.F. Edwards. The statistical mechanics of polymers with excluded volume. *Proc. Phys. Soc.*, 85:613–624, 1965.

[67] M.K Kosmas and K.F. Freed. Self-Consistent field theories of the polymer excluded volume problem. IV. The linear polymer. *J. Chem. Phys.*, 68(11):4878–4895, 1978.

[68] J.C. Le Guillou and J. Zinn-Justin. Critical exponents from field theory. *Phys. Rev. B.*, 21(9):3976–3998, 1980.

[69] J.P. Valleau. Distribution of end-to-end length of an excluded-volume chain. *J. Chem. Phys.*, 104(8):3071–3074, 1996.

[70] S. Förster and C. Burger. Scattering functions of polymeric core-shell structures and excluded volume chains. *Macromolecules*, 31:879–891, 1998.

[71] P. Debye. Molecular-weight determination by light scattering. *J. Phys. Coll. Chem*, 51:18–32, 1947.

[72] K.S. Schweizer and J.G. Curro. PRISM Theory of the structure, thermodynamics, and phase transitions of polymer liquids and alloys. *Adv. Polym. Sci.*, 116:319–377, 1994.

[73] M. Fuchs and M. Müller. Intermolecular structure factors of macromolecules in solution: Integral equation results. *Phys. Rev. E.*, 60(2):1921–1929, 1999.

[74] A. Yethiraj and K.S. Schweizer. Self-consistent polymer integral equation theory: Comparison with Monte Carlo simulations and alternative closure approximations. *J. Chem. Phys*, 97(2):1455–1464, 1992.

[75] E.F. David and K.S. Schweizer. Integral equation theory of block copolymer liquids. I. General formalism and analytic predictions for symmetric copolymers. *J. Chem. Phys.*, 100(10):7767–7795, 1994.

[76] H. Benoit and M. Benmouna. Scattering from a polymer solution at an arbitrary concentration. *Polymer*, 25:1059–1067, 1984.

[77] M. Gradzielski, D. Langevin, L. Magid, and R. Strey. Small-angle neutron scattering from diffuse interfaces. 2. Polydisperse shells in water-n-alkane-$C_{10}E_4$ microemulsions. *J. Phys. Chem.*, 99:13232–13238, 1995.

[78] Lord Rayleigh. . *Proc. R. Soc. London.*, A84:24, 1911.

[79] O. Glatter. A new method for the evaluation of small-angle scattering data. *J. Appl. Cryst.*, 10:415–421, 1977.

[80] O. Glatter. Evaluation of small-angle scattering data from lamellar and cylindrical particles by the indirect transformation method. *J. Appl. Cryst.*, 13:577–584, 1980.

[81] P.R. Bevington and D.K. Robinson. *Data reduction and error analysis for the physical sciences.* McGraw-Hill, 1994.

[82] W.H. Press, S.A. Teukolsky, W.T. Vetterling, and B.P. Flannery. *Numerical recipes in C.* Cambridge university press, 1992.

[83] W.H. Jefferys. On the method of least squares. *Astron. J.*, 82(2):177–181, 1980.

[84] W.H. Jefferys. On the method of least squares II. *Astron. J.*, 86(1):149–1155, 1981.

[85] J.S. Pedersen. Analysis of small-angle scattering data from colloids and polymer solutions: modeling and least-squares fitting. *Adv. Colloid Interface sci.*, 70:171–210, 1997.

[86] E.T. Jaynes. Probability theory: The logic of science. Available from http://bayes.wustl.edu/etj/prob.html.

[87] G. Bricogne. Maximum entropy and the foundations of direct methods. *J. Appl. Cryst.*, A40:410–445, 1984.

[88] C.J. Gilmore. Maximum entropy and baysian statistics in crystallography: A review of practical applications. *J. Appl. Cryst.*, A52:561–589, 1996.

[89] R.B. Ash. *Information theory.* Dover Publications, 1965.

[90] N. Metropolis, A.W. Rosenbluth, M.N. Rosenbluth, A.H. Teller, and E. Teller. Equation of state calculations by fast computing machines. *J. Chem. Phys.*, 21(6):1087–1092, 1953.

[91] J.S. Pedersen, M.L. Laso, and P. Schurtenberger. Monte Carlo study of excluded volume effects in wormlike micelles and semiflexible polymers. *Phys. Rev. E.*, 54(6):5917–5920, 1996.

[92] J.S. Pedersen and P. Schurtenberger. Static properties of polystyrene in semidilute solutions: A comparison of Monte Carlo simulation and small-angle neutron scattering results. *Europhys. Lett.*, 45(6):666–672, 1999.

[93] J.S. Pedersen and P. Schurtenberger. Scattering functions of semiflexible polymers with and without excluded volume effects. *Macromolecules*, 29(23):7602–7612, 1996.

[94] H. Goldstein. *Classical mechanics.* Addison-Wesley, Reading, Massachusetts, 1980.

[95] M.P. Allan and D. J. Tildesley. *Computer simulation of liquids.* Clarendon Press, Oxford, 1987.

[96] B.M. Forrest and U.W. Suter. Generalized coordinate hybrid Monte Carlo. *Molecular Physics*, 82(2):393–410, 1994.

[97] E. Leontidis, J.J. de Pablo, M. Laso, and U.W. Suter. A critical evaluation of novel algorithms for the fff-lattice Monte Carlo simulation of condensed polymer phases. In L. Monneire and U.W. Suter, editors, *Advances in polymer science*, volume 116, pages 283–318. Springer-Verlag, 1994.

[98] K. Kremer and K. Binder. Monte Carlo simulation of lattice models for macromolecules. In *Computer Physics Reports*, pages 259–310. Elsevier Science Publishers, 1988.

[99] A. Baumgärtner. Simulation of Macromolecules. In K. Binder, editor, *The Monte Carlo method in condensed matter physics*, pages 285–316. Springer verlag, 1995.

[100] M. Lal. 'Monte Carlo' computer simulation of chain molecules. I. *Molecular Physics*, 17(1):57–64, 1969.

[101] N. Madras and A. D. Sokal. The pivot algorithm: A highly efficient Monte Carlo method for the self-avoiding walk. *J. Stat. Phys.*, 50(1/2):109–186, 1988.

[102] S.D. Stellman and P.J. Gans. Efficient computer simulation of polymer conformation. I. Geometric properties of the hard-sphere model. *Macromolecules*, 5(4):516–526, 1972.

[103] S.D. Stellman, M. Froimowitz, and P. J. Gans. Efficient computation of polymer conformation energy. *J. Comput. Phys.*, 7:178–181, 1971.

[104] D. Frenkel, R.J. Vos, C.G. de Kruif, and A. Vrij. Structure factors for polydisperse systems of hard spheres. A comparison of Monte Carlo simulations and Percus-Yevick theory. *J. Chem. Phys.*, 84:4625, 1986.

[105] B. Stoustrup. *The C++ programming language.* Addison-wesley, 2000.

[106] J.S. Pedersen and M.C. Gerstenberg. Scattering form factor of block copolymer micelles. *Macromolecules*, 29:1363–1365, 1996.

[107] J.S. Pedersen. Form factors of block copolymer micelles with spherical, ellipsoidal and cylindrical cores. *J. Appl. Cryst.*, 33:637–640, 2000.

[108] B. Hammouda. Structure factor for starburst dendrimers. *J. Polym. Sci., Part B: Polym. Phys.*, 30:1387–1390, 1992.

[109] M. Kotlarchyk and S.H. Chen. Analysis of small angle neutron scattering spectra from polydisperse interacting colloids. *J. Phys. Chem.*, 79(5):2461–2469, 1983.

[110] J.S. Pedersen. Structure factor effects in small-angle scattering from block copolymer micelles and star polymers. *J. Chem. Phys.* accepted for publication.

[111] T. Neugebauer. *Ann. Phys. (Leipzig)*, 42:509, 1953.

[112] H. Utiyama, Y. Tsunashima, and M. Kurata. Rayleigh scattering by linear flexible macromolecules. *J. Chem. Phys.*, 55(7):3133–3145, 1971.